UNIVERSITY OF CALIFORNIA,

IRVINE

Improving estimates of the permafrost carbon-climate feedback with year-round measurements, inventories, and ecosystem manipulations

DISSERTATION

Submitted in partial satisfaction of the requirements for the degree of

DOCTOR OF PHILOSOPHY

in Earth System Science

by

Shawn Alexander Pedron

Dissertation Committee:

Associate Professor Claudia I. Czimczik (chair)

Professor Michael L. Goulden

Ralph J. and Carol M. Cicerone Professor James T. Randerson

Professor Jeffrey M. Welker

2021

DEDICATION

To my father Stephen Pedron,

who gave me ambition, self-worth, and maxims to succeed by-

"Use the right tool for the job."

"If you want something done right, do it yourself."

To my mother Nicole Pedron,

who taught me the high value of female leadership.

And to my partner Jessica Vaisz,

whose deep beauty and ardent devotion make me feel complete.

TABLE OF CONTENTS

LIST OF FIGURES

LIST OF TABLES

ACKNOWLEDGEMENTS

I have learned a great amount during this degree, about science, myself, others, and some ways that all of these connect. One thing I see more clearly than ever is how directly my capacity for success is related to the quality of my relationships, personal and professional.

From my undergraduate at University of Arizona, I credit my composure in the lab to Mary Kay Amistadi, who always took the time to explain what the stakes were and how to train for them. In my graduate career at University of California, Irvine, my first-year professors taught me to use numbers and words as tools to operate like a scientist. I have also benefitted tremendously from the mentorship of my thesis committee, especially my advisor Claudia Czimczik, who is never afraid to look at something a new way. Claudia, thank you for being an endless fountain of great ideas, and being keenly interested while still allowing me creative freedom. Mike Goulden, thank you for giving me a deeper understanding of the way that carbon moves through ecosystems. James Randerson, thank you for helping me understand the importance and mechanics of models; your demeanor of endless interest and curiosity is an inspiration.

Through my Earth System Science research, I have had opportunities to work and travel with brilliant and interesting people from an incredible variety of backgrounds, with technical expertise ranging from nuclear physics to dog sledding. The ambitious enthusiasm of undergraduate researchers has helped advance my research in the field and lab. Jennifer Walker laid the foundation for the new instruments in Chapter 2 and trained me how to avoid blowing up glassware (mostly). Xiaomei Xu, Guaciara dos Santos, John Southon, and the ^{14}C lab do pioneering work, which I am very grateful to have access to. Cyril McCormick and Ricardo Jimenez helped me think like an engineer, and Colin Edgar has an intuitive understanding of sensory equipment from eddy covariance to battery banks that he shares without hesitation. Jebediah Tim, Amanda Young, and the Toolik staff are so adept and professional that I have been able to collect data and samples from the middle of the Alaskan tundra since my first year.

My partner Jessica Vaisz has never wavered in her support of my love for science, even while raising two enormous puppies alone when I left for a field campaign. She and her family have supported my mental and physical health in the easiest and most difficult times, and I am lucky to have them in my life. My own family has also been a constant support. My father taught me the dedication, curiosity, and creativity that have helped me progress as a researcher. The cohort who I began the degree with are all smart individually, and even better together. Regular get-togethers with Dillon Elsbury, Kevin Wright, and Zach Wolff, always answered questions and generated new ideas, and expanded my cinematic horizons. Nikki Fiori has also been a terrific collaborator and friend.

My work is made possible with funding from the Jenkins family (for my first year), NSF EAGER (Ch. 2-3) NASA ABoVE, and the International Tundra Experiment (Ch. 4). Ridge 2 Reef also funded part of my degree, allowing me to learn what ambitious science outreach looks like from Steven Allison, and to build my geospatial analysis experience with community partners. I am grateful for the opportunity to work in an ancestral hunting ground of the Nunamiut people and share their respect for the pristine land which has made my research possible. I am also grateful to my Alaskan collaborators Jeffrey Welker, Eric Klein, and Gus Jespersen for welcoming me into their world, and look forward to our future work together.

CURRICULUM VITA

Shawn Alexander Pedron

EDUCATION

- PhD, Earth System Science — University of California, Irvine, USA — 2021
- MS, Earth System Science — University of California, Irvine, USA — 2019
- BS, Chemistry — University of Arizona, Tucson, USA — 2015

RESEARCH EXPERIENCE

Czimczik Lab Aug. 2016-Present — Irvine, CA, USA

International Tundra Experiment (ITEX) – Arctic Observatory Network (AON) — Toolik Lake, AK

- Investigated permafrost soil carbon stock and flux responses to increased snow duration and thickness
- Lead design and installation of new passive soil $^{14}CO_2$ sampling technology
- Performed instrument and datalogger repair and maintenance in cooperation with field support

NSF Early-Concept Grants for Exploratory Research (EAGER) — Toolik Lake, AK, USA

- Developed and tested a technique for quasi-continuous, year-round sampling of soil-respired CO_2 for ^{14}C and ^{13}C analysis to investigate soil carbon vulnerability to remineralization in permafrost
- Partitioned soil respiration into hetero- and auto-trophic components and calculated year-round flux-weighted isotopic signatures for soil column

NASA Arctic Boreal Vulnerability Experiment (ABoVE) — Fairbanks, AK, USA

- Constrained satellite remote sensing data of Arctic boreal post-fire forest succession and shrub expansion with ground-truthing techniques such as tree, shrub, and soil core samples, leaf-area index, Landsat-derived NDVI, and vegetation surveys
- Research location targeted 102 tree + 5 shrub sites around Fairbanks and the Dalton Highway

Ridge to Reef (NSF NRT*)* Aug. 2017-Present — Irvine, CA, USA

- Co-developed urban ecosystem management solutions with scientists and project managers
- Designed ArcGIS layer for restoration and plant functional type change at Crystal Cove State Park

AZ Lab for Emerging Contaminants Aug. 2013-Aug. 2016 — Tucson, AZ, USA

- Performed high-throughput (10,000+ samples $year^{-1}$) CZO (Critical Zone Observatory) and private water sample analyses, data QA/QC, training, and assistance with field sampling
- Trained to operate and maintain analytical instruments including ICP-MS, AF4, EC (C/N/S), TOC-TN (solid/liquid), XRF, IC, HPLC, Spectrofluorimetry, UV-Vis
- Trained to handle biohazards, radioactive material, compressed gases

PEER-REVIEWED PUBLICATIONS

- Fiore, N. M., Goulden, M. L., Czimczik, C. I., **Pedron, S. A.**, & Tayo, M. A. (2020). *Do recent NDVI trends demonstrate boreal forest decline in Alaska?*. Environmental Research Letters.
- **Pedron, S.A.**, Xu, X., Walker, J., Ferguson, J.C., Jespersen, R.G., Welker, J.M., Klein, E.S., Czimczik, C.I., (in press). *Time-integrated collection of CO_2 for ^{14}C analysis from soils.*

Under construction

- **Pedron, S.A.**, Euskirchen, E., Ferguson, J.C., Jespersen, R.G., Welker, J.M., Czimczik, C.I., (2020). *Closing the winter gap – Year-round measurements of soil respiration sources in Arctic tussock tundra.*

- **Pedron, S.A.**, Welker, J.M., Czimczik, C.I., (2020). *Subsidence and compaction due to snow-induced permafrost thaw increases soil C and N exposure.*
- Jespersen, R.G., **Pedron, S.A.**, Ferguson, J.C., Czimczik, C.I., Welker, J.M., (2020). *Snow-induced permafrost thaw mobilizes ancient C year-round at depth and surface.*
- **Pedron, S.A.**, Jespersen, R.G., Martinez, B., Goulden, M. L., Czimczik, C.I., (2020). *Growing season temperature increase drives low Arctic shrub expansion.*

CONFERENCE PRESENTATIONS

Oral

- **Pedron, S.A.**, Czimczik, C.I., Walker, J.C., Klein, E.S., Euskirchen, E.S., Welker, J.M., *Closing the winter gap – Year-round measurements of soil respiration sources in Arctic tussock tundra.* 2nd Annual Radiocarbon Summit at JPL, La Cañada Flintridge, CA, USA, February 5, 2020 (**Invited**)
- **Pedron, S.A.**, Xu, X., Holden, S.R., Natasha, A., Czimczik, C.I., Jespersen, R.G., Ferguson, J.C., Welker, J.M., *Accessibility of permafrost carbon in a changing Arctic: Assessing the influence of experimentally- increased snowpack height on microbial carbon sources.* American Geophysical Union, San Francisco, CA, USA, December 9-13, 2019

Poster

- Jespersen, R.G., **Pedron, S.A.**, Czimczik, C.I., Welker, J.M., Ferguson, J.C., Xu, X., *Ancient C emissions from Arctic tundra: soil carbon isofluxes ($^{14}CO_2$) in response to long-term changes in winter snow depth.* American Geophysical Union, San Francisco, CA, USA, December 9-13, 2019
- Fiore, N.M., Goulden, M.L., Czimczik, C.I., **Pedron, S.A**., Tayo, M.A., *Composition and structure of browning and greening forests in interior Alaska.* 5th ABoVE Science Team Meeting, San Diego, CA, USA, May. 20-23, 2019
- Martinez, B., **Pedron, S.A**., Niu, L., Tayo, M.A., Fiore, N.M., Goulden, M.L., Czimczik, C.I., *Implications of Shrub Expansion for Carbon and Nitrogen Cycling in Arctic Tundra.* 5th ABoVE Science Team Meeting, San Diego, CA, USA, May. 20-23, 2019
- **Pedron, S.A**., Xu, X., Walker, J., Welker, J.M., Klein, E., Euskirchen, E., Czimczik, C.I., *Apportioning seasonality of soil respiration sources: A passive, quasi-continuous $^{14}CO_2$ sampler.* American Geophysical Union, Washington, D.C., USA, Dec. 8-14, 2018
- Fiore, N.M., Goulden, M., Czimczik, C.I., **Pedron, S.A**., *Forest composition, structure and productivity of browning and greening forests in Interior Alaska.* American Geophysical Union, Washington, D.C., USA, Dec. 8-14, 2018
- **Pedron, S.A**., Xu, X., Walker, J., Welker, J.M., Klein, E., Euskirchen, E., Czimczik, C.I., *Closing the winter gap in permafrost carbon emissions: A passive, quasi-continuous $^{14}CO_2$ sampler.* Toolik All Scientists Meeting, Portland, OR, USA, Jan. 27-28, 2017 *and* American Geophysical Union, New Orleans, LA, Dec. 11-15, 2017 (updated)

COMPUTATIONAL SKILL

- R — statistical analysis, data visualization, large datasets, time series
- Autodesk Fusion360 — computer-assisted design and rendering
- ArcGIS — geospatial analysis, gridded datasets
- Additional experience in Python, MATLAB, NetCDF Operators, Unix, Excel

SELECTED FELLOWSHIPS AND AWARDS

- Outstanding Contributions to the Department award, ESS, UCI — 2019
- Ridge to Reef research fellowship — 2018-2019
- Associated Graduate Students travel grant to AGU — 2018
- Permafrost Young Researcher Network travel grant to AGU — 2017
- University of Alaska, Fairbanks travel grant to Toolik All Hands Meeting — 2017

TEACHING AND MENTORING

- 1-on-1 research and mentoring (lab, field, data processing) with 6 undergraduate students, representing female, international, underrepresented minority, and 1st generation college students
- Climate Literacy Empowerment and iNquiry (CLEAN): Design and engage in local under-served K-12 school classroom activities to promote understanding of the Earth's climate system
- 6 quarters of Teaching Assistantships in introductory and advanced Earth System Science courses

SERVICE

- Diverse Educational Community and Doctoral Experience (DECADE) — Irvine, CA, USA
- Graduate student representative for Earth System Science — Irvine, CA, USA
- Ridge to Reef Council member — Irvine, CA, USA
- Tucson Samaritans — Tucson, AZ, USA
- Autism mentoring — Dallas, TX, USA

MEMBERSHIP

- American Geophysical Union (AGU) — 2017-Present
- US Permafrost Association (USPA) — 2017-Present
- Permafrost Young Researcher Network (PYRN) — 2017-Present

ABSTRACT OF THE DISSERTATION

Improving estimates of the permafrost carbon-climate feedback
with year-round measurements, inventories, and ecosystem manipulations

by

Shawn Alexander Pedron

Doctor of Philosophy in Earth System Science

University of California, Irvine, 2021

Associate Professor Claudia Czimczik

Rapid warming and changing precipitation patterns in northern regions are alleviating temperature and nutrient limitations on microbial activity in soils and jeopardizing the stability of vast amounts of ancient organic carbon (C) stored in near-surface permafrost. Like fossil fuels, permafrost C is depleted in radiocarbon (^{14}C) and its emission to the atmosphere contributes to climate change. While tundra systems continue to sequester C during the growing season, evidence is emerging that the non-growing season (fall through spring) is a critical period of microbial activity – turning the Arctic into a net C source.

In my dissertation, I developed and deployed new technology to elucidate which C sources fuel microbial activity during the non-growing season and to quantify emissions of permafrost C. First, I present a new sampler for collecting depth-resolved, time-integrated soil-respired CO_2 for ^{14}C analysis from upland permafrost soils year-round. Second, I describe the

first continuous, depth-resolved time series of microbial C emissions and annual flux-weighted signature of ecosystem-respired $^{14}CO_2$ from graminoid tundra derived from year-round *in situ* measurements of soil $^{14}CO_2$. Results show that soil microorganisms shift from using modern C during the growing season to increasingly older C pools in fall to winter. Third, I couple the sampler with bulk soil analyses, incubations, and soil thaw and land-atmosphere C flux observations to show that permafrost thaw, compaction and subsidence from 25 years of experimental snow augmentation has mobilized significant amounts of ancient C and profoundly impacted nitrogen cycling. These studies illustrate greater than expected seasonal dynamics in microbial C oxidation, further highlighting the role of the non-growing season for permafrost C emissions and paving the way for a regional-scale assessment of permafrost C emissions in the rapidly changing Arctic.

Chapter 1: Introduction

The Arctic is an important component of the Earth system that is experiencing rapid climate change. Northern high latitudes are warming twice as fast relative to global rates, a process known as "Arctic amplification," and receiving greater amounts of precipitation (Box *et al.*, 2019; Jeffries *et al.*, 2013; Overland *et al.*, 2019). Temperatures have increased the most in coastal regions affected by declining sea ice cover and during the fall and winter. This accelerated climate change has already brought the Arctic region beyond the 2˚C-warming threshold targeted by the UN Paris climate agreement (U Nations 2015), and has started to transform Arctic ecosystems and landscapes (Post *et al.*, 2019) from a "brake" to "accelerator" of climate change (Steffen, 2006).

A major consequence of Arctic climate change is the warming of permafrost (Biskaborn *et al.*, 2019; Chadburn *et al.*, 2017; Osterkamp, 2003). Permafrost, defined as ground that remains at or below 0˚C for 2 or more consecutive years, underlies 22% of the land surface of the Northern Hemisphere (Obu *et al.*, 2019, Fig. 1). Between 2007 and 2016, permafrost temperatures averaged across polar and high-mountain regions have increased by 0.29 ± 0.12 °C (Pörtner *et al.*, 2019). The Coupled Model Intercomparison Project CMIP6 models project that the annual mean frozen volume in the top 2 m of the soil could decrease by 10%–40% $^{\circ}C^{-1}$ of global mean surface air temperature increase (1.7 to 2.7 × 10^6 km^2 $^{\circ}C^{-1}$) (Burke *et al.*, 2020).

The warming and loss of permafrost has important consequences for the global carbon (C) cycle. Soils are a large reservoir of organic C (containing about 2 to 3 times the amount of C in the atmosphere), and an estimated 30-50% of the global reservoir of soil C is currently frozen in permafrost (472±27 Pg C for 0–1 m) (Hugelius *et al.*, 2014). Much of this carbon has slowly

accumulated over millennia as a consequence of syngenetic soil formation processes (Ping *et al.*, 1998; Schirrmeister *et al.*, 2011a, 2011b; Strauss *et al.*, 2012).

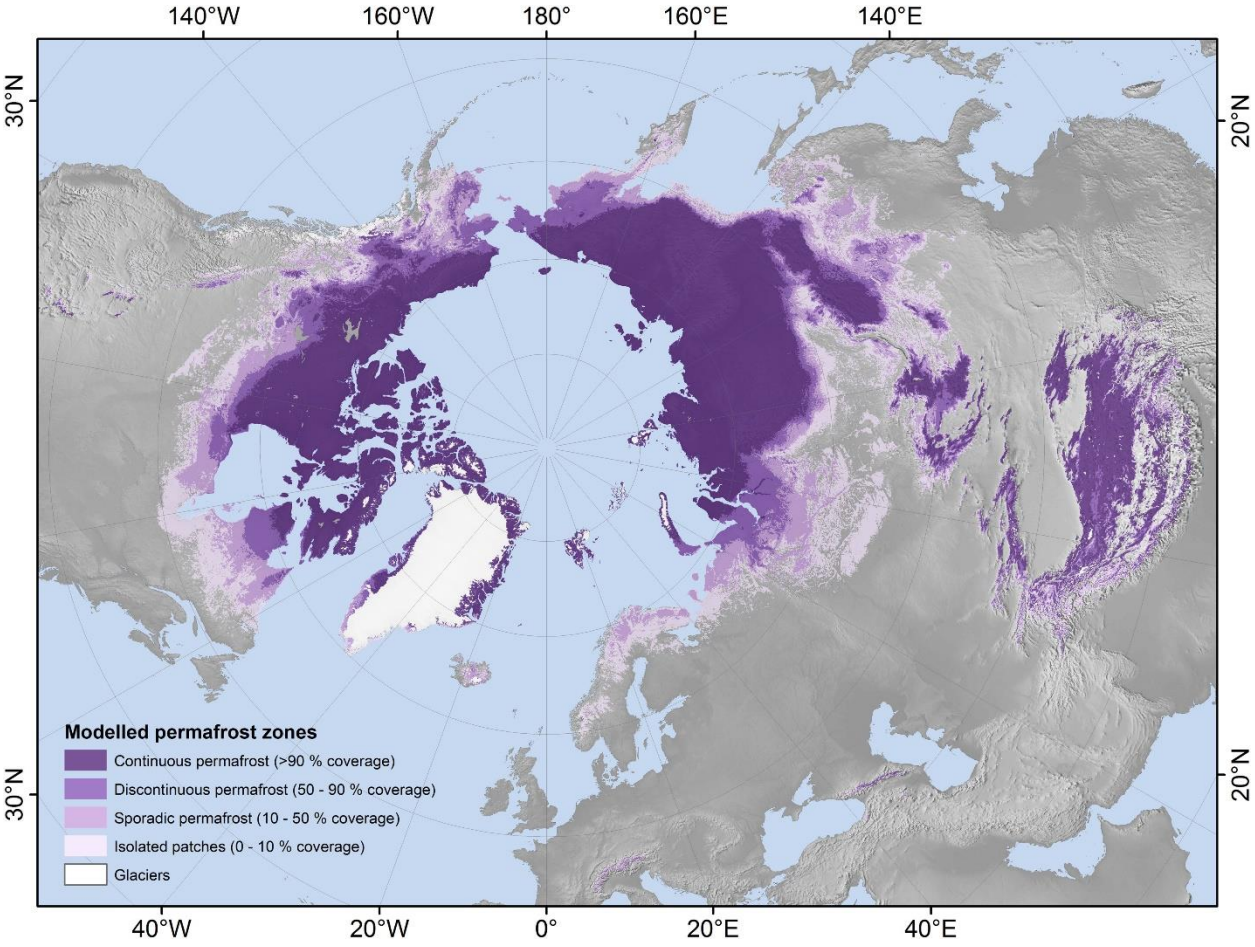

Fig. 1.1 Distribution of permafrost in the Northern Hemisphere (Obu *et al.*, 2019).

Climate change is alleviating temperature limitations on the activity of microorganisms in soils (Schmidt *et al.*, 2011) that decompose soil organic matter and release soil C as the greenhouse gases CO_2 and CH_4 into the atmosphere. The loss of permafrost is projected to release up to 240 Pg C to the atmosphere by 2100 (Meredith *et al.*, 2019), but the magnitude and timing of permafrost thaw and C emissions remain highly uncertain (Elder *et al.*, 2018; Estop-Aragonés *et al.*, 2018; Lupascu *et al.*, 2014a; McGuire *et al.*, 2018; Schuur *et al.*, 2015).

Permafrost thaw can manifest via a deepening of the active layer (Burke *et al.*, 2020), the seasonally thawing and freezing top layer of permafrost soils (Koven *et al* 2013, Fig. 1.2), and warmer active layer temperatures. Moreover, abrupt thaw and mass wasting can rapidly expose permafrost C to decomposition (Turetsky *et al.*, 2020).

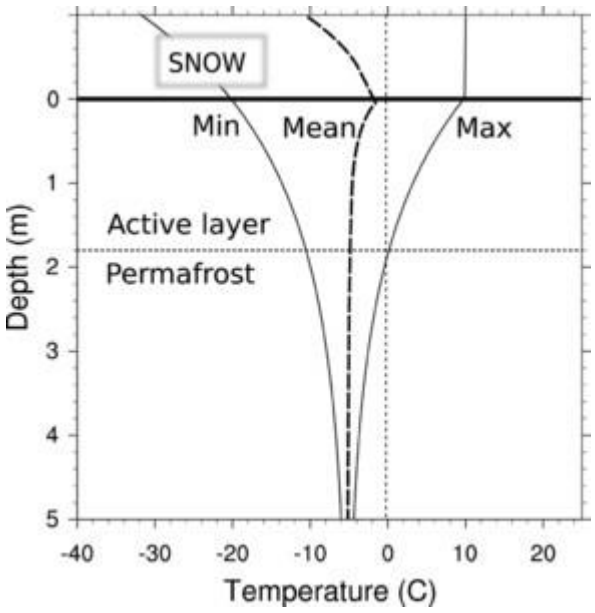

Fig. 1.2 Conceptual view of the thermal dynamics of permafrost soils (Koven *et al.*, 2013).

While Arctic ecosystems have long been considered dormant during the long (6-9 months) and dark winter, advances in measurement technology and our understanding of microbial ecology now paint the non-growing season (September to May) as a critical period for the annual C budget of tundra ecosystems (Euskirchen *et al.*, 2012; Fahnestock *et al.*, 1998; Lupascu *et al.*, 2018; Morgner *et al.*, 2010; Oechel *et al.*, 1997; Raz-Yaseef *et al.*, 2017; Welker *et al.*, 2004, 2000). Moreover, climate change and winter emissions in the Arctic may be turning the Arctic into a net source of C to the atmosphere (Commane *et al.*, 2017; Natali *et al.*, 2019).

Measurements of the radiocarbon (^{14}C) content of soil CO_2 and soil/ecosystem CO_2 emissions (or "respiration") offer a unique insight into soil C cycling. First, they offer an opportunity to quantify emissions of C from permafrost (Lupascu *et al.*, 2018; Natali *et al.*, 2011; Schuur *et al.*, 2009) because permafrost C pools are strongly depleted in ^{14}C due to radioactive decay and distinct from C that has more recently participated in the global C cycle. Second, such measurements allow us to understand how rapidly soils may sequester or lose C in response to

changes in environmental conditions or net primary productivity (Shi *et al.*, 2020; Trumbore, 2006) by providing an estimate of transit time (the age of C leaving the soil). Third, ^{14}C data can also be used to apportion emissions into plant and microbial contributions (Estop-Aragonés *et al.*, 2018; Lupascu *et al.*, 2014c; Schuur *et al.*, 2009). Most soil $^{14}CO_2$ measurements to date, however, have focused on the growing season and represent snapshots of C cycling in soils (Borken *et al.*, 2006; Czimczik *et al.*, 2006; Estop-Aragonés *et al.*, 2018; Hicks Pries *et al.*, 2017, 2013; Lupascu *et al.*, 2014a, 2014b; Muhr *et al.*, 2010; Schuur & Trumbore, 2006), especially in the permafrost region.

To improve our understanding the permafrost C feedback to climate change, we urgently require direct, year-round observations of C emissions and their sources from permafrost landscapes, especially during the non-growing season. During my graduate research, I designed a new sampler for collecting depth-resolved, time-integrated soil-respired CO_2 for ^{14}C analysis from upland permafrost soils year-round. I deployed this new technology at two field sites to (1) capture the first continuous, depth-resolved time series of microbial C emissions and annual flux-weighted signature of ecosystem-respired $^{14}CO_2$, and (2) study the impact of active layer deepening on ecosystem $^{14}CO_2$. Together, my research significantly advances our ability to directly observe non-growing season fluxes and quantify permafrost C emissions in the rapidly changing Arctic.

Chapter 2: Time-integrated collection of CO_2 for ^{14}C analysis from soils

Adapted from:

Time-integrated collection of CO_2 for ^{14}C analysis from soils

Pedron S, Xu X, Walker J C, Ferguson J C, Jespersen R G, Welker J M, Klein E S and Czimczik C I 2021 *Radiocarbon* **In press**

2.1 Introduction

Soil respiration, the emission of carbon dioxide (CO_2) from soils, is a major flux in the global carbon (C) cycle, and its radiocarbon content (here reported as fraction modern carbon (*F*) (Trumbore *et al.*, 2016)) allows insights into the cycling of C in terrestrial ecosystems (Trumbore, 2009). The *F* of soil respiration (soil FCO_2) is a measure of the amount of time that has passed since the constituent C atoms were last in the atmosphere, integrating the transit through various reservoirs, including plant and microbial biomass, soil organic matter, and carbonates (Sierra *et al.*, 2017).

In organic and acidic soils, soil FCO_2 provides an important constraint on how rapidly soils may sequester or lose organic C in response to changes in net primary productivity or environmental conditions (Shi *et al.*, 2020). Along with its $\delta^{13}C$ signature (Hicks Pries *et al.*, 2013), soil FCO_2 can be used to partition soil C emissions into contributions from the rhizosphere (respiration of roots and associated microorganisms) relative to those from microorganisms that decompose soil organic matter to reveal how plant and microbial activity and microbial C sources

are influenced by changes in environmental conditions (Hicks Pries *et al.*, 2013; Trumbore, 2000, 2006).

Many investigations of soil FCO_2 collect net soil respiration from chambers or soil pore space CO_2 from gas wells (Borken *et al.*, 2006; Czimczik *et al.*, 2006; Estop-Aragonés *et al.*, 2018; Hicks Pries *et al.*, 2017, 2013; Lupascu *et al.*, 2014a; Schuur & Trumbore, 2006). However, these methods use pumps or evacuated canisters and accumulate CO_2 prior to collection, which can affect the gradient of CO_2 within the soil profile and may change soil FCO_2. These approaches also collect CO_2 about once a month over periods of minutes to about one day and may miss episodic C emissions (Lupascu *et al.*, 2014b; Muhr *et al.*, 2010). Furthermore, most soil respiration source studies in seasonal environments have focused on the growing season. The scarcity of time-integrated and non-growing season data is of particular concern in high latitude ecosystems (Lupascu *et al.*, 2018; Natali *et al.*, 2019), where permafrost soils with vast C stocks are rapidly warming and active layer depths are changing (Box *et al.*, 2019; Pulliainen *et al.*, 2020). Thus, the evaluation of environmental change on C cycling in soils over time and across landscapes could be improved by more continuous and passive measurements of soil FCO_2.

To achieve time-integrated samples, gas intake rates into evacuated steel canisters have traditionally been modulated by adjusting the length and inner diameter of a critical flow path, i.e. a capillary (Lupascu *et al.*, 2014c; Trumbore *et al.*, 2015; Walker *et al.*, 2015). In cold environments, however, a capillary upstream from the membrane is likely to become obstructed by condensing or freezing water vapor. Our sampler uses a tubular diffusive membrane intake to exclude liquid water while transmitting gas. Passive CO_2 trapping for $^{14}CO_2$ analysis is a technique with increasing use and popularity (Walker *et al.*, 2015; Wotte *et al.*, 2017a, 2017b). Trace-gas

sampling wells and chambers with passive CO_2 traps have been used with diffusive silicone (Si) membranes in periodically saturated soils and waters since 2001 (Garnett *et al.*, 2009; Jacinthe & Groffman, 2001; Kammann *et al.*, 2001; Wotte *et al.*, 2017a), and modified to perform depth-resolved C isotope sampling in peatlands (Clymo & Bryant, 2008; Garnett *et al.*, 2012, 2011) and mineral soils (Hartley *et al.*, 2013). Here, we adapted such a sampler for usage in upland environments (mineral soil) without soil collars (trenching). Our sampler is designed to be permanently installed year-round in extreme conditions (-36 to +15°C, ice-bound to 100% volumetric water content (VWC)), with negligible routine maintenance and easy and efficient exchange of CO_2 traps to capture winter and shoulder-season (spring/autumn) permafrost dynamics. Fully steel components (excluding PTFE ferrules for airtight connections and Si tubing) and cold- and vacuum-rated valves ensure high durability and accuracy in the harsh winter. We also investigate some environmental predictors (VWC, temperature, CO_2 concentration ($[CO_2]$)) that likely relate to sampling rate and soil respiration F and $\delta^{13}C$ values.

We present a rugged, and lightweight sampler that collects soil CO_2 passively (capturing CO_2 by diffusion) for subsequent F (and $\delta^{13}C$) analysis over periods of two weeks to two months from soil depths of 20-80 cm below the surface. We designed the sampler to withstand Arctic conditions, including freeze-thaw cycles, waterlogging, and herbivory, in a remote location without power. Our method allows the collection of soil FCO_2 year-round to provide seasonal to annual estimates of C cycling rates in terrestrial ecosystems.

2.2 Methods

2.2.1 CO_2 isotope sampler

The sampler consists of a soil gas access well ("access well") that is permanently installed in the soil, and an exchangeable, rechargeable molecular sieve trap ("MS trap") to capture soil CO_2 for C isotope (F & $\delta^{13}C$) analysis (Fig. 2.1). The soil gas inlet (Fig. 2.1A) is composed of a platinum-cured Si rubber tube (1 m, ¼" OD, 2124T5, McMaster-Carr, USA), which forms a membrane between the interior of the tubing and the (semi-) saturated soil surrounding it. Silicone rubber (and other Si-polymeric membranes) are known to be permeable to many gases, with gas-specific permeability proportional to molecular diameter and temperature (Kammermeyer, 1957; Robb, 1968). The tubing excludes liquid water but allows gas to diffuse into the sampler without disturbing the CO_2 gradient within the soil profile. Diffusivity of CO_2 in Si rubber is governed by Fick's law, whereby diffusion of a gas across a fluid barrier (the Si tube) is a function of the concentration difference across the barrier, the barrier thickness, and the (temperature-dependent) diffusion coefficient of the gas (Bertoni *et al.*, 2004). The length of the tubing which we use directly translates to a greater surface area over which diffusion can occur. Diffusivity is also determined by t he polarity of the material and permeating gas molecule (Zhang & Cloud, 2006), which should make (polar, hydrophobic) Si effective at reducing water vapor uptake.

Two generations of inlets were used. In the original version, Si tubing is sealed on one end and connected to the sampler via a ¼" hose connection. This connects to ¼" OD stainless steel tubing that passes through a bore-through connection to the interior of a ¾" OD tube to create a water sump (Fig. 2.1D), which prevents the obstruction of the gas flow path by ice or water from water vapor permeating the inlet and condensing or freezing along the inner walls.

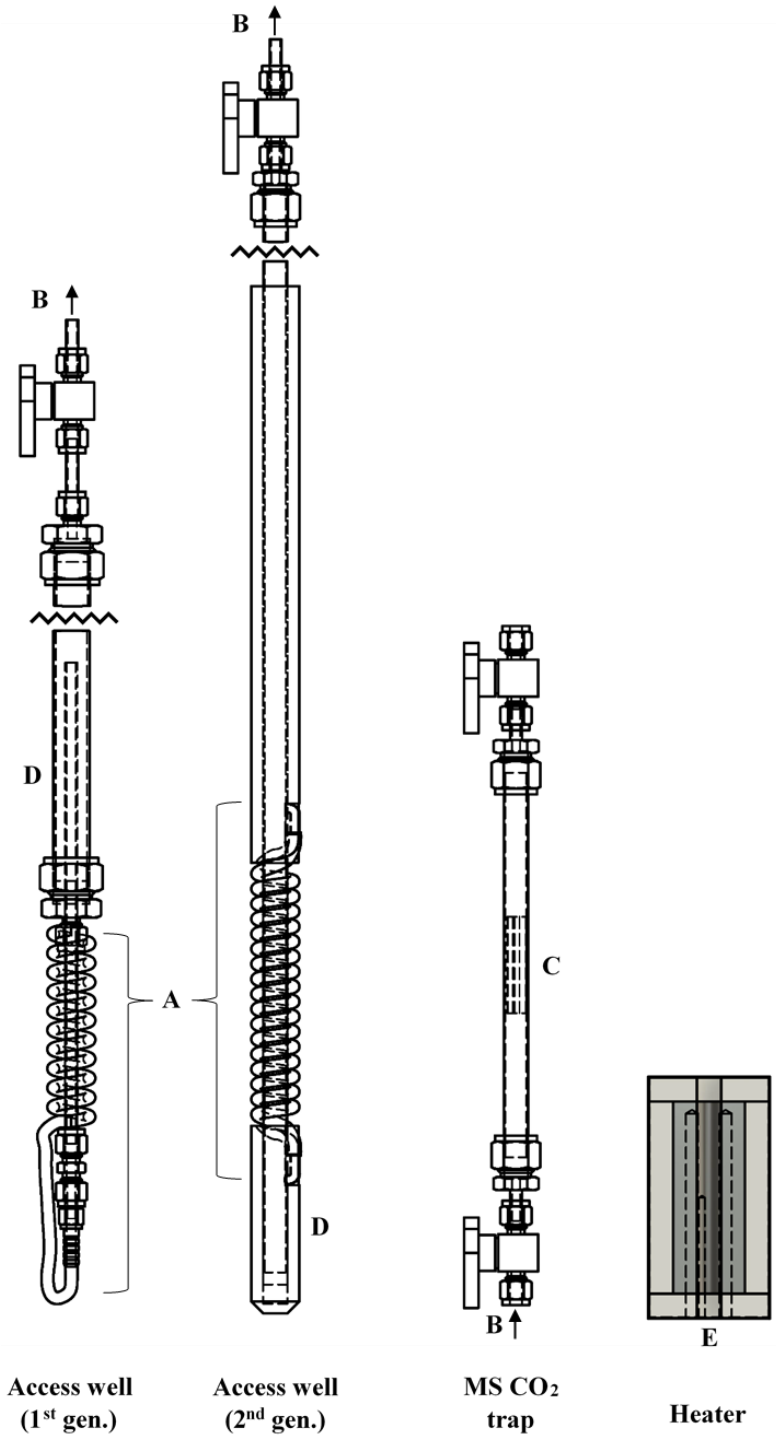

Fig. 2.1 Soil $^{14}CO_2$ sampler components consisting of a permanently installed access well (2 generations), exchangeable MS trap, and CO_2 extraction heater. Soil CO_2 passes through gas-permeable silicone tubing (A) and passively diffuses along flow path through junction (B) to be adsorbed upon molecular sieve (C). Interior ice deposits melt and pool in sump (D) in spring. CO_2 is thermally desorbed in laboratory using clamshell-style heaters (E).

In the optimized 2nd version, Si tubin g is coiled around the sampler and connected at both ends by a steel 90° elbow tube silver-soldered to the interior of a 1.5 m long ½" OD smooth-bore stainless-steel tube. This central steel tubing ends above ground and is capped 5 cm below the Si coil to create the water sump (Fig. 2.1D). After soldering on the bottom cap, the steel tubing is washed with 20% HCl (#7647-01-0, Klean Strip Green, USA) and rinsed with MQ water. The steel tubing sections above and below the Si coil, which are expected to be below the soil surface, are sleeved with PVC tubing (1" OD, 1/2" ID) to seal the hole augured into the soil for well insertion to minimize gas flux in the vertical axis. All wells in the 2nd gen. are the same length to maintain a consistent internal diffusion path, independent of how deep they are inserted in the soil.

A junction (Fig. 2.1B) spanning two plug valves (PTFE components and Si-based lubricant, SS-4P4T, Swagelok, USA) connects the access well to a removable MS trap and enables MS trap exchanges without exposure of the interior of the access well to ambient atmosphere. Expected snow depths determine the overall length of the access wells. Prior to attaching the first MS trap, each access well is evacuated to -25" Hg pressure with a hand pump (MITMV8500, MightyVac, USA).

The design and extraction technique of the MS trap was based on work by Walker *et al.* (2015). With open valves, CO_2 is collected by sorption onto pre-cleaned zeolite MS (Fig. 2.1C; 1.5 g, 45-60 mesh, 13X, 20304 Sigma-Aldrich, USA) contained within a 316 stainless steel mesh envelope (0.114 mm ID mesh opening, 9419T34, McMaster-Carr, USA). The envelope is folded to contain the zeolite and stay in place through friction with the interior of a steel tube (½" OD, 8" length) that is pre-baked at 550°C in air for 1 hour (to oxidize any residual organics from fabrication) and capped with ½" to ¼" reducers and SS-4P4T valves. All connections are stainless

steel to avoid differential expansion. Alternatively, soil gas can be collected from the access well with an evacuated steel canister.

2.2.2 Laboratory analyses of CO_2

We built two clamshell-style heaters to thermally desorb CO_2 from MS traps in the laboratory (Fig. 2.1E). One half of each heater was built by installing insertion heaters (4877133 x2, McMaster-Carr, USA) and a high-temperature thermocouple (9353k31, McMaster-Carr, USA) into an insulated steel block. Two symmetrical halves were both connected to a digital temperature control (sensitivity ±2°C, SL4848-RR, AutomationDirect, USA) to form a full heater. The MS trap is clamped within a heater and attached to a vacuum line, where CO_2 is extracted under vacuum at 425°C for 30 min, cryogenically purified, and graphitized using a sealed-tube zinc reduction method (Xu *et al.*, 2007). The extraction is followed by a cleaning sequence at 500°C with 100 mL min^{-1} UHP N_2 flush for 20 min, then 100 mL min^{-1} UHP CO_2-free (zero) air flush for 10 min. After cleaning, the MS trap is pressurized to just over 1 atm with UHP zero air to minimize leaking caused by pressure changes during air transport.

For samples with a total yield >0.3 mg C, an aliquot of CO_2 is split and analyzed for ^{13}C (GasBench II coupled with DeltaPlus XL, Thermo, USA). The ^{14}C of the graphite is measured with accelerator mass spectrometry (NEC 0.5MV 1.5SDH-2 AMS) alongside processing standards and blanks at the KCCAMS laboratory of UC Irvine (Beverly *et al.*, 2010; Santos *et al.*, 2007).

We report stable isotope measurements using conventional δ notation (‰) [Eq. 2.1]:

$$\boldsymbol{\delta^{13}C = 1000 \cdot \left(\frac{R_{sample}}{R_{standard}} - 1\right)} \qquad \text{[Eq. 2.1]}$$

Where R_{sample} denotes the heavy-to-light isotope ratio of a sample and $R_{standard}$ is the isotope ratio of the standard (0.0112372 for Vienna Pee Dee Belemite (PDB) $^{13}C/^{12}C$ standard (Gonfiantini, 1984). We report radiocarbon results using the fraction modern (F) notation [Eq. 2.2]:

$$\boldsymbol{F = \frac{R_{SN}}{R_{ON}} = \frac{R_S(\frac{0.975}{1+\delta/1000})^2}{0.95R_{O,-19}}} \quad \text{[Eq. 2.2]}$$

Where R_{SN} is the measured $^{14}C/^{12}C$ ratio of the sample normalized for fractionation to a $\delta^{13}C$ value of -25‰, with δ being the measured $\delta^{13}C$ value of the sample, and R_{ON} is the $^{14}C/^{12}C$ ratio of the oxalic acid I standard measured in 1950 ($1.176\pm0.010\cdot10^{-12}$), normalized for fractionation to its measured $\delta^{13}C$ value of -19‰ (Trumbore *et al*. 2016). The measurement uncertainty for all samples and standards was <0.003 F based on long-term reproducibility of secondary standards.

2.2.3 Sampler performance

We took three approaches to evaluate the samplers: *(1)* We examined isotope sampling accuracy and potential memory effect on both the standalone MS traps and full-process replications by collecting pure certified reference material standards for up to 24 hours and periods of 1-4 weeks, respectively. *(2)* We optimized access well dimensions for sample intake rate by attaching varied lengths of Si membrane and Bev-A-Line (56280, 1/8" ID x 1/4" OD Bev-A-Line IV, United States Plastic Corp., USA) to evacuated steel canisters and MS traps. To further test sampling rate and gas seal, we exposed the full-process replications to varied [CO_2] and temperature. *(3)* We evaluated real-world performance by deploying a complete sampler in the field for two years.

2.2.3.1 Isotope sampling

To assess the suitability of each MS trap for isotope analysis, we compared the C isotope data of reference materials analyzed with and without MS trap exposure. As "known" values, we used literature consensus *F* values, and measured $\delta^{13}C$ of pure aliquots (Table 1). Specifically, we used two modern oxalic acid standard materials OX I (SRM4990B) and OX II (SRM4990C) (Mann, 1983), one aged wood standard, (TIRI B) (Scott, 2003), and one

^{14}C-free material (ABA-cleaned bituminous coal, USGS Pocahontas #3) (Trent *et al.*, 1982; Xu *et al.*, 2007). These reference materials were combusted to CO_2, purified, and allowed to passively transfer onto each MS trap on a vacuum line. After 12-24 hrs., CO_2 was extracted and measured for *F* and $\delta^{13}C$ (see **Laboratory analysis of CO_2)**. To quantify potential memory effects (i.e., "hysteresis", CO_2 that survives the post-extraction cleaning), some traps were tested multiple times, so that standards with known signatures (0.571-1.040 *F*, *n*=12; -23.1 to -19.4‰ $\delta^{13}C$, *n*=5) could be compared to values of the previous samples held by those traps.

Table 2.1 Summary statistics for standard material tests on MS traps. *Known* values are accepted literature consensus *F* values, and measured $\delta^{13}C$ of pure aliquots (‰). 2-tailed Student's t-test p-values use the *Known* value as true.

Standard		**MS trap**					
		Known	Mean	st.dev	st.err	N	p-value
OX II	*F*	1.341	1.328	0.005	0.002	4	0.011
	$\delta^{13}C$	-17.4	-17.3	0.1	0.1	4	0.652
OX I	*F*	1.040	1.038	0.004	0.001	24	0.013
	$\delta^{13}C$	-19.0	-18.8	0.2	0.0	16	0.000
TIRI-B	*F*	0.571	0.570	0.002	0.001	4	0.349
	$\delta^{13}C$	-24.5	-24.4	0.1	0.1	4	0.277
Coal	*F*	0.000	0.003			1	
	$\delta^{13}C$	-23.1	-22.9			1	

A MS trap method blank was evaluated from a set of MS traps that were subjected to the entire sampling process aside from actual exposure to soil CO_2, in order to capture the average contaminating CO_2 intrusion which may leak into a MS trap in routine sampling. MS traps were shipped to the field site filled with ~1 atm UHP CO_2-free air, attached to access wells (but never opened), and shipped back to the lab (58-59 days, *n*=8). These were extracted and used to calculate the size and *F* of the method blank (only 2 were large enough for ^{14}C, but not ^{13}C analysis).

Full-process replications were created by enclosing Si inlet assemblies (as in Fig. 2.1A, 1st gen.) in sealed glass mason jars with ports through which the internal atmosphere could be evacuated and then filled with CO_2. These full-process sampler + jar systems were evacuated to $<10^{-2}$ torr and filled with 1 atm UHP zero air, and reference material was injected into the jars and allowed to diffuse into the samplers for 1-4-weeks (*n*=20). We evaluated the response of the measured isotopes to varied ambient [CO_2] (0.33-0.71%), temperature (-20 and 20°C), path length (0.03-1.3 m), and unique reference material signature (0.571-1.040 *F*; -24.5 to -19.04‰ $\delta^{13}C$) by varying the amount of reference material injected into each jar, and either enclosing the mason jar in a freezer or leaving it at lab temperature. We used stepwise optimization of multivariate linear regression models (R *step* and *lm* functions, *stats v3.6.2* package) to determine the unbiased significance of each predictor variable to each response (*F*, $\delta^{13}C$, sampling rate). By using Aikaike information criteria to eliminate irrelevant predictors, we arrived at multivariate models for each response that maximized goodness of fit while minimizing model complexity.

2.2.3.2 Access well

We optimized several access well components in the laboratory to maximize the CO_2 uptake rate in intermittently waterlogged and frozen soil without disturbing the CO_2 gradient. First,

we tested the influence of Si surface area, diffusion path length, and collection system (canister or MS trap) by attaching diffusive Si tubing (0-3 m, sealed on one end) to gas-impermeable Bev-A-Line tubing (0-3 m). This well-prototype was connected to MS traps and, or 0.5, 6, or 32 L evacuated stainless-steel canisters and exposed to ambient [CO_2] (n=41). The uptake rate was calculated by extracting CO_2 after 1-58 days. We selected Si tubing lengths up to the maximum amount that could be installed without causing dramatic site disturbance, and path lengths that would allow us to access the collection system above typical snowpack heights.

Second, we evaluated the predictive value of [CO_2], temperature, and path length on the sampling rate response for the same full-process replications described in *Isotope sampling*.

2.2.3.3 Field sampling

To assess the performance of the sampler in the field, we continuously collected soil CO_2 from a moist acidic tussock (dominated by *Eriophorum vaginatum* L.) / wet sedge (*Carex bigelowii*) tundra (O horizon pH=3.7±0.1, B horizon 4.6±0.4 mean±se (Hobbie & Gough, 2002)) near Toolik Field Station, AK, USA (68.625478 N, 149.602199 W, 724 m, -6.8 to -5.8^{o}C MAT, 44 to 52 cm y^{-1} MAP 2017-2019) between June 2017 and August 2019. The values presented here are from samplers that were part of a larger experiment, but we focus only on assessing the sampler performance.

The 1st gen. access well (n=1) was installed at 20 cm below the surface in June 2017. Soil gas samples were collected over 3-6 weeks in evacuated canisters (0.5 to 32 L) from June 2017 to September 2017, with MS traps from September 2017 to 2018, and with alternating MS traps and evacuated canisters from September 2018 to August 2019. Episodically (n=6), when $F$$CO_2$ was also measured using traditional sampling approaches with dynamic chambers (n=42) as described

in Lupascu *et al*. (2014a), we also collected gas samples over 3-6 days in 0.5 L evacuated canisters. The 2nd gen. access wells (n=20) were installed between 20 and 80 cm depth in July 2019 and were only sampled over 8 weeks with MS traps.

To gauge the sampler's efficiency and quantify the temporal variability of soil pore space [CO_2], we co-deployed [CO_2] (non-dispersive infrared, Carbocap GMP343 with vertical soil attachment and PTFE membrane, Vaisala, Finland) and VWC and temperature probes (VWC from dielectric permittivity, temperature from thermistor, Decagon 5TM, METER, USA) with the 1st gen. access well (n=1 each at -20 cm). [CO_2] data were collected from June 2017 to August 2019 at 30-second resolution on a computer, using software made in LabVIEW (Laboratory Virtual Instrument Engineering Workbench, National Instruments, USA, 2017) to simply capture data output from the probes and save it to a text file located on a cloud drive. A CO_2 temperature-correction was applied by the GMP343 firmware at the time of measurement. VWC and temperature data were collected from September 2017 to August 2019 at 15-minute resolution and stored on a Decagon Em50 battery-powered data logger and accessed during field campaigns.

We evaluated the response of the measured isotopes and sample collection rate to the dynamic soil environment. We again used stepwise optimization of a multivariate linear regression model to determine the significance of each predictor variable. These include the mean of measured environmental predictors over each sampling period ([CO_2], VWC, temperature), state of water at the depth of the gas inlet, and the collection system used. Sample collection rate was also considered as a predictor for ^{13}C and ^{14}C. Where gaps in the data existed due to sensor malfunction or differences in installation date, the day-of-year means over the sampling period (~2% of CO_2, ~7% of VWC and temperature data) were used.

2.2.3.4 Data corrections

We corrected the measured C isotopes for three likely sources of exogenous C: method blank (full-process replications and field samples), contaminating lab-air CO_2 dissolved in Si tubing (full-process replications only), and mixing of ambient air CO_2 into soil (field samples only). Calculated method blank or air fractions (i.e., impurities) were used to correct isotope values [Eq. 2.3]:

$$\Delta_{sample} = \Delta_{impurity} \cdot f_{impurity} + \Delta_{corrected} \cdot (1 - f_{impurity}) \quad \text{[Eq. 2.3]}$$

Where Δ represents either FCO_2 or $\delta^{13}CO_2$. Calculated fractions were also used to correct yield (and thereby sampling rate) [Eq. 2.4]:

$$Yield_{corrected} = Yield_{sample} - Yield_{sample} \cdot f_{impurity} \quad \text{[Eq. 2.4]}$$

We corrected samples with yields <1 mg C for method blanks using the blank size and *F* (see *Isotope sampling*). Given a fixed blank value, the significance of the blank to the total sample signature will decrease as the sample size increases. With our blank *F* (0.5875, 0.6013, *n*=2) and size (8.5±6 µg C, *n*=8), blank corrections for samples >1 mg C would approach our analytical uncertainty (0.003 *F*). MS trap results were not corrected for $\delta^{13}C$ method blanks.

To account for lab-air CO_2 that was dissolved in the Si tubing used for full-process replications, we calculated the total mass of CO_2 which was dissolved in the Si tubing at the experimental start time given the tubing dimensions and an approximate solubility of 2.2 m^3 CO_2 m^{-3} Si atm (Robb, 1968). We then took the ratio of this mass to the total yield for the contaminating fraction (<7% for all samples). We assume that the isotopic composition of the lab air was similar to that of the field air given that: CO_2 is a well-mixed gas, lab-air measured no more than 600 ppm

when testing the GMP343 probes, and human-respired $\delta^{13}CO_2$ is not different enough from ambient (approximately -22‰ vs -9‰ respectively (Affek & Eiler, 2006)) to have a large effect on the correction.

To account for mixing of ambient air CO_2 into soil, which dilutes the soil respiration isotope signatures, we calculated the fraction of air present in the soil over each sampling period as the ratio between [CO_2] in ambient air (from Imnavait, about 8 km away) and at the inlet depth. The isotopic composition of the field air was measured at the site during campaigns (n=11 FCO_2, n=10 $\delta^{13}CO_2$) as described in Lupascu *et al*. (2014a).

2.3 Results and Discussion

2.3.1 Isotope sampling.

Our MS traps allowed for reproducible and accurate C isotope measurements of CO_2. The mean standard error for three reference materials (OXI, OXII, and TIRI-B) absorbed upon standalone MS traps was 0.0014 *F* and 0.056‰ $\delta^{13}C$ (Fig. 2.2A, B, Table 1). *F* of the recovered reference materials was not very different from their consensus values (Table 1). Although the two-tailed Student's t-test indicated a p-value only slightly greater than 0.01 for two of the standards, the greatest mean difference (i.e. sample-known values, 0.013±0.002 *F* for OXII) is less than the standard deviation of full-process replicates (0.020 *F* for OXI, 0.024 *F* for TIRI-B, Fig. 2.2E, G, I), indicating that ^{14}C error of MS traps is less than that of individual samples. Only one bituminous coal standard was run as an extreme test of sorption hysteresis; it is shown in Fig. 2.2A-D. $\delta^{13}C$ was greater than pure aliquot values by <0.5‰ consistently. It is known that MS material fractionates $\delta^{13}C$ upon absorption (Davidson, 1995; Garnett & Hardie, 2009), with a typical value of 4‰ under ambient [CO_2]. It is likely that we do not see this magnitude of

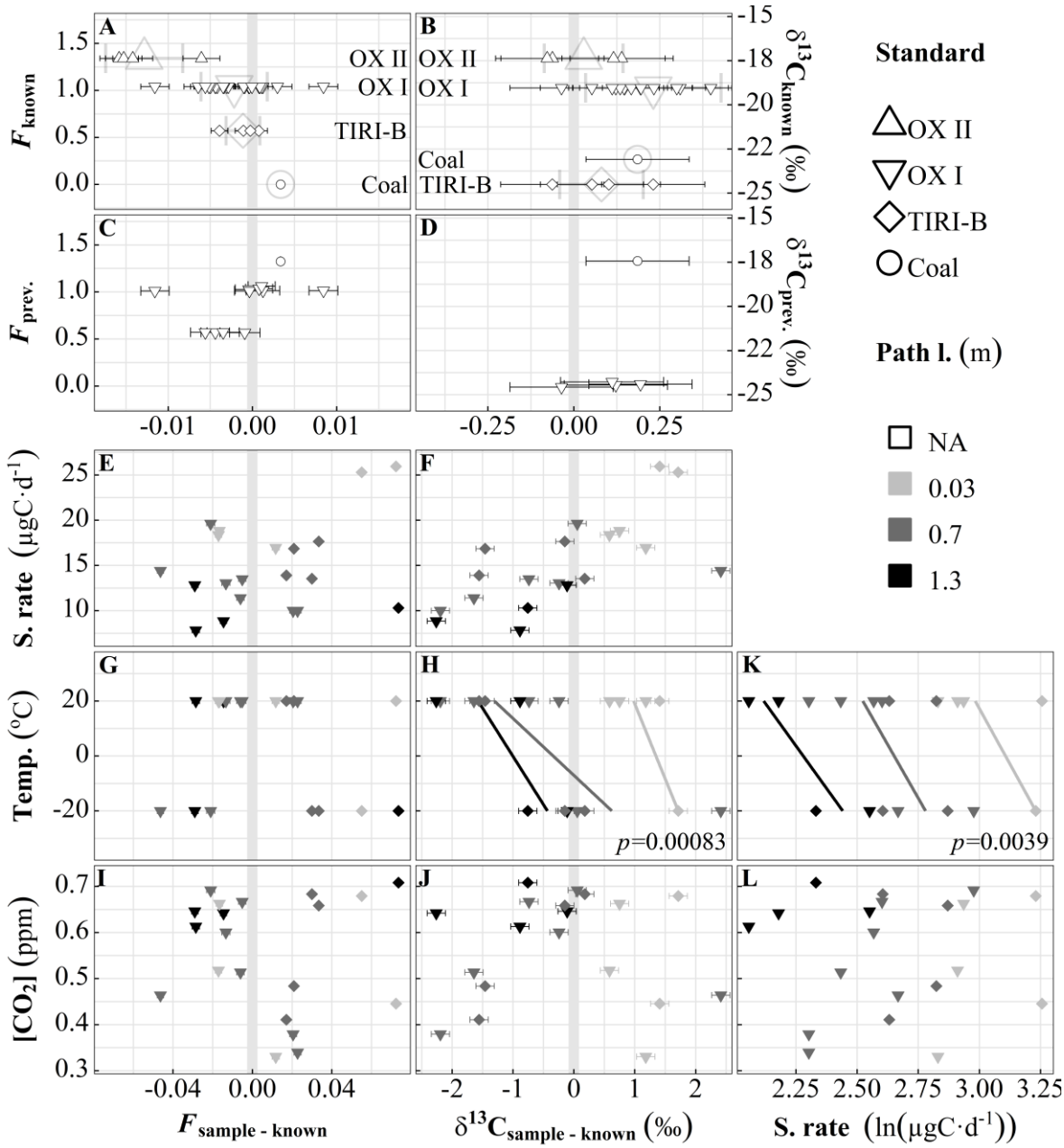

Fig. 2.2 Recovery of reference materials from standalone and full-process tests of CO_2 traps. A-J: Deviation of recovered isotope values from known values of FCO_2 and $\delta^{13}CO_2$ of reference materials (grey vertical band shows no difference). Small error bars show instrumental error (1σ). A-D: Open symbols, performance of standalone MS traps (0.18- 0.92 mg C). A, B show recovery of pure reference material for standalone traps (on top of large light-grey standard mean±sd), and C, D show this relative to a trap's previous sample value. E-L: Closed symbols, performance of full-process replications as a function of relevant predictors. Regressions and significance level are shown for significant predictors as determined by stepwise minimization of Akaike information criterion. For full-process replicates, reference material signature is significant for *F* deviation, and path length and temperature are significant for $\delta^{13}C$ deviation and sampling rate (all p<0.004).

fractionation because pure CO_2 was used, and therefore absorption was not inhibited or slowed by non-absorbable gases (N_2 and O_2) as it would be in atmospheric or soil gas environments.

Additionally, the diffusion pathway between the vacuum extraction line and the MS traps was short, and complete absorption only took <5 min. Wotte *et al*. 2017b also report insignificant $\delta^{13}C$ fractionation for their testing of a similar MS trap design. We observe no hysteresis for ^{14}C or ^{13}C (Fig. 2.2C, D), which would be evident as a strong linear relationship between previous signature and current deviation from known. The MS trap blank (not shown) was 8±6 µg C, equivalent to 0.15±0.11 µg C day^{-1} (mean±sd, n=8), with F of 0.5875 and 0.6013 (n=*2*).

The deviation from known is larger for full-process replications (Fig. 2.2E-J) than for standalone MS traps. It is likely that our attempt to create a controlled ambient environment around the inlets resulted in an imperfect seal, causing recovered reference materials to deviate towards the value of ambient air (Northern Hemisphere FCO_2 was 0.98 in 2013 (Reimer *et al.*, 2013), while atmospheric $\delta^{13}CO_2$ is approximately -9‰). This is most apparent in F results: TIRI-B samples were more enriched than known, while OX I were more depleted (known F of 0.571 and 1.040, respectively). The larger deviation of samples taken at -20°C leads us to believe that the suboptimal seal on the mason jar intended to contain the ambient atmosphere was exacerbated by different thermal expansion coefficients of the jar materials (i.e., metal will contract more than glass). Stepwise regression assigns significance to the reference material signature for ^{14}C, and temperature and path length for ^{13}C. We see no influence of sampling rate, temperature, or [CO_2] on F, and no radical values that would reveal methodological contamination. The significant temperature + path length $\delta^{13}C$ trend (Fig. 2.2H) is likely the combined result of air leakage from imperfect seal and fractionation along the diffusive path from inlet to MS material, as it is not evident in (fractionation-corrected) F results (Fig. 2.2G). This observed fractionation may

contribute to the ~4‰ $\delta^{13}C$ depletion reported in previous research on passive MS trapping (Davidson, 1995; Garnett & Hardie, 2009). While it appears to be correctable, we will not attempt to do so until the phenomenon is better understood.

2.3.2 Access well

In the prototyping tests, the CO_2 sampling rate varied from 7-44 µg C day^{-1} depending on Si tubing length and path length, temperature, [CO_2], and to a smaller degree, on collector (canister or MS trap). We found sampling rate to be directly related to Si tubing length and inversely to path length (Fig. 2.3A). At equivalent Si and path lengths and temperatures, the rate for canisters (which actively draw all ambient gas into the sampler with negative pressure) is 3.7±1 (mean±sd, *n*=17) times greater than for MS traps, which adsorb CO_2 molecules passively diffusing into the sampler. We also observe a small direct sampling rate proportionality to canister volume (not shown), however it was far outweighed by the other controls.

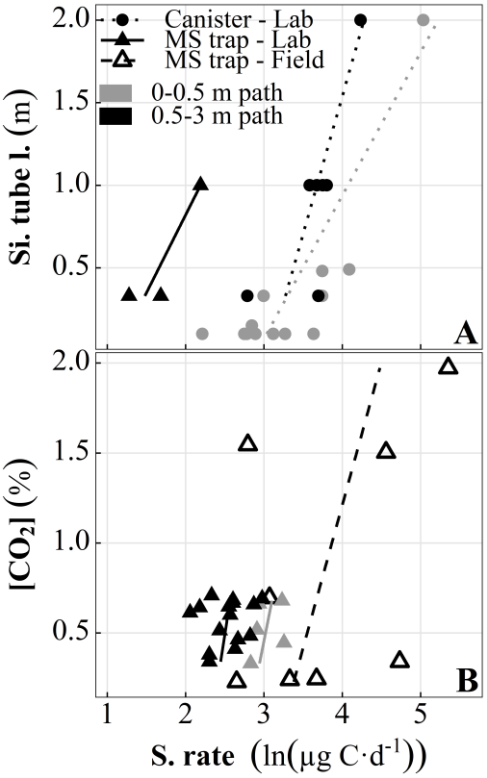

Fig. 2.3 Response of CO_2 sampling rate to (A) varied silicone inlet lengths at equivalent [CO_2] (lab only) and (B) varied ambient [CO_2] at equivalent silicone tubing length of 1 m (lab and field at temperatures >0°C). Path length is from inlet connection to MS trap joint.

A Si tubing length of 1 m was chosen to optimize sampling rate while minimizing site disturbance, producing reasonable yields over a range of path lengths for sampling periods >2 weeks given the anticipated soil [CO_2]. Stepwise regression assigns significance to temperature and path length as predictors of sampling rate (Fig. 2.2K). We transform (natural log) sampling

rate here and throughout the figures for easy comparison with field results, which demonstrate bimodal distribution (i.e. frozen vs thawed) and a strong exponential relationship between sampling rate and temperature (Fig. 2.4E). The inverse temperature effect on sampling rate was unexpected, as CO_2 permeability of Si rubber *increases* with increasing temperature (a dramatic reduction is only seen below approximately -40^oC (Robb, 1968)). The most likely explanation is once more the poor seal of the mason jars containing the inlets, allowing more freezer air to enter the system. This potentially contributes to the temperature dependence of ^{13}C as well. If the influence of temperature on sampling rate is ignored, [CO_2] becomes a significant predictor in a simple linear model of [CO_2] and path length (p=0.03, Fig. 2.3B, solid symbols).

2.3.3 Field sampling

In the field, at temperatures >0^oC, the response of the sampler's CO_2 uptake rate to varying [CO_2] (i.e. slope) was comparable to that in the lab (Fig. 2.3B, open symbols). We observed more variable CO_2 uptake rates (7.0-45 µg C day^{-1} lab vs 2.5-210 µg C day^{-1} field) in the field, likely due to a much broader [CO_2] range (0.33-0.71% lab vs 0.063-4.7% field) and changes in environmental conditions such as soil VWC (9.2-79%), temperature (-8.1-13^oC), and pore space volume with freeze-thaw cycles. While our calibrations focused on the most significant controls of sampling rate, future investigations should also consider soils with different textures to understand the influence of soil moisture and pore space volume. The approximate maximum adsorption capacity for 13X zeolite MS (25^oC at 100 kPa, without water vapor) is ~4 mol CO_2 kg^{-1} zeolite based on experimental data on adsorption equilibria (Wang & LeVan, 2009), which equates to a maximum of 72 mg CO_2-C given the 1.5 g of zeolite material used in our MS traps. The range of uncorrected yields captured on MS traps attached to 1st gen. access wells in this

experiment was 0.087-5.3 mg CO_2-C, and 0.56-13 mg CO_2-C on 2nd gen. access wells using the same MS traps. The higher 2nd-gen. yields are likely due to more methodical coiling of Si tubing and the dual ports to the interior diffusion pathway, as well as greater sampling periods. Since all samples collected over the two-year period were less than half the capacity of the MS trap, we assume that sample uptake was linear over each sampling period.

Our three models of field-collected FCO_2, $\delta^{13}CO_2$, and sampling rate considered [CO_2], VWC, temperature, water state of matter, and collector type as predictor variables (Fig. 2.4). The [CO_2], state of water, and collector used did not significantly influence any response. Sample collection rate was calculated as the total yield over the collection period, and was strongly

responsive to temperature (Fig. 2.4E). When samples collected at subzero temperatures are considered (as opposed to Fig. 2.3B field samples), [CO_2] loses significance as a predictor of sampling rate, but still appears to have bimodal linear responses for frozen and thawed states, implying unique summer and winter controls on sampling rate (Fig. 2.4H). We theorize that winter reductions in sampling rate are due to reduced microbial and plant respiration, followed by restriction of soil C transport when soil water freezes (Lee *et al.*, 2010; Mikan *et al.*, 2006). It is known that the availability of liquid water in soils near freezing temperatures is a strong control on microbial activity (Schimel & Clein, 1995). Like Lee *et al*., (2010), we observe extremely high [CO_2] in the months before the start of the growing season – likely due to a reduction of the pore volume near the [CO_2]-sensor – without a corresponding spike in sampling rate. The CO_2 permeability of Si rubber is a direct function of temperature, in the same direction as the observed trend. However, the magnitude is much smaller than what we observe. According to (Robb, 1968), Si rubber has permeabilities of 323 and 293 cc cm s^{-1} cm^2 cm Hg at temperatures of 28 and -40^{o}C,

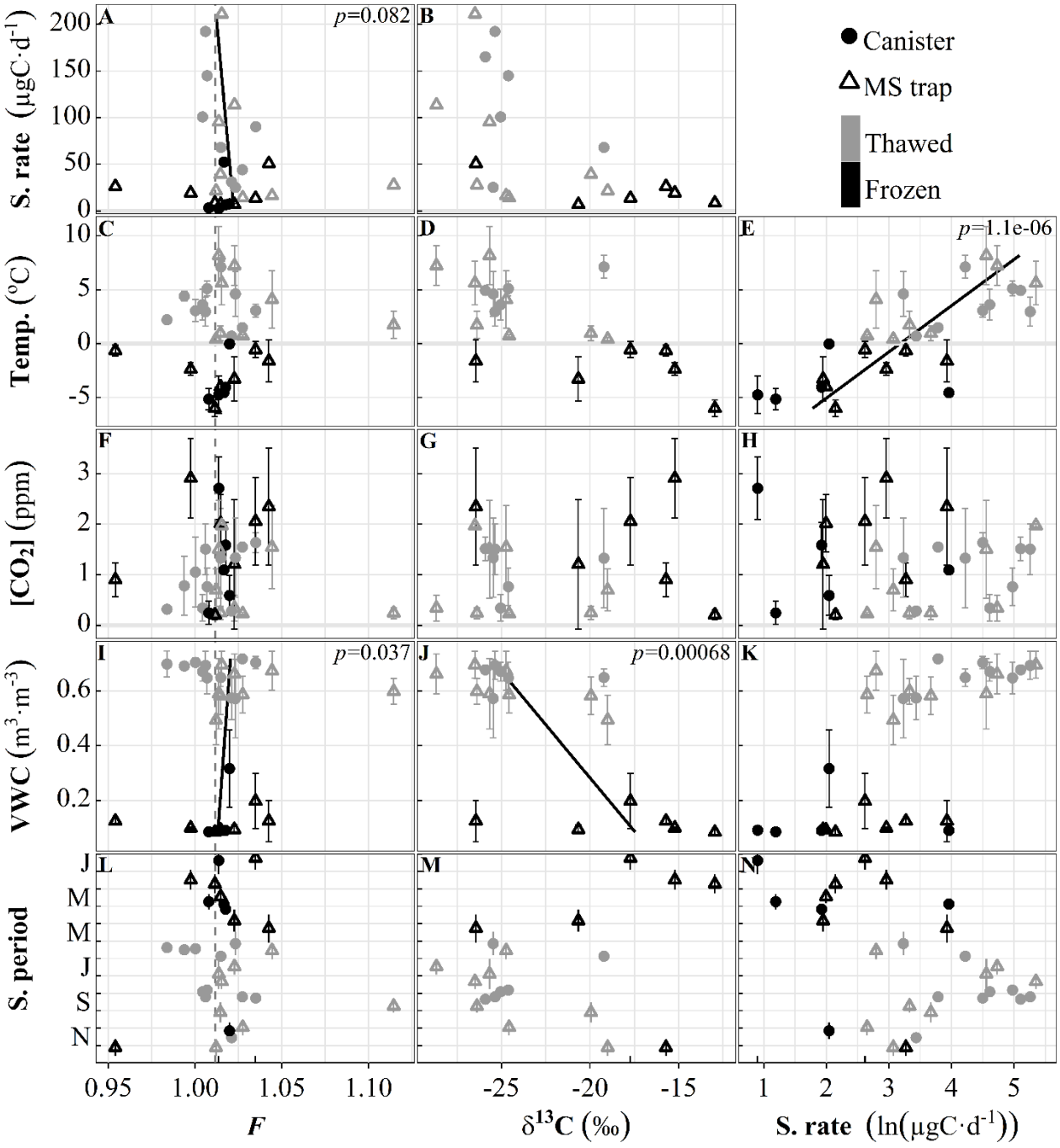

Fig. 2.4 Response of 2 years of soil CO_2 *F*, $\delta^{13}C$, and sampling rate (one sampler, depth = -20 cm) to relevant predictors. Bars for *Sampling period* panels (L-N) span on and off dates. Error bars of environmental predictor panels (C-K) show standard deviation of the predictor over the sampling period. Regressions are shown for predictors that maximize the quality of a multivariate linear regression for each response (x-axes). The vertical dashed line for *F* is the mean value for ambient air over the experimental period (6±8‰, *n*=9).

respectively. This equates to a linear slope of 0.14% permeability per ^{o}C, while our observed range of CO_2 sampling rate spans 3 orders of magnitude.

Although we do not see the same sampling-rate-dependent $\delta^{13}C$ fractionation in the field that was evident in full-process replications, further work is needed to explore this effect. The VWC dependence of $\delta^{13}CO_2$ (Fig. 2.4J) could be related to physical or microbial processes. For example, kinetic fractionation occurs in the partitioning between gas-phase and dissolved CO_2 (Thode *et al.*, 1965), resulting in enrichment in the gas phase, which is inversely proportional to temperature. It is also known that microbial methanogenesis processes yield CO_2 enriched in $\delta^{13}C$ (Aravena *et al.*, 1993; Charman *et al.*, 1999; Whiticar *et al.*, 1986), which is also an inverse function of temperature. While we have observed local indicators of methanogenesis (blue-grey mineral soil, bubbles in nearby standing water), and the environent is likely suitable (anoxia caused by frequent inundation and/or continuous winter snowpack), we did not directly collect any methane.

Soil FCO_2 is not strongly correlated to any predictor variables (all $p>0.03$), but does show some seasonality and the model is improved when predicted by VWC and sampling rate (Fig. 2.4L, I, and A respectively). The sampling rate correlation is logical, as maximum sampling rates are observed during the peak growing season (Fig. 2.4N), when autotrophic respiration (modern *F*) is greatest. FCO_2 of field samples during the growing season (1.021±0.031 mean±sd, n=15, June-September) varied similarly to the observed FCO_2 of traditional soil respiration chambers (1.040±0.026‰ mean±sd, n=39) measured during campaigns. The sampler signature at 20 cm depth is near enough to the soil surface to be close to representative of the growing season isotopic flux but is also able to capture older C (oldest sample F=0.954‰, November/December 2018)

during the non-growing season. As plant respiration slows at the end of the growing season and soil water freezes to ice, heterotrophs become confined to their local environment. This corresponds with a change in available substrate from more modern, labile C (i.e. plant exudates and litter from the growing season) (Grogan & Chapin, 1999) to older C which is potentially still easily degradable and high in carbohydrates (Mueller *et al.*, 2015), due to a history of physical vertical mixing from freeze-thaw cycles common to tundra ecosystems (Bockheim, 2007; Schimel & Clein, 1995). Winter and shoulder-season (i.e. spring and autumn) fluxes of ancient C have also been seen in high-latitude forests (Czimczik *et al.*, 2006; Hirsch *et al.*, 2002; Winston *et al.*, 1997), peatlands (Garnett & Hardie, 2009), and tundra (Hartley *et al.*, 2013; Hicks Pries *et al.*, 2013; Lupascu *et al.*, 2018). Our sampler offers a device capable of capturing a continuous year-round record of soil CO_2 isotopes in permafrost environments.

2.4 Conclusions

We present a novel sampler designed for time-integrated, year-round collection of soil-respired CO_2 and subsequent C isotope analysis in remote environments that facilitates a deeper understanding of C cycling in soils, i.e., plant and microbial contributions to soil-atmosphere CO_2 fluxes and microbial C sources. Soil CO_2 diffuses into the sampler via a water-proof Si membrane and accumulates in lightweight, compact MS traps, but can also be collected in evacuated canisters. The CO_2 collection rate is proportional to soil temperature. The deployment of the sampler in Arctic tundra demonstrates its ruggedness and suitability for use in organic and mineral soils and sediments with a wide range of moisture and temperature conditions.

Acknowledgements

We thank the Toolik Field Station Science Support and Environmental Data Center teams, D. Helmig (CU Boulder), and the KCCAMS staff and C. McCormick (UCI) for their logistical and technical support. Funding was provided by the U.S. NSF OPP (#1649664 to C.I.C., #1650084 to J.M.W. & E.S.K.).

Chapter 3: Closing the winter gap: Year-round measurements of soil respiration sources in Arctic tussock tundra

Adapted from:

Closing the winter gap: Year-round measurements of soil respiration sources in Arctic tussock tundra

Pedron S, Welker J M, Euskirchen E. Klein E S, Xu X and Czimczik C I 2021 *Environmental Research Letters* **In prep**

3.1 Introduction

Climate change is rapidly transforming the Arctic (Post *et al.*, 2019; Steffen, 2006). Permafrost thaw as a consequence of warming and precipitation increases (Mekonnen *et al.*, 2021) may facilitate microbial decomposition of vast amounts of soil organic carbon (C) (472±27 Pg C for 0–1 m) (Hugelius *et al.*, 2014) into the greenhouse gases CO_2 and CH_4 (Schuur *et al.*, 2015), further strengthening positive feedbacks and ecosystem changes. From 1971-2017, mean annual air temperatures have increased by 0.6°C per decade and precipitation by 40 mm per decade (Box *et al.*, 2019). Permafrost temperatures in the northern circumpolar continuous permafrost zone have increased by 0.39 ±0.15ºC (2007-2016, Biskaborn *et al* 2019), concurrently with increases in active layer thickness (*medium confidence*, Meredith *et al* 2019). The area underlain by near-surface (within 4 m) permafrost may decrease by 2-66% (RCP2.6) or 30-99% (RCP8.5) by 2100, and this loss is projected to release up to 240 Pg C to the atmosphere (Meredith *et al.*, 2019), but the magnitude, timing, and proportions of CH_4 and CO_2 fluxes remain highly uncertain (Schuur *et al.*, 2015; Turetsky *et al.*, 2020).

Non-growing season C emissions are emerging as an important contribution to the annual C balance of Arctic ecosystems (Euskirchen *et al.*, 2012; Fahnestock *et al.*, 1998; Morgner *et al.*, 2010; Oechel *et al.*, 1997; Raz-Yaseef *et al.*, 2017; Welker *et al.*, 2004, 2000), turning the Arctic into a net annual C source (Commane *et al.*, 2017; Natali *et al.*, 2019). It remains unclear, however, which soil C pools fuel microbial respiration from fall to spring. Some of this may originate from older C in thawing permafrost, which like fossil fuel combustion, has not participated in the global C cycle for millennia, but may increasingly contribute to land-atmosphere C emissions. To reduce the uncertainty in our understanding of non-growing season emission and the permafrost C feedback to climate change, we urgently need direct, year-round observations of C emission and their sources from permafrost landscapes.

Measurements of the radiocarbon (^{14}C) content of soil-atmosphere C emissions can be used to estimate how rapidly soils may sequester or lose C in response to changes in environmental conditions or net primary productivity (Trumbore, 2006). These data provide an estimate of transit time (the age of C leaving the soil) and can be used to apportion emissions into plant- and microbial contributions and to quantify losses of permafrost C (Estop-Aragonés *et al.*, 2018; Lupascu *et al.*, 2014c; Schuur *et al.*, 2009) (Lupacu *et al.* 2014b, Estop-Aragonés *et al.* 2018; Schuur *et al.* 2009).

Soil C emissions are a major component of ecosystem C emissions. A significant proportion of soil C emission originates from the rhizosphere, i.e., respiration of plant roots and microorganisms that consume root exudates, which have a similar $\Delta^{14}C$ signature as ambient air CO_2. Currently (2021), the $\Delta^{14}C$ of atmospheric CO_2 is about 0‰ following a 70-year decline of ^{14}C in the atmosphere from a maximum during the 1950s and ‘60s, when testing of thermo-nuclear weapons resulted in the formation of additional (bomb or modern) ^{14}C that subsequently mixed

into marine and terrestrial C pools and became diluted by emissions of ^{14}C-free CO_2 from fossil fuels (Graven *et al.*, 2020; Levin *et al.*, 2010). Microbial emissions constitute the remainder of the soil C efflux and are either slightly depleted ($\Delta^{14}C < 0‰$, "old") when derived from decomposition of pre-1950 substrate, or enriched ($\Delta^{14}C > 0‰$, "modern") from post-1950 substrate. In permafrost soils, microbial emissions of previously frozen C are strongly depleted in ^{14}C due to radioactive decay ($\Delta^{14}C << 0‰$, "ancient").

Currently, soil C source apportionment studies combine ^{14}C analysis of ecosystem (or soil), rhizosphere, and microbial emissions ($^{14}CO_{2\ eco}$, $^{14}CO_{2\ rhizo}$, and $^{14}CO_{2\ micro}$, respectively) to determine the relative contribution of rhizosphere (R_{rhizo}) and microbial emissions (R_{micro}) to the total (R_{eco}) [Eq. 3.1-3.2]. Ecosystem C emissions are collected in the field, rhizosphere C emissions can be measured by incubating roots or approximated from ^{14}C measurements of ambient air CO_2 or the tissue of annual plants, and microbial C emissions in laboratory incubation experiments.

$$\mathbf{f}_{eco} = \mathbf{f}_{rhizo} + \mathbf{f}_{micro} = \frac{\mathbf{R}_{rhizo}}{\mathbf{R}_{eco}} + \frac{\mathbf{R}_{micro}}{\mathbf{R}_{eco}} \qquad \text{[Eq. 3.1]}$$

$$\mathbf{^{14}CO_{2\ eco}} = \mathbf{f}_{rhizo}\,\mathbf{^{14}CO_{2\ rhizo}} + \mathbf{f}_{micro}\,\mathbf{^{14}CO_{2\ micro}} \qquad \text{[Eq. 3.2]}$$

While past studies have significantly advanced our understanding of soil C emissions and their sources from permafrost soils (Hicks Pries *et al.*, 2013, 2016; Lupascu *et al.*, 2014b; Street *et al.*, 2020) they suffer shortcomings. First, to collect sufficient mass for ^{14}C analysis, common approaches accumulate soil CO_2 in chambers (Lupascu *et al.*, 2014c) and some remove ambient atmospheric CO_2 from the headspace prior to accumulating soil C emissions (Czimczik *et al.*, 2006; Hicks Pries *et al.*, 2013; Plaza *et al.*, 2019). The chambers cover the ground for 0.5 to 48 hours during which the soil CO_2-depth gradient is disturbed. More importantly, this approach only provides a snapshot of emissions and may miss advective fluxes in response to changes in

atmospheric pressure or precipitation events (Lupascu *et al.*, 2014b). Furthermore, due to the high cost of ^{14}C analysis, most studies collect chamber samples about once a month and few have collected outside the growing season (Lupascu *et al.*, 2018; Winston *et al.*, 1997). Second, the source of microbial C emissions is assessed in laboratory incubations (Schädel *et al.*, 2014; Treat *et al.*, 2015) that disrupt the autotroph–heterotroph respiratory continuum (Högberg & Read, 2006). However, we commonly observe a greater range of microbial-respired $^{14}CO_2$ in the field than in laboratory incubation studies (Lupascu *et al.*, 2014b).

As permafrost thaws, it is prudent to investigate the vulnerability of its organic matter to decomposition *in situ*. Here, we use a recently developed a passive CO_2 sampler (capturing CO_2 by diffusion, Pedron *et al.* 2021) to collect soil $\Delta^{14}CO_2$ from a graminoid tundra system in Arctic Alaska for two years (06/2017 – 08/2019). These data are then used to apportion soil C emissions into rhizosphere and microbial contribution. The resulting annual $^{14}CO_2$-depth profiles allow us to investigate microbial C sources during the non-growing season. Our approach finally quantifies the mean age of the land-atmosphere C flux on a monthly to annual scale, and thus provides a basis for a more systematic quantification of permafrost C losses in the rapidly changing Arctic.

3.2 Methods

3.2.1 Field site and sample collection

We continuously captured soil CO_2 for $\Delta^{14}CO_2$ analysis from a moist acidic tundra system near Toolik Field Station, AK, USA (68.625478 N, 149.602199 W, 724 m) with passive samplers consisting of a permanently installed access well (diffusive silicone tubing inlet attached to steel tubing path) connected to an exchangeable evacuated cylinder or molecular sieve (MS) trap to which CO_2 will absorb (Pedron *et al.*, 2021). Access wells were buried within the active layer at

depths of 20 cm (O horizon, *n*=1 each, tussock/swale) and 36 cm (A horizon, *n*=1) and suspended above the surface (20 cm, *n*=1), all within a 1 m^2 area (Fig. 3.1B). Samples were collected from June 2017 to August 2019 over periods of 3-6 weeks using canisters (06/2017-09/2017), MS traps (09/2017-09/2018), and alternating canisters and MS traps (09/2018-08/2019). We also collected high-resolution (<2-week) samples in 0.5 L canisters during field campaigns (*n*=22, 2017 (June, Sep., Nov.), *n*=20, 2018 (Mar., Aug.), *n*=4, 2019 (June)).

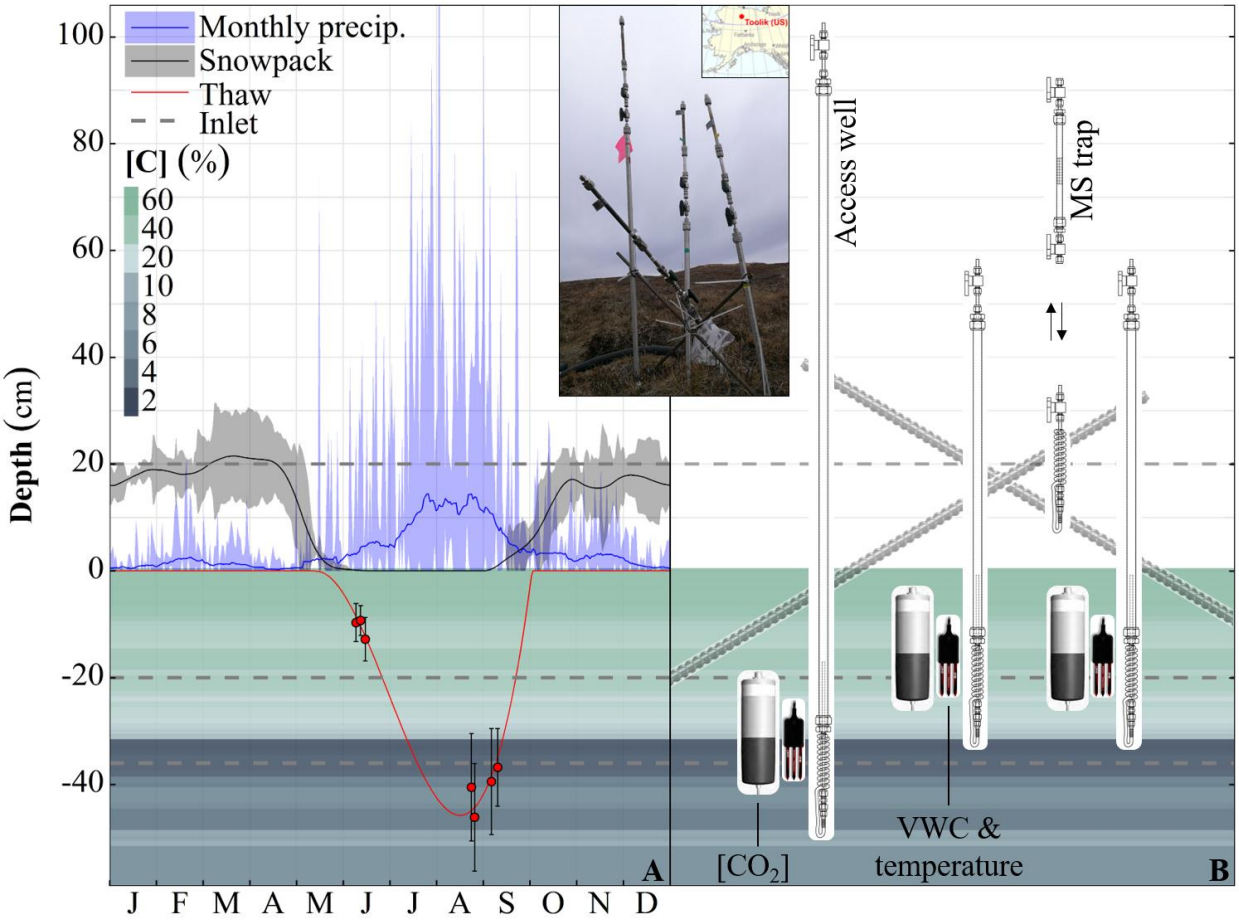

Fig. 3.1 (A) Environmental data during the sampling period (06/2017–09/2019), averaged by day of year and either smoothed (precipitation, snowpack, from Toolik EDC) or modeled from observations (thaw depth). The soil is shaded based on the C percent of bulk organic matter (averaged from soil cores) and scaled to distinguish organic (green >20%) from mineral (blue <20%) soil. (B) Site setup. Permanent access wells attached to exchangeable molecular sieve (MS) traps were suspended above the surface (20 cm, *n*=1) or buried within the active layer with silicone inlets at -20 (O horizon, *n*=2 (tussock/swale)) and -36 cm below the surface (A horizon, *n*=1) alongside [CO_2] and VWC + temperature probes within a 1 m^2 area in a moist acidic tundra system near Toolik Field Station, AK, USA (68.625478 N, 149.602199 W, 724 m).

The sampler-isotope data were sequentially corrected for: (1) leakage of ambient air CO_2 into traps or canisters; and (2) mixing of ambient air CO_2 into the soil pore space, given the high porosity of our soils (Hirsch *et al.*, 2004) [Eq. 3.3].

$$\mathbf{^{14}CO_{2\ cor}} = \frac{\mathbf{^{14}CO_{2\ spl} - {}^{14}CO_{2\ air} * f_{air}}}{\mathbf{1 - f_{air}}} \quad \text{[Eq. 3.3]}$$

where $^{14}CO_{2\ cor}$ and $^{14}CO_{2\ spl}$ represent the corrected or measured $\Delta^{14}CO_2$ of a sample, respectively, f_{air} the proportion of ambient air CO_2, and $^{14}CO_{2\ air}$ the $\Delta^{14}CO_2$ of ambient air. We note here that the samplers are also capable of capturing $\delta^{13}CO_2$ with the same corrections, however we relegate these additional data and results to the supplement considering that the method was designed and thoroughly tested for ^{14}C and may exhibit temperature- or sampling rate-dependent $\delta^{13}CO_2$ fractionation.

The proportion of MS trap air-CO_2 from leakage was calculated from extraction of a set of cleaned traps that were shipped back and forth from the field site and attached, but never opened to access wells (n=8, 0.16±0.1 ug C d^{-1}). The proportion of air-CO_2 due to soil-air mixing was calculated from the ratio of air [CO_2] to soil [CO_2] at the depth of each inlet, averaged over each sampling period.

We episodically monitored thaw depth during sampling campaigns with a steel-tipped tile probe in swales, and retrieved continuous environmental data (air and soil temperatures, insolation, precipitation, snow depth) from Toolik's Environmental Data Center (Environmental Data Center Team, 2020) and atmospheric CO_2 concentrations and ecosystem CO_2 fluxes from an eddy covariance (EC) tower at Imnavait Creek (wet sedge tundra, ~12 km WSW; Euskirchen *et al.* 2019) (Figs. S1 & S2). We deployed soil [CO_2] (Carbocap GMP343, 06/11/2017-08/25/2019, 30-sec resolution, Vaisala, Finland) and temperature and volumetric water content (VWC) (Decagon

5TM, 09/12/2017-08/26/2019, 15-min resolution, METER, USA) probes (n=3 of each) with the buried access wells (Fig. 3.1B). Data gaps were filled using day-of-year means over the sampling period (~14% of [CO_2], ~19% of VWC and temperature daily values).

To validate the samplers, we measured the ecosystem CO_2 respiration flux (R_{eco}) with traditional dynamic soil chambers installed in June 2017, 10 m away from the access wells. Chamber bases were inserted to about 2 cm depth and vegetation was not clipped (n=3 each, tussock/swale). We collected ambient air CO_2 and chamber R_{eco} samples for isotopic analysis in June, Sept., & Nov. 2017 (n=37), March & Aug. 2018 (n=11), and Aug. 2019 (n=2), and measured R_{eco} rate in June & Sept. 2017 (n=39) (Lupascu *et al.*, 2018, 2014b).

Growing season chambers were flushed with ambient air before being attached to bases, and isotopes were subsequently corrected for air volume. Chambers sampled in November 2017 (n=3) were left attached to bases at the end of the 2017 growing season, with Bev-A-Line tubing connected to a central point, accessible above snowpack. We scrubbed their headspace CO_2 by circulating it through soda lime and sampled after 24 hours of accumulation, thereby minimizing contamination from prior accumulation.

Growing season R_{eco} fluxes were quantified with an infrared gas analyzer and data logger (LI-840, LI-1400, LI-COR Biosciences, Lincoln, NE, USA) at a rate of 0.5 L min^{-1}. Emission rates were calculated from the slope of time vs. CO_2 concentration curves using linear regression (we do not attempt to calculate winter emission rates).

To sample CO_2 for isotope analyses, we left the growing season chambers closed until the CO_2 concentration inside the chamber was at least double that of ambient air (up to 24 h). After measuring its concentration, the CO_2 was dried (Drierite, W.A. Hammond Drierite Co. Ltd., Xenia, OH, USA) and collected onto u-shaped MS traps ("u-traps", 2 g of powder-free 13X 8×12 beads,

Grace, USA) by recirculating the headspace air at a rate of 0.5 L min^{-1} for 15 min. These MS u-traps used to collect chamber or ambient air CO_2 are distinct from the MS traps previously described in both shape (u-shaped vs. straight) and MS dimension (8×12 beads vs. 45-60 mesh), but operate by the same principle of size-selective molecule retention. These data were corrected for mixing of ambient air CO_2 [Eq. 3], where the fraction of air-CO_2 was calculated from ratio of air [CO_2] to chamber-headspace [CO_2]. Isotope data with a calculated fraction of air >40% (*n*=23, 47% of $\Delta^{14}C$; n=20, 45% of $\delta^{13}C$) were likely affected by leakage around the chamber base – a common issue in relatively permeable peat-rich soil and tussock/swale terrain affected by freeze-thaw cycles – and excluded from results.

To conduct time-resolved source partitioning, a continuous R_{eco} flux measurement was also necessary. We approximated this using the Imnavait Creek EC net ecosystem exchange data, that is partitioned into R_{eco} and gross primary productivity as described in (Euskirchen *et al.*, 2019). Imnavait R_{eco} fell below the standard error of our chamber flux magnitudes and was scaled to our site by multiplying the magnitude at each timestep by the mean quotient of our chamber fluxes to the reported values. Fig. 3.9A shows the values as reported from the eddy covariance derived R_{eco} (solid gray line) and scaled to our site (dashed black line) with their standard errors over the experimental period.

We collected soil samples for laboratory incubations and bulk soil analyses by cutting roughly rectangular columns of soil from 6 m south of the samplers with either a utility saw (*n*=1 each tussock/swale in thawed soil, Sept. 2017) or an electric chainsaw (*n*=1 each tussock/swale in frozen soil, March 2018). Cylindrical cores collected by powered corer (*n*=3, 2015) and a modified rotary hole saw (*n*=2, 2019) from a nearby site (moist acidic tussock tundra, <1 km away) were also used after comparison of bulk soil isotopes revealed no significant differences (all 2-sample

Student's t-test $p>0.05$ for 10-cm depth bins). Soils were stored in plastic freezer bags and kept frozen from the day of collection.

3.2.2 Laboratory analyses

At UC Irvine, CO_2 was thermally desorbed from chamber and ambient air u-traps and MS traps (Pedron *et al.*, 2021) or extracted from canisters (Lupascu *et al.*, 2014b) on a vacuum line and converted to graphite using a sealed-tube zinc reduction method (Xu *et al.*, 2007). Graphite was analyzed for $\Delta^{14}C$ with accelerator mass spectrometry (NEC 0.5MV 1.5SDH-2 AMS) alongside processing standards and blanks with a measurement uncertainty of <3‰ (Beverly *et al.*, 2010). For samples ≥0.3 mg C, an aliquot was analyzed for its $\delta^{13}C$ (GasBench II-DeltaPlus XL, Thermo, Waltham, MA, USA), with an uncertainty of 0.1‰.

Soil cores were separated into organic or mineral soil groups and sectioned into intervals (1.5-14 cm) while frozen. For bulk soil analysis, soil was dried at 60°C to constant mass, weighed, and ground to powder using rotary blade and ball mills for organic and mineral soils, respectively. For $\Delta^{14}C$ analysis, samples were combusted in pre-combusted, evacuated quartz tubes with cupric oxide (900°C, 3 h) and the resulting CO_2 processed as described above. Bulk soil C and N elemental and stable isotopic composition was measured alongside processing standards and blanks with EA-IRMS (Fisons NA-1500NC, DeltaPlus XL, Thermo, USA). The measurement uncertainty (1σ, from long-term measurements of secondary standards) was 0.1‰ for $\delta^{13}C$ and 0.4‰ for $\delta^{15}N$. Bulk density and VWC were calculated using the wet and dry masses.

Incubations (2-158 g soil) were performed on field-moist samples at 22, 7, and -20°C in glass mason jars (0.5-2 L) flushed with CO_2-free air and kept in the dark. CO_2 concentrations were measured periodically with a LI-COR 820, and the respired CO_2 was extracted and converted to

graphite as previously described once concentrations reached 30% (17-49 days). Short (~1-day) incubations were also performed on roots harvested from the 09/2017 soil cores on the same day of collection to quantify rhizosphere emissions. These data provided predictive relationships between microbial CO_2 emissions (R_{micro}), depth, and temperature.

3.2.3 Data processing and soil C emission partitioning

Using the data collected during the 2-year study period, we averaged meteorological, soil [CO_2], temperature, VWC, and access well $\Delta^{14}CO_2$ data month to month over one year. Access well aggregates were weighted by the period overlapping the beginning and end of each timestep. To account for our 2-6-week sampling periods and data gaps, we chose to represent out data products at calendar month resolution. We found no significant differences in soil $\Delta^{14}CO_2$ and $\delta^{13}CO_2$ collected at 20 cm depth under tussock or swale (paired two-tailed t-test p-value >> 0.05).

We created a monthly $\Delta^{14}CO_{2\,eco}$ -depth model using measured predictors along depth (bulk soil $\Delta^{14}C$) and time (days snow-free, days snow-covered) from the deepest inlet depth (-36 cm) to the organic soil surface (0 cm). Model details are described in **3.6.1.1: *Multivariate adaptive regression splines***, and results in Table 3.2 & Fig. 3.12.

We used our incubation results with the field temperature data to model microbial respiration at each depth. Summing the column values at each timestep allowed us to estimate the contribution of R_{micro} to R_{eco} surface emissions for a temporal partitioning of f_{micro} vs. f_{rhizo} [Eq. 1]. Model details are described in **3.6.1.1: *Non-linear least squares***, and results in Table 3.1 & Fig. 3.10.

Applying this partitioning to our modeled $^{14}CO_{2\,eco}$ at each depth [Eq. 2], we calculated $^{14}CO_{2\,micro}$. The column $^{14}CO_2$ value (i.e., the surface signature) is the sum of a flux-weighted

multi-endmember mixing model at every timestep, where each discrete depth is an endmember. We used Point Barrow air ($\Delta^{14}C$=4.0±3.9 over the sampling period) for $^{14}CO_{2\ rhizo}$ (Xiaomei Xu, pers. com.).

Our technique for soil C emission partitioning makes five assumptions:

(1) A laboratory-derived model of the R_{micro} response to temperature can be used to predict R_{micro} in the field. Note that this is different from previous approaches that prescribe $\Delta^{14}CO_{2\ micro}$ per depth based on incubations to calculate R_{micro} (e.g. Czimczik *et al.* 2006), and motivated by the fact that in permafrost soils and outside the growing season $\Delta^{14}CO_2$ of emissions are commonly outside the range of microbial $\Delta^{14}CO_2$ observed in incubations and ambient $\Delta^{14}CO_2$ (Czimczik & Welker, 2010; Lupascu *et al.*, 2014b).

(2) The integration of this modeled R_{micro} across the soil volume (surface to 36 cm depth) is equivalent to the surface R_{micro} flux at any time. The same relationship holds for R_{rhizo} and R_{eco}.

(3) Imnavait EC R_{eco} data may be reasonably scaled by *in-situ* chamber R_{eco} to approximate annual R_{eco} at our site.

(4) A source partitioning calculated for the total surface R_{eco} holds true to the rooting/active-layer depth at any time.

(5) $\Delta^{14}C_{\ rhizo}$ is the same as atmospheric $\Delta^{14}CO_2$ over the experimental period ($\Delta^{14}CO_2$ = 4.76±8‰, n=11, mean±sd), and $\delta^{13}CO_{2\ rhizo}$ as CO_2 produced from root incubations (-25.4±0.2‰, n=2).

3.3 Results and Discussion

3.3.1 Bulk soil properties

The active layer mineral soil at our study site is a mottled silt loam (1.0-19% C, 0.06-1.1% N) overlain by an approximately 20-cm thick organic layer (21-46% C, 0.52-2.8% N) (Fig. 3.2C, D). As expected for cryoturbated and hummocky terrain, the ash free bulk density increases with depth, yet is highly variable (0.12-2.1 g cm^3 mineral, 0.008-0.38 g cm^3 organic; Fig. 3.2B). Thaw depth (Fig. 3.1A) varies from 2-73 cm, with a maximum in August, and no

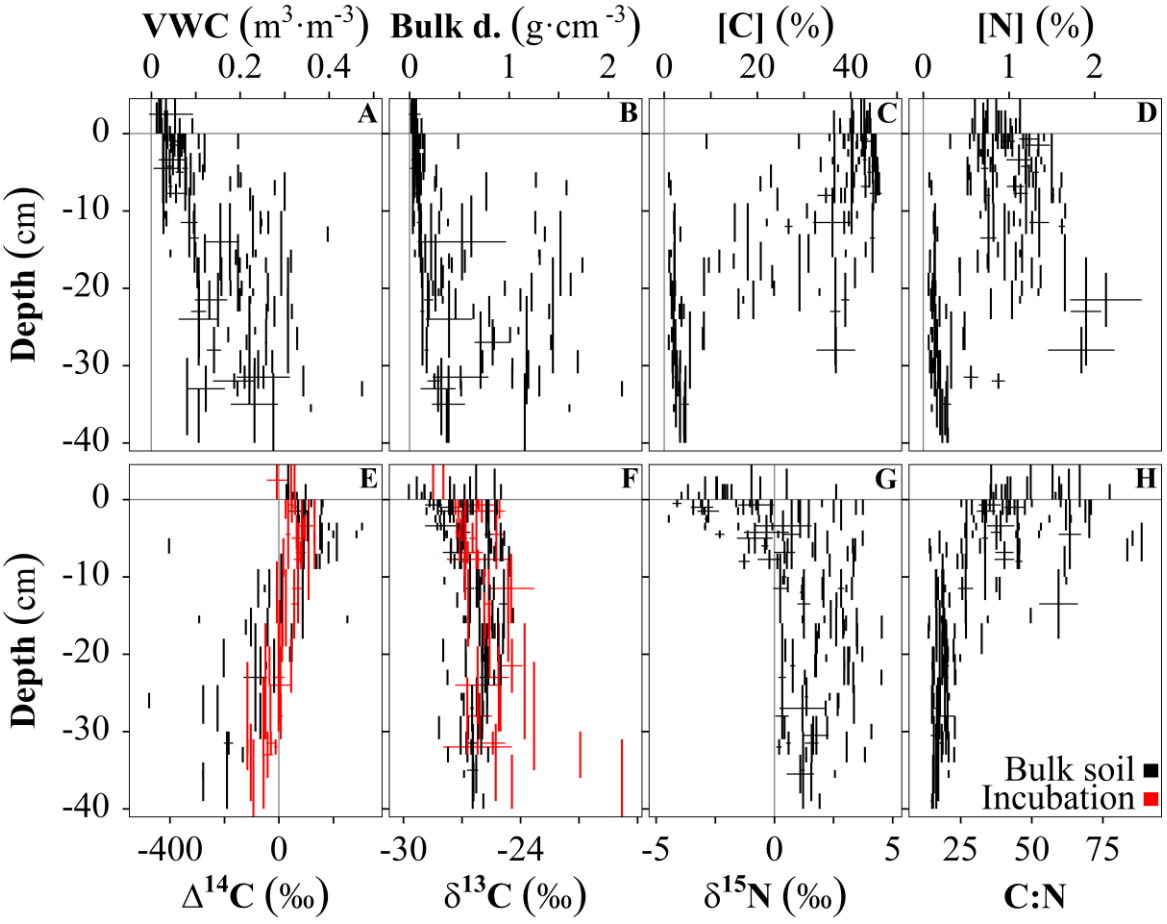

Fig. 3.2 Profiles of bulk soil and incubation properties. Vertical segments span top and bottom depths of individual core segments. Horizontal error bars are standard deviation of replications of the same core segment. Values greater than zero are live biomass (i.e. 0 is the organic soil surface). Incubations were performed at -20, 8, and 22°C with negligible influence on the isotopic values.

annual air temperature change has been documented for the region in recent decades (Bieniek *et al.*, 2015).

The mean age of the bulk organic matter increases with depth from modern ($\Delta^{14}C \geq 0‰$; organic material deposited/formed after 1950) to approximately 2,000 years BP at about 40 cm depth (Fig. 3.2E). The bomb-spike is apparent at 5-10 cm depth – indicating organic material deposited/formed during the mid-20th century. Consistent with previous work (Lupascu *et al.*, 2018), microbially-respired CO_2 follows a similar trend with depth, but is consistently younger than bulk C (enriched or depleted relative to old ($\Delta^{14}C < 0‰$) or modern ($\Delta^{14}C > 0‰$) bulk C, respectively) at the same depths and for the same cores – reflecting preferential microbial consumption of younger organic matter during the laboratory incubation experiment. Respired $\delta^{13}CO_2$ is also enriched relative to bulk soils (Fig. 3.2F), which is expected (Koarashi *et al.*, 2012), but notable in magnitude and proportionality to depth. Enrichment of $\delta^{13}C$ is discussed in detail in **3.6.2: CO_2 isotope traps**.

Bulk soil $\delta^{15}N$ in the top 10 cm is live material (mostly moss, shown as depth >0; Stewart *et al.* 2011), and enriched relative to air below (Fig. 3.2G). This reflects the increasing level of decomposition and enrichment through trophic fractionation (Högberg, 1997; Mariotti *et al.*, 1981; Natelhoffer & Fry, 1988).

3.3.2 Seasonal patterns in the age of Reco

Year-round collection of soil $\Delta^{14}CO_2$ revealed two spatiotemporal patterns (Fig. 3.3A, B). First, CO_2 captured near the surface is always older at depth, whic h is typical for soils developing in stable landscape positions (Shi *et al.*, 2020). Interestingly, we also observe that soil $\Delta^{14}CO_2$ varies around the mean of incubation-derived $\Delta^{14}CO_{2\ micro}$ within ±6 cm of the inlet

depths (dashed lines) throughout the growing season. This suggests that short-term laboratory incubation experiments capture the typical growing season average of microbial C sources but fail to represent winter emissions.

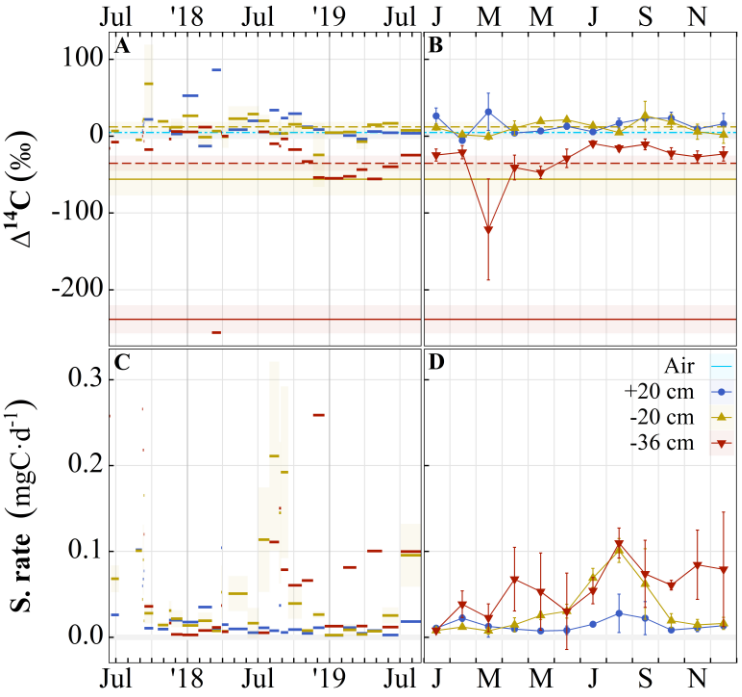

Fig. 3.3 Time series of process-blank corrected (A) $\Delta^{14}C$ and (C) sampling rate of soil CO_2 in graminoid tundra (06/2017–09/2019). Horizontal segments span collection dates for each sample. The *horizontal dot-dash line* indicates the mean $\Delta^{14}CO_2$ in ambient air, *dashed lines* $\Delta^{14}CO_2$ emitted from microbial respiration during laboratory incubations of soils collected within ±6 cm of the mean inlet depths, and *solid lines* $\Delta^{14}C$ of the bulk soil. Shading around lines and segments shows standard error. Panels (B) and (D) show the same data as (A) and (C), respectively, averaged by month of year and weighted by sample period within month with standard error bars.

Second, the age of soil CO_2 changes significantly throughout the year (Fig. 3.3A, B). During the growing-season (Jun-Aug.), soil $\Delta^{14}CO_2$ is significantly younger than that of bulk soil C, indicating that CO_2 production is fueled to a considerable extent by C recently assimilated by plants, as also see in the High Arctic (Czimczik & Welker, 2010). From fall and throughout the non-growing season (Sep.-Mar.), soil $\Delta^{14}CO_2$ becomes older, reaching a minimum in March (Fig. 3.3A, B). As previously reported (e.g. Czimczik *et al.* 2006; Lupascu *et al.* 2014a), soil $\Delta^{14}CO_2$ also changes throughout the growing season, with the oldest C respired during maximum thaw, temperature (Fig. 3.4E), VWC (Fig. 3.4F), and CO_2 production (Fig. 3.4G). These trends are further illustrated using our depth-resolved, monthly model of the data (Figs. 4A, S7; R^2=0.81).

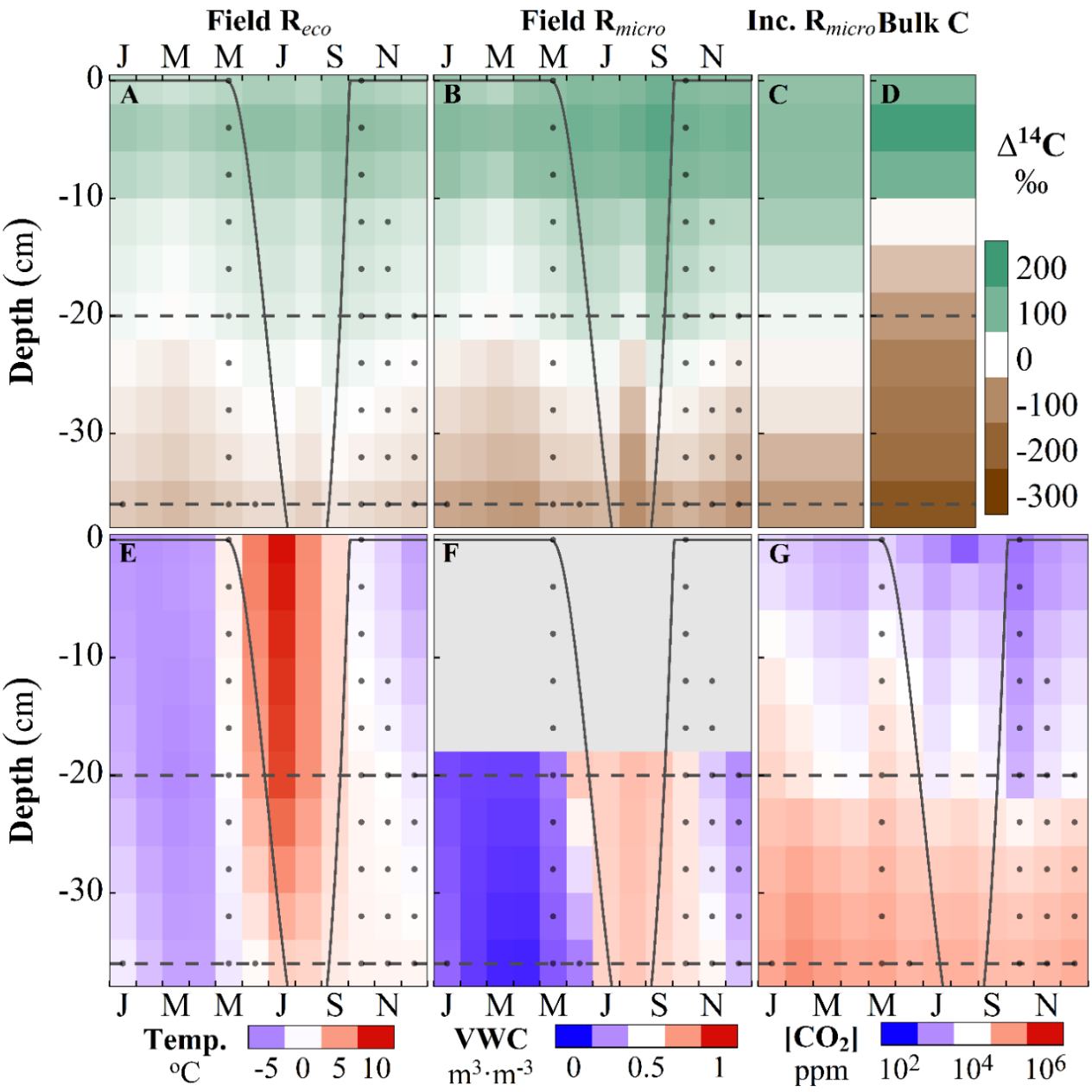

Fig. 3.4 Upper panels compare $\Delta^{14}C$ of (A) soil CO_2 modeled from passive sampler observations, (B) microbial CO_2 modeled from (A) using temperature-dependent emissions, (C) microbial CO_2 from incubations, and (D) bulk soil organic matter as a function of depth (0 cm = top of O horizon) and month of year. Bottom panels (E-G) show linear interpolations of month of year mean values of environmental data from *in-situ* probes. Surface values for temperature and $[CO_2]$ were taken from Toolik EDC and the Imnavait Fen EC tower, respectively. Dashed horizontal lines show mean depths of access wells. Grey spline shows modeled thaw depth, while gray dots show temperature = 0±1°C.

Furthermore, this soil $\Delta^{14}CO_2$ profile resembles that of microbial-respired CO_2 produced during laboratory incubations (Fig. 3.4C).

Above the soil surface, we capture CO_2 with a similar $\Delta^{14}C$ to that of CO_2 in ambient air following melt-off and during the early growing season (late May-July) (Fig. 3.3A, B). As the growing season progresses and into the early winter (Aug.-Oct.), we record a mixture of ambient air CO_2 and modern C, from the decomposition of soil organic matter assimilated since 1950. In winter, we capture snowpack gas that is intermittently enriched or depleted in ^{14}C relative to ambient air CO_2. At 20 cm depth (Figs. 3A, B & 4A), we recover soil CO_2 that is (a) enriched in ^{14}C relative to CO_2 in ambient air (C assimilated since 1950) during spring melt-off (late May/early June) and the end of the growing season (Aug.) and (b) ^{14}C-depleted throughout winter ($\Delta^{14}CO_2 < 0‰$, assimilated before 1950). This seasonal pattern is amplified at 36 cm depth, with soil CO_2 dominated by modern C in early spring and much older C in late winter.

Our continuous observations uncovered a large seasonal variation in soil $\Delta^{14}CO_2$, with older C pools fueling CO_2 production during the non-growing season. The data also show that the active layer remains at around 0˚C (Fig. 3.4E), allowing for CO_2 production (Fig. 3.3C, D & 4G), throughout the fall and early winter (Sep.-Dec.). Thus, our work provides further evidence that non-growing season emissions contribute significantly to the loss of old soil C pools from warming permafrost (Commane *et al.*, 2017; Natali *et al.*, 2019).

3.3.3 Microbial C sources in the dark

Previous studies conducted during the growing season (Czimczik *et al.*, 2006; Czimczik & Welker, 2010; Hicks Pries *et al.*, 2016; Schuur & Trumbore, 2006; Schuur *et al.*, 2009) used incubation experiments to estimate microbial contributions to R_{eco} fluxes. Our results (Fig. 3.4B,

C) show that this approach is a reasonable representation of microbial C sources during the growing season. However, apportioning R_{eco} fluxes during the non-growing season requires a more dynamic understanding of microbial C sources.

As in previous research (Czimczik & Welker, 2010; Lupascu *et al.*, 2014b), we find that the range of microbial $\Delta^{14}CO_2$ in the field (Fig. 3.4B) is greater than that of microbial $\Delta^{14}CO_2$ observed during incubations (Fig. 3.4C). The age of microbial-CO_2 observed in the field outside the growing season (Aug.-Mar.) is frequently older than any CO_2 captured by incubations. In summer and early fall, the presence of older CO_2 may result from the sampler capturing CO_2 originating below it and diffusing upwards. As the active layer refreezes, however, it is more likely that the older CO_2 originates from the decomposition of locally available, older material. We find that the microbial $\Delta^{14}CO_2$ approaches $\Delta^{14}C$ of the bulk C (Fig. 3.4D).

Our results show that short-term incubation experiments do not capture the full range of C sources utilized by soil microorganisms in soils and support the emerging view of a plant-microbe-soil continuum (Högberg & Read, 2006; Sokol *et al.*, 2019) and of dissolved organic matter as a source of microbial C and energy (Roth *et al.*, 2019). Our data suggest that microorganisms rely increasingly on local C sources in fall and winter as they become disconnected from fresh plant exudates and other mobile C sources. Hence, we can expect climate change, via warmer soil temperatures and active layer deepening, to accelerate the loss of older C from permafrost soils during the polar night.

3.3.4 Microbial C contributions to R_{eco}

Ecosystem and microbial respiration in Arctic tundra follow a temperature-dependent seasonal dynamic and are greatest during the growing season, with a maximum in July (Fig.

3.5A). We found that microbial contributions ranged from 38-68% of R_{eco} (Figs. 3.5A, 3.11). Growing season R_{micro} peaked (f_{micro}=52%) in July, with rhizosphere contributions dominating in August and September. The annual column mean $\Delta^{14}CO_2$ values of ecosystem and microbial respiration were 33±2.8‰ and 57±6.2‰, respectively (Fig. 3.5B). Column $\Delta^{14}CO_{2\ eco}$ was not significantly different from the growing season chamber $\Delta^{14}CO_{2\ eco}$ (one sample t-test p-value=0.84, overlapping 95% CI in Fig. 3.5B).

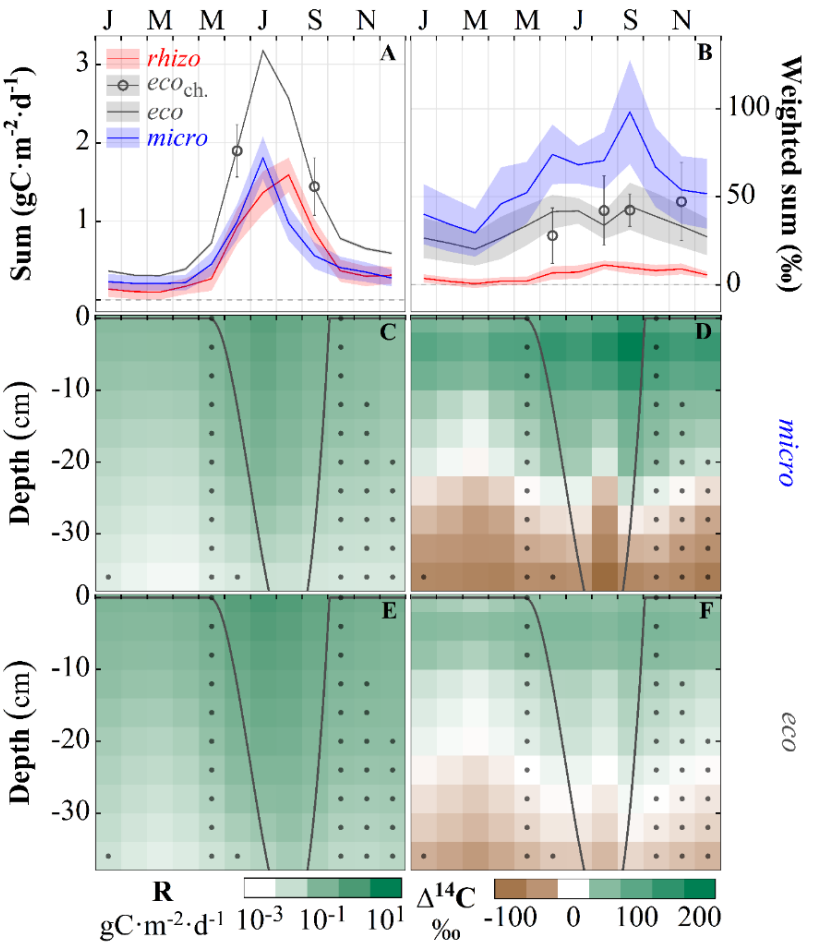

Fig. 3.5 (Top row) Flux (A) and $\Delta^{14}C$ (B) of total surface CO_2 emissions (R_{eco}) and contributions from the rhizosphere (R_{rhizo}) and decomposition of organic matter by heterotrophic microorganisms (R_{micro}). (Middle row) Depth-resolved flux (C) and $\Delta^{14}C$ (D) of microbial emissions (R_{micro}). (Bottom row) Depth-resolved flux (E) and $\Delta^{14}C$ (F) of soil CO_2. (C) and (F) are model products, while (D) and (E) are derived by partitioning the fluxes in (A). Finally (B), ambient air (Barrow, red) is used with component groups (C+D or E+F) to produce weighted surface fluxes. Circles show month of year chamber mean, and all error indicators (bands and bars) show 95% CI. Gray spline shows modeled probe thaw depth, while gray dots show temperature=0±1°C.

The large uncertainties associated with the annual age of emissions are primarily a result of seasonal shifts in microbial contributions to surface emissions and microbial C sources. As expected, we find that the oldest microbially-derived C is produced in mid-summer/maximum thaw (Fig. 3.5D), but that these emissions are masked by the

greater magnitude of respiration in the organic horizons. After plants senesce, microbes contribute more significantly to surface emissions and utilize older C sources.

This study demonstrates that continuous observations of soil and ecosystem $\Delta^{14}CO_2$ provide unprecedented insight to microbial C sources and enable a more systematic observation of C cycling in Arctic soils (Shi *et al.*, 2020) by quantifying the loss of ancient permafrost C from thawing permafrost.

3.4 Conclusions

Here, we combine year-round observations of soil $\Delta^{14}CO_2$ in Arctic graminoid tundra with short-term laboratory incubation experiments and bulk soil analyses to reveal seasonally dynamic microbial C sources. We show that microbial C emissions during the non-growing season are fueled by older soil C pools and further highlight the polar night as a critical period for climate-vulnerable permafrost C pools.

Acknowledgements

We thank the Toolik Field Station Science Support and Environmental Data Center teams, D. Helmig (CU Boulder), and the KCCAMS staff and C. McCormick (UCI) for their logistical and technical support. Funding was provided by the U.S. NSF OPP (#1649664 to C.I.C., #1650084 to J.M.W. & E.S.K.).

3.5 Supplement

3.5.1 Methods

3.5.1.1 Models

Polynomial

Thaw-probe depth was modeled as a 3-degree polynomial of DOY and set to zero outside of the growing season (where the polynomial touches or crosses above zero). This polynomial represents the maximum depth reachable by thaw-probe at our site throughout the year and was fit simply to contextualize other data in figures.

Non-linear least squares

[CO_2] was measured regularly over the course of the incubations at 22, 7, and -20^oC. Fluxes were calculated as the difference between measurements relative to the time gap, and averaged as a mean, weighted by the day of measurement. Although the initial CO_2 pulse at the start of incubations was purged, a weighted average emphasizes the latter stabilized flux measurements, incorporating all measurements while reducing model error. Flux by mass was converted to flux over a surface area by averaging overlapping cores into defined depth steps (Fig. 3.10A, 4 cm steps). The model for R_{micro} CO_2 flux was selected to approximate the form of common Q_{10} equations, while considering the numerous predictors which may influence the favorability of microbial activity that decay with depth down the soil column. Using depth as a variable relates the model to measurable values such as bulk properties (Fig. 3.2A&B), concentrations (Fig. 3.2C&D), and incubation fluxes, as well as things which are more difficult or unknown, without requiring any measurement and retaining simplicity and minimal error. R_{micro} CO_2 flux at

individual depths were modeled (Table 3.6, Fig. 3.10A&C) from laboratory soil incubations as an exponentially decaying nonlinear least squares fit (R *nls* function) of temperature and depth [Eq. 3.4]:

$$\mathbf{R}_{\boldsymbol{micro}} = \boldsymbol{a} * \mathbf{exp}\,(\boldsymbol{b} * \mathbf{Temperature} + \boldsymbol{c} * \mathbf{Depth}) \qquad \text{[Eq. 3.4]}$$

Multivariate adaptive regression splines

We used multivariate adaptive regression splines (commonly "earth" models due to trademarking) (R *earth v5.1.2*) to find natural nodes in linear, nonlinear, and interactive data, while minimizing variables (and over-fitting) with cross-validated backwards pruning. *Earth* models were selected because they have greater flexibility than linear regressions, but are more easily interpreted than e.g. machine learning models, making them suitable to extrapolate $\Delta^{14}CO_{2\ eco}$ and $\delta^{13}CO_{2\ eco}$ for a full soil profile (above the depths of the shallowest access well and sensors) while also potentially aiding a mechanistic understanding of each response to one or more predictors.

Each response variable was interpolated between -20 cm and -36 cm to allow the greatest number of observations with which to build the model. In this way, the *earth* model can attribute appropriate significance to soil predictors that vary with depth across the entire range of depths sampled, rather than being limited to two unique depths. We selected a minimum number of predictor variables which were easily measured and demonstrated a clear relationship with the response; correlations with other environmental variables are shown in Fig. 3.16.

$\Delta^{14}CO_{2\ eco}$ was predicted by three variables: (a) local bulk soil $\Delta^{14}C$, (b) the amount of time elapsed since smoothed Toolik EDC snow depth data was greater than zero (i.e. melt-off), and (c) the amount of time elapsed since Toolik EDC snow depth data was equal to zero (i.e. the onset of a semi-continuous snowcap) (Table 3.7, Fig. 3.12). We considered these predictors reasoning that

(a) microbes respire CO_2 derived in part from the bulk substrate, (b) the snow-free season comes with both fresh rhizosphere OM inputs (modern ^{14}C) and increased temperatures (as well as increased plant respiration), and (c) continuous snow cover (therefore frozen or near-freezing soil surface) represents a kind of lid, which coincides with impacted substrate availability from plant senescence and limited DOM and CO_2 mobility.

3.5.1.2 Soil respiration partitioning

Our CO_2 traps measure $\Delta^{14}CO_{2\,eco}$ and $\delta^{13}CO_{2eco}$ at different soil depths (*d*), which we use to inform the *earth* model to predict between the minimum sampler depth and the soil surface for each month of year (Fig. 3.12, 3.13). We know the signature of rhizosphere CO_2 from Point Barrow air samples ($\Delta^{14}CO_{2\,rhizo}$, Xu, X, pers. com.) and root incubations ($\delta^{13}CO_{2\,rhizo}$). We scale a local EC source as an approximation of R_{eco} at our site (Fig. 3.9A), where R_{eco} is obtained from the Imnavait Creek Fen and scaled to our site by multiplying the magnitude at each timestep by the mean quotient of our chamber fluxes to the Imnavait values. We use an incubation model to predict R^{d}_{micr} at different soil depths (Fig. 3.10C and **Models: *Non-linear least squares***). We use these components in a system of equations to partition R and $\Delta^{14}CO_2$ within the soil column and as the surface sum. We perform the same partitioning steps for $\delta^{13}CO_2$, which may be substituted for $\Delta^{14}CO_2$ in all equations.

The total surface R_X for any component *X* (*eco, rhizo, micr*) is calculated as the sum of R^{d}_{X} over each of *n* depth steps from the total depth to the soil surface [Eq. 3.5]:

$$\mathbf{R_X = \sum_{d=n}^{d=0} R_X^d} \qquad \text{[Eq. 3.5]}$$

In Fig. 3.11A, we show the column sum of R_{micro} model results, as well as scaled R_{eco}, and R_{rhizo} (the difference); 3.11B shows the fraction of R_{eco} for each component.

We must assume that this ratio of fluxes on any given day holds constant to the bottom of the soil column [Eq. 3.6]:

$$\frac{\mathbf{R_X}}{\mathbf{R_{eco}}} = \frac{\mathbf{R_X^d}}{\mathbf{R_{eco}^d}} \quad \text{or equivalently} \quad \mathbf{f_X} = \mathbf{f_X^d} \qquad \text{[Eq. 3.6]}$$

In other words, on any day the surface R_{eco} is made up of R_{micro} and R_{rhizo} [Eq. 3.1], and the relative rate of production of each of these components to each other is the same at the surface of the soil as at the maximum relevant depth. While this does not necessarily hold true at every depth in the active layer, our experimental design lacks the means to resolve partitioning with depth. This is likely the biggest source of error in the surface isotope flux calculation. However, the error of the assumption should be minimized because the magnitude of R_{micro} decays exponentially with depth (Fig. 3.10A&C), becoming a minor fraction of the column sum below ~30 cm (where the partitioning is more removed from the surface reality). Root density (and therefore R_{rhizo}) should decrease with depth as well.

The components of ecosystem CO_2 flux are partitioned at each depth with a 2-endmember mixing model of microbial and rhizosphere endmembers [Eqs 3.7-3.9]:

$$\mathbf{R_{eco}^d} \bullet \mathbf{^{14}CO_{2\,eco}^d} = \mathbf{R_{micro}^d} \bullet \mathbf{^{14}CO_{2\,micro}^d} + \mathbf{R_{rhizo}^d} \bullet \mathbf{^{14}CO_{2\,rhizo}} \qquad \text{[Eq. 3.7]}$$

$$\mathbf{R_{eco}^d} = \mathbf{R_{micro}^d} + \mathbf{R_{rhizo}^d} \qquad \text{[Eq. 3.8]}$$

$$\mathbf{^{14}CO_{2\,micro}^d} = \frac{\mathbf{R_{eco}^d}}{\mathbf{R_{micro}^d}} \bullet \mathbf{^{14}CO_{2\,eco}^d} - \frac{\mathbf{R_{eco}^d}}{\mathbf{R_{micro}^d}} \bullet \mathbf{^{14}CO_{2\,rhizo}} + \mathbf{^{14}CO_{2\,rhizo}} \qquad \text{[Eq. 3.9]}$$

Combining Eqns. 3.6 ($R_X = R_{micro}$) & 3.9 yields an expression which accepts surface flux ratios [Eq. 3.10]:

$$\mathbf{^{14}CO_{2\ micro}^{d}} = \frac{\mathbf{R_{eco}}}{\mathbf{R_{micro}}} \bullet \mathbf{^{14}CO_{2\ eco}^{d}} - \frac{\mathbf{R_{eco}}}{\mathbf{R_{micro}}} \bullet \mathbf{^{14}CO_{2\ rhizo}} + \mathbf{^{14}CO_{2\ rhizo}} \quad \text{[Eq. 3.10]}$$

Knowing $^{14}CO_{2\ X}^{d}$ allows us to calculate $^{14}CO_{2\ X}$ as the sum of an *n*-endmember mixing model from the total depth to the surface by assuming that the surface $^{14}CO_{2\ X}$ flux is equivalent to the flux-weighted mean of what is produced at each depth [Eq. 3.11]:

$$\mathbf{R_X} \bullet \mathbf{^{14}CO_{2\ X}} = \mathbf{R_X^0} \bullet \mathbf{^{14}CO_{2\ X}^0} + \mathbf{R_X^1} \bullet \mathbf{^{14}CO_{2\ X}^1} + \cdots + \mathbf{R_X^n} \bullet \mathbf{^{14}CO_{2\ X}^n}$$

$$\Rightarrow \quad \mathbf{^{14}CO_{2\ X}} = \frac{\mathbf{1}}{\mathbf{R_X}} \bullet \sum_{\mathbf{d=n}}^{\mathbf{d=0}} \left(\mathbf{R_X^d} \bullet \mathbf{^{14}CO_{2\ X}^d}\right) \quad \text{[Eq. 3.11]}$$

This is directly used to solve for $^{14}CO_{2\ micro}$. While we do not know R_{eco}^{d}, we can rearrange Eq. 3.6: $\frac{R_{micro}}{R_{eco}} = \frac{R_{micro}^{d}}{R_{eco}^{d}} \Rightarrow \frac{R_{eco}^{d}}{R_{eco}} = \frac{R_{micro}^{d}}{R_{micro}}$. This allows Eq 3.11 to also be solved for $^{14}CO_{2\ eco}$ through substitution of the flux ratios.

3.5.2 Results and Discussion

3.5.2.1 Sensory data

Meteorological data obtained from Toolik EDC were averaged by DOY over the experimental period and smoothed with a ±11 day running average (Fig. 3.6). Photosynthetically active radiation (PAR) is greatest May-June, after which increased cloud cover concurs with maxima in precipitation and humidity. Air temperature crosses above 0°C near the beginning of May, coinciding with snow melt-off (~June 17). Regional snow depth increases more gradually when temperatures drop below freezing in September. Snow depth was continuously greater than

zero after ~Sep. 6. The continuity of snowpack has impacts on gas fluxes, limiting but not prohibiting diffusion from high subsoil [CO_2] to low atmospheric [CO_2]. Thaw depth was modeled from observations (n=85, 4 campaigns) as a 3rd-degree polynomial between the surface soil thaw-out and freeze-up days (Fig. 3.6F). These days were calculated as the first and last day for which smoothed, interpolated temperature at 0 cm was >0^{o}C (5/10 and 10/12, respectively). While the thermodynamic state of permafrost water is both a function of depth and time, and soil at depths below the surface remain unfrozen (and biologically active) well into the winter, the freezing of the surface horizon is still a phenomenon with potential biophysical impacts on soil gas fluxes along the same line of reasoning as snowpack continuity.

Data collected from probes co-deployed with soil CO_2 samplers (Fig. 3.7, left panels) were averaged by DOY and depth (-20 cm probes) over the experimental period. We used local ambient temperature and [CO_2] data from Toolik EDC and Imnavait EC, respectively, as surface values with which to vertically interpolate for a complete soil profile (Fig. 3.7 B&F). The thaw curtain (0±1^{o}C) is seen as the patterned region of DOY-depth space in Fig. 3.7B. This zone persists well into the winter, with temperatures staying within a range suitable for microbial activity year-round at -36 cm. This is also the depth at which we collect our oldest samples each year (-258 and -56‰ $\Delta^{14}C$ over 3/4-3/28 2018 and 4/8-5/16 2019, respectively). These samples capture respiration produced at the very end of winter, when soil decomposers have been isolated from fresh carbon sources by reduced unfrozen water availability for the greatest time.

VWC was interpolated between the two depths for each timestep (Fig. 3.7D). The Jan-Feb changes at -36 cm are noteworthy as evidence of changing water availability late into the winter. Decagon 5TM probes measure the dielectric permissivity of their environmental medium to calculate VWC. The dielectric permissivity of ice is much lower than that of water, resulting in a

stark decrease in calculated VWC in soils passing through the thaw curtain (Watanabe & Wake, 2009). Conductivity probes are still capable of measuring changes in unfrozen water content in the presence of ice, as seen from the VWC changes below <0°C.

This possibility of continued heterotrophic activity at depth throughout the winter is supported by this evidence of changing water availability, as well as a continuous buildup of [CO_2]. It is also likely that [CO_2] increases as space within the thaw curtain is compressed by expanding ice above and below.

3.5.2.2 CO_2 isotope traps

During the growing season (JASO), soil $\delta^{13}CO_2$ varies about the average of CO_2 respired from incubations of soils ±6 cm of the inlet depth (Fig. 3.8A&B). We see strong seasonality in data aggregated by month (Fig. 3.8B). Surface and near-surface soil $\delta^{13}C$ converge in late winter, suggesting some vertical CO_2 diffusion from soil to air through the snowpack. Soil $\delta^{13}CO_2$ exhibits a strong correlation with VWC and temperature (Fig. 3.16), which possibly stems from a combination of physical and microbial processes. Gas-phase $\delta^{13}CO_2$ enrichment may occur from gas-liquid equilibrium carbonate chemistry, as an inverse function of temperature (Mook *et al.*, 1974; Thode *et al.*, 1965), while bulk soil $\delta^{13}C$ enrichment in (especially permafrost soil) is mostly understood to indicate increasing levels of heterotrophic OM transformation (Gentsch *et al.*, 2015). This observed fractionation has several proposed mechanisms, including decomposer preference for ^{12}C, and enhanced stabilization of ^{13}C-enriched matter (Natelhoffer & Fry, 1988; Torn *et al.*, 2002). Recently fixed material will also be more depleted in ^{13}C due to dilution of atmospheric CO_2 with (low $^{13}C/^{12}C$) fossil fuels. Soil microbial and fungal carboxylation reactions (i.e. dark reactions) have been proposed to consume ambient CO_2 in catabolism, which

may have a different $^{13}C/^{12}C$ than the material being decomposed. If the ambient is enriched relative to the OM, the decomposer should become enriched relative to the substrate, to a progressively greater degree with increasing levels of decomposition (Ehleringer *et al.*, 2000). CO_2 respired from decomposition of this enriched OM will of course be enriched as well. By this logic, enriched $\delta^{13}CO_2$ respired in late winter aligns with $\Delta^{14}CO_2$ results, which indicate decomposition of old material during the same time. Indeed, if soil gas becomes trapped by ice in late winter and CO_2 is recycled and concentrated by decomposers and ice compression, this could result in enhanced [CO_2] (Fig. 3.7E&F) and the dramatic $\delta^{13}CO_2$ enrichment observed. While incubation (Fig. 3.2F) and chamber (Fig. 3.9C) observations also yield enriched $\delta^{13}CO_2$ in these soils, it is also possible that the sampling system contributed a sampling-rate-dependent fractionation, resulting in enriched CO_2 during periods of low sampling rate (Pedron *et al.*, 2021).

3.5.2.3 Models

Multivariate adaptive regression splines

The $\Delta^{14}CO_{2\ eco}$ model calculated two hinges in the bulk soil $\Delta^{14}C$ predictor (-127.0 & -168.8‰). These values are approximately the bulk soil $\Delta^{14}C$ close above and below the -20 cm inlet depth (Figs. 3.2E&3.2A, B). Importantly, this predictor allows the model to reproduce the bomb-spike.

The model also calculated two hinges for onset of snowpack (14.54 & 181.8 days since onset). We speculate that the higher value represents a late winter minimum temperature threshold (Fig. 3.7A&B), after which soil temperatures begin to rise.

$\delta^{13}CO_{2\ eco}$ was only predicted by temperature (Table 3.8, Fig. 3.14). Four hinges were calculated, that may be loosely interpreted as: (>1.5^{o}C) growing-season values approach signature plant respiration (-25 to -27‰), (1.5-0.7; 0.7-0.46^{o}C) near-freezing temperature coincides with active frost-heave and winter dormancy, with an increasingly large fraction R_{micro}, and (0.46 to -3.9; <-3.9^{o}C) temperature-dependent enrichment phenomenon seems to be increasingly important in the sub-zero regime.

3.5.2.4 Soil respiration partitioning

The $\delta^{13}CO_{2\ eco}$ model and $\delta^{13}CO_{2\ micro}$ partitioning results are show in Fig. 3.14A&B, respectively. The modeled $\delta^{13}CO_{2\ micro}$ profile (Fig. 3.14B) has a more dynamic appearance than the incubation and bulk carbon $\delta^{13}C$ profiles (Fig. 3.14C&D, respectively). Column $\delta^{13}CO_{2\ eco}$ (Fig. 3.15D) is like air in summer and becomes more enriched in winter. More winter chamber data would be extremely useful in validating these results. The seasonally variable R_{micro} enrichment relative to R_{rhizo} is consistent with the incubation trend of microbial respiration fractionation increasing in magnitude with removal from fresh SOM, albeit in time rather than depth.

3.5.3 Tables and Figures

Table 3.1 Summary of R_{micro} *nls* flux model developed from laboratory incubations of local soils. Residual standard error was 0.115 on 24 degrees of freedom.

	Estimate	Std. Error	t value	Pr(>|t|)
a	0.121513	0.036242	3.353	0.00265
b	0.155155	0.013614	11.397	3.61E-11
c	0.081441	0.003676	22.154	< 2e-16

Table 3.2 Summary of $\Delta^{14}CO_{2\ eco}$ *earth* model developed from field data 2017-2019 (R^2=0.81). The model was implemented with default parameters and: *nfold* = 10 (cross-validation folds); *ncross* = 30 (cross validations); *degree* = 1 (no interaction); *varmod.method* = "earth" (method to construct variance model for error prediction). The model was weighted by the inverse squared standard error of the response.

Predictor	Rank	Hinge		Coefficient
		min	max	
Intercept				4.443
Bulk soil $\Delta^{14}C$	1	-127.0		-0.184
		-168.8	-127.0	0.176
Days snow-covered	2	14.54	181.8	0.351
			14.54	-0.146
Days snow-free	3			-0.217

Table 3.3 Summary of $\delta^{13}O_{2\ eco}$ *earth* model developed from field data 2017-2019 (R^2=0.92). The model was implemented with default parameters and: *nfold* = 10 (cross-validation folds); *ncross* = 30 (cross validations); *degree* = 1 (no interaction); *varmod.method* = "earth" (method to construct variance model for error prediction). The model was weighted by the inverse squared standard error of the response.

Predictor	Hinge		Coefficient
	min	max	
Intercept			-53.45
Temperature (^oC)		-4.0	5.779
	-4.0	0.5	-18.90
	0.5	0.7	22.47
	0.7	1.5	6.513
	1.5		-9.865

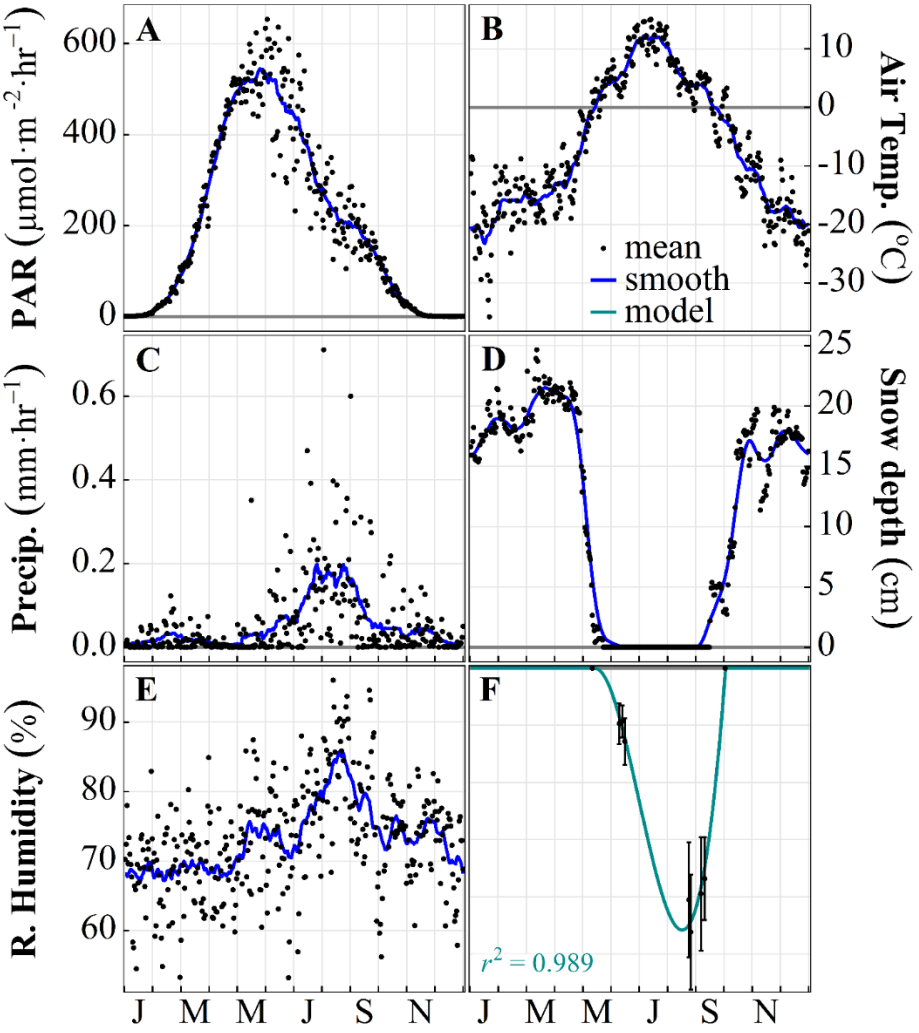

Fig. 3.6 Environmental data over the sampling period, aggregated by day of year. Panels A-E are Toolik EDC data, with ±11-day running averages. The thaw depth model (F) is a 3^{o} polynomial (set==0 when ≥0 cm) built from empirical day of year mean(±sd) thaw probe measurements (*n*=85) taken during campaigns.

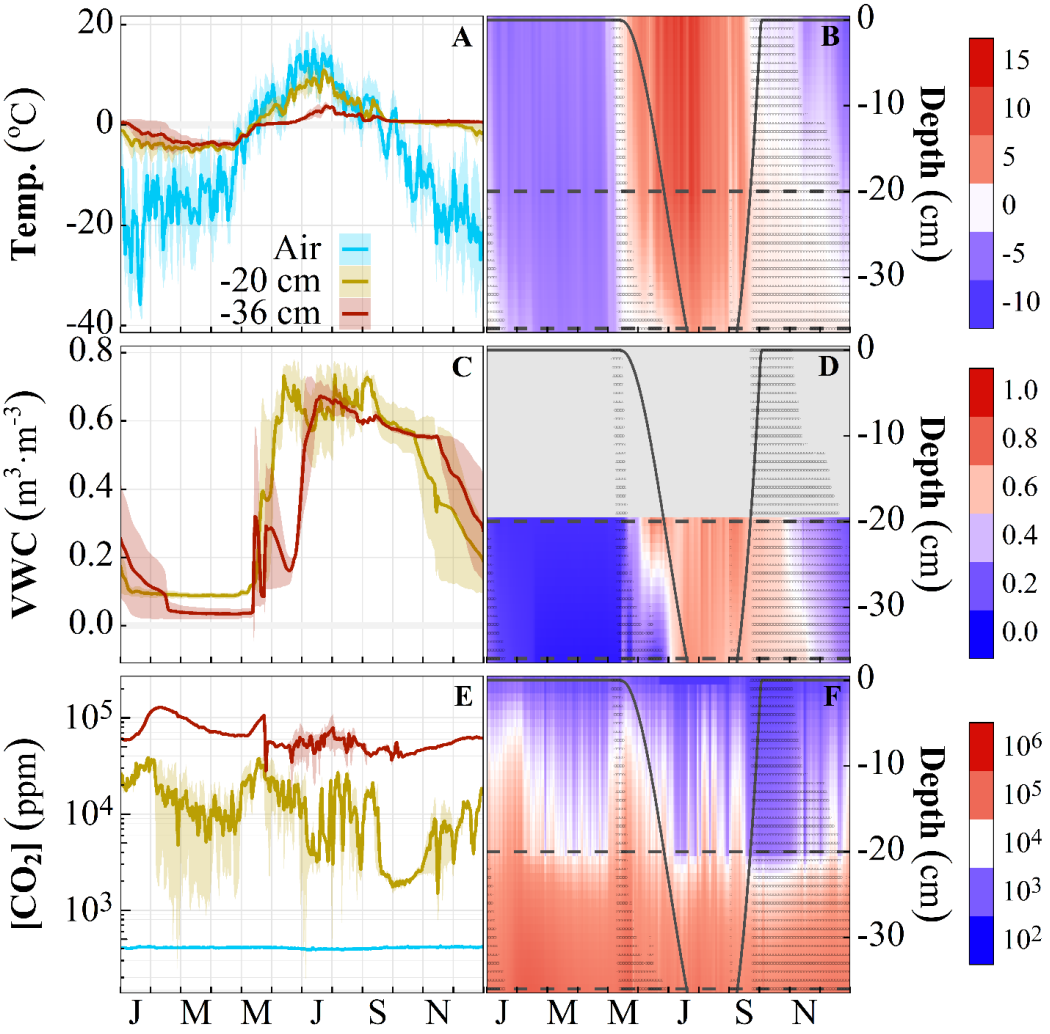

Fig. 3.7 Day of year mean±sd data (A, C, E) beside linear interpolations (B, D, F) of environmental *in-situ* probes. Surface values for temperature and [CO_2] were taken from Toolik EDC and the Imnavait Fen EC tower, respectively. In right panels, *horizontal dashed lines* are depths of sensors, *spline* shows modeled probe thaw depth, and *dot pattern* shows temperatures 0±1°C (from B).

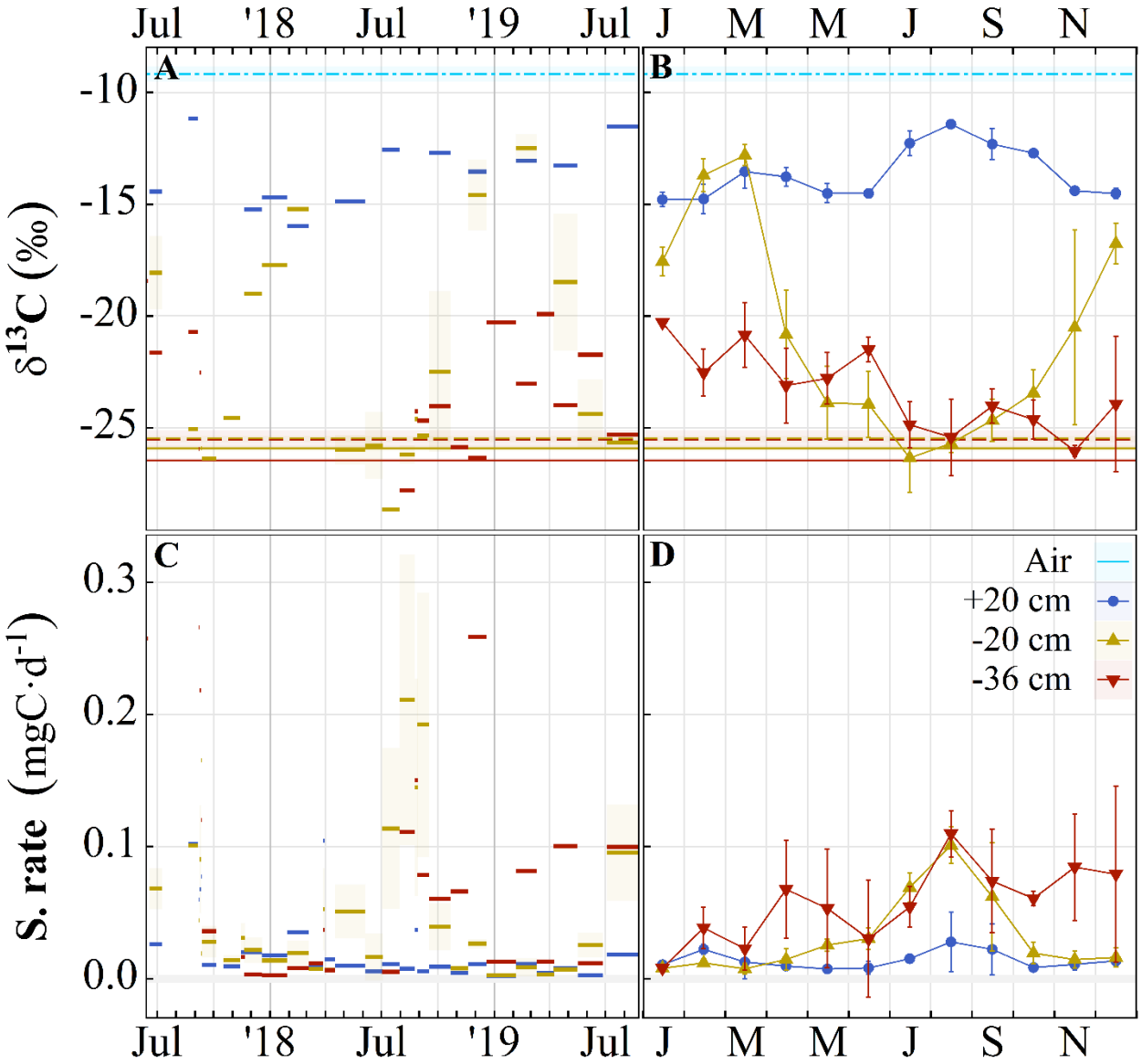

Fig. 3.8 Time series of process-blank corrected (A) $\delta^{13}C$ and (C) sampling rate of soil CO_2 in graminoid tundra (06/2017–09/2019). Horizontal segments span collection dates for each sample. The *horizontal dot-dash line* indicates the mean $\delta^{13}CO_2$ in ambient air, *dashed lines* $\delta^{13}CO_2$ emitted from microbial respiration during laboratory incubations of soils collected within ±6 cm of the mean inlet depths, and *solid lines* $\delta^{13}C$ of the bulk soil. Shading around lines and segments shows standard error. Panels (B) and (D) show the same data as (A) and (C), respectively, averaged by month-of-year (weighted by sample period within month) with standard error bars.

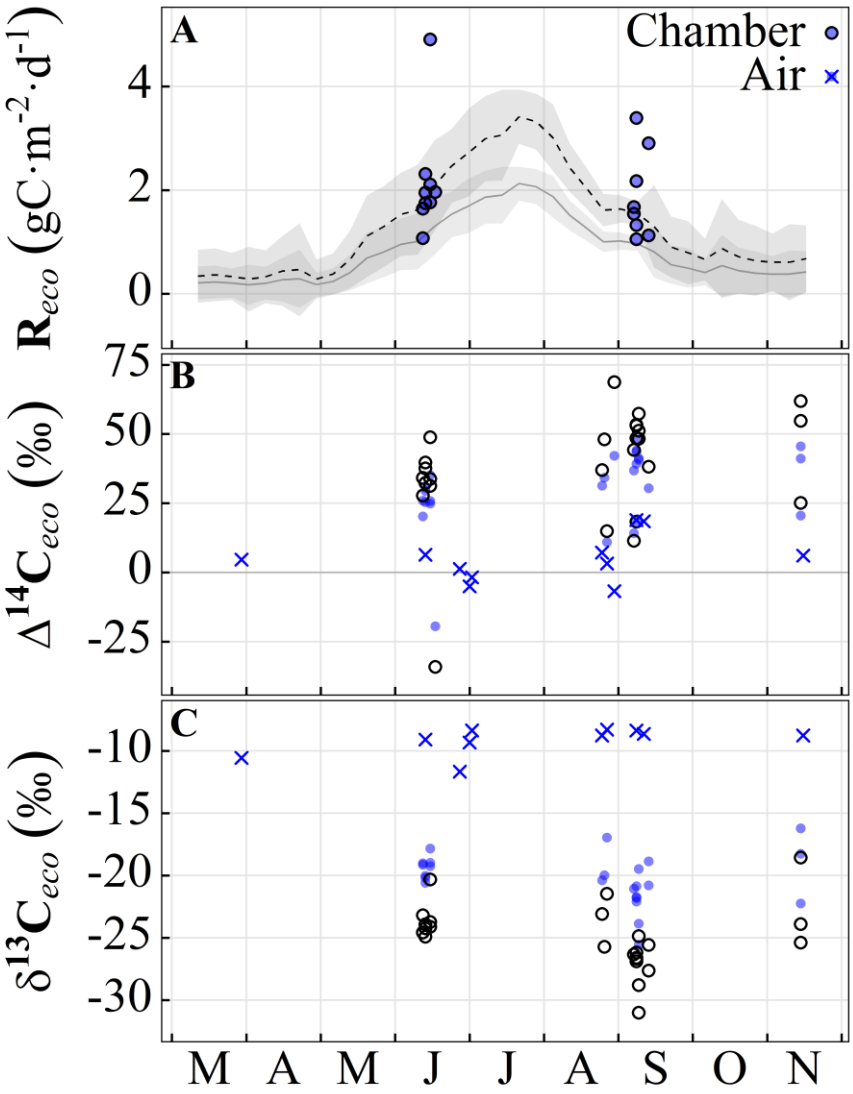

Fig. 3.9 Closed-top soil respiration chamber and reference air CO_2 sampled during campaigns. Open symbols are corrected for ambient air in the chamber, while blue closed circles correspond to the raw data. The *solid gray* line is Imnavait Fen eddy covariance R_{eco} over the sampling period, while the *dashed black* line is linearly scaled to our site.

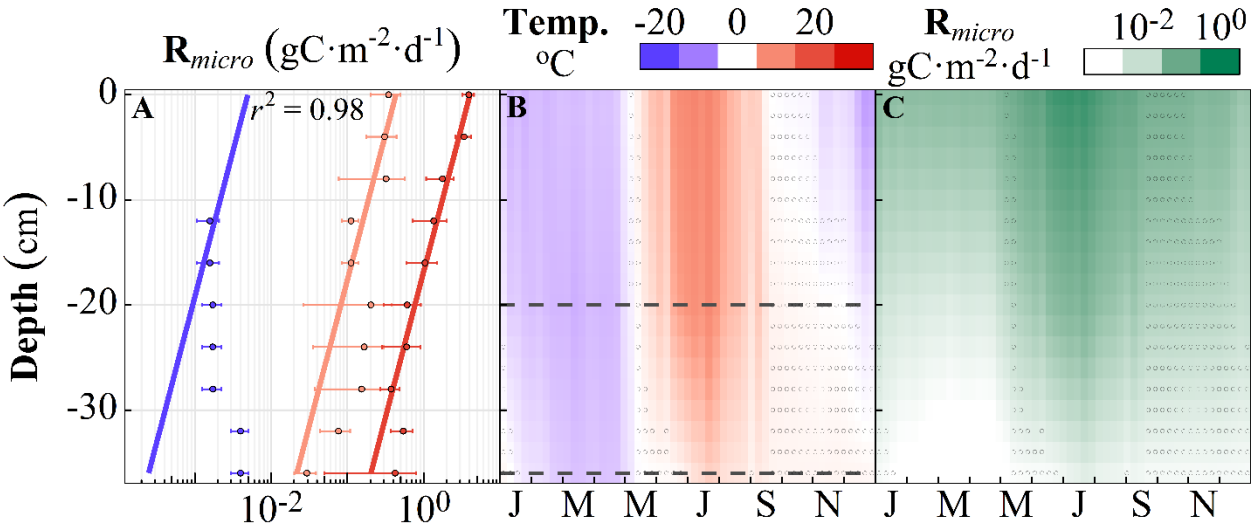

Fig. 3.10 Summary of incubation CO_2 flux (R_{micro}) model. (A) Mean(±se) CO_2 flux from incubations at -20, 8, and 22°C, averaging overlapping cores into 4 cm depth steps, with model predictions (slanted lines). Fluxes were modeled as an exponential function of temperature and depth in a nonlinear least-squares fit (Eq. S1, Table 3.1). (B) Interpolated probe temperature was used for (C) flux predictions. *Dot pattern* shows temperatures 0±1°C.

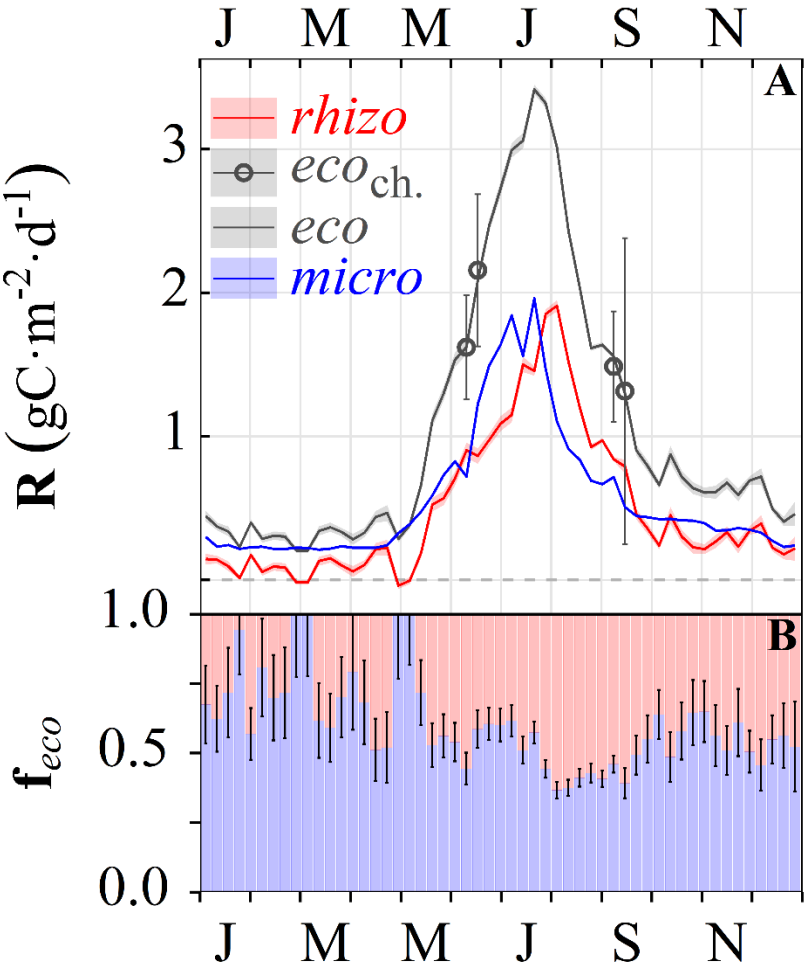

Fig. 3.11 (A) Components of CO_2 respiration. R_{eco} is scaled from Imnavait Fen. R_{micro} is the column sum of modeled R^d_{micro} at each time, and R_{rhizo}=R_{eco}-R_{micro}. (B) Fraction of R_{eco}, ±se.

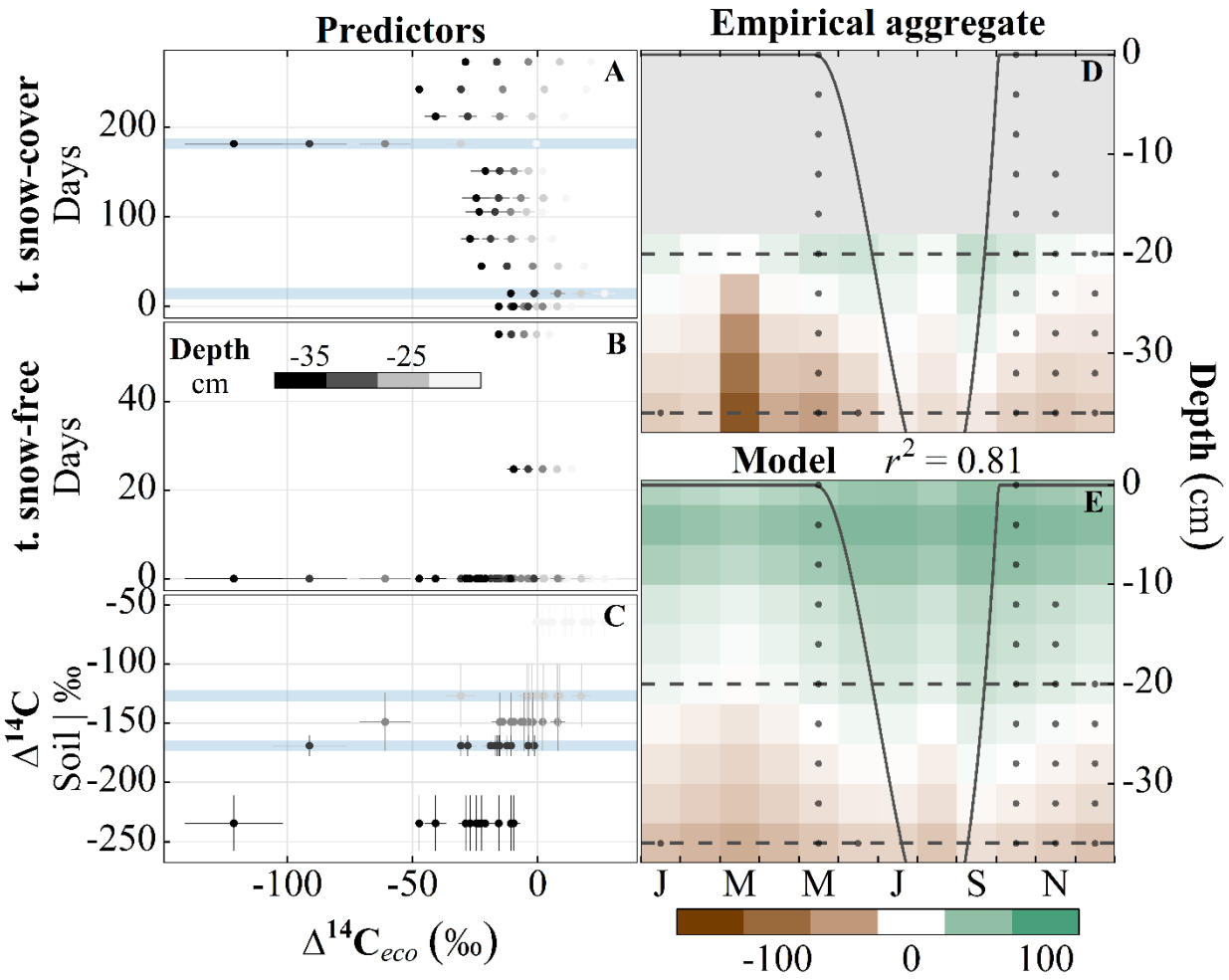

Fig. 3.12 (A-C) Summary of $\Delta^{14}CO_{2\ eco}$ predictors, (D) interpolated response and (E) model prediction. Empirical $\Delta^{14}CO_{2\ eco}$ results were aggregated by month of year and modeled as a function of (A) the amount of time which has passed since the last snow-free day, (B) the amount of time which has passed since the onset of semi-continuous snowpack and (C) $\Delta^{14}C$ of bulk soil from cores. Hinges calculated by *earth* model are shown as horizontal light blue bars. *Dashed horizontal lines* show mean depths of sampler inlets. *Spline* shows modeled probe thaw depth, while *dot pattern* shows temperature=0±1°C.

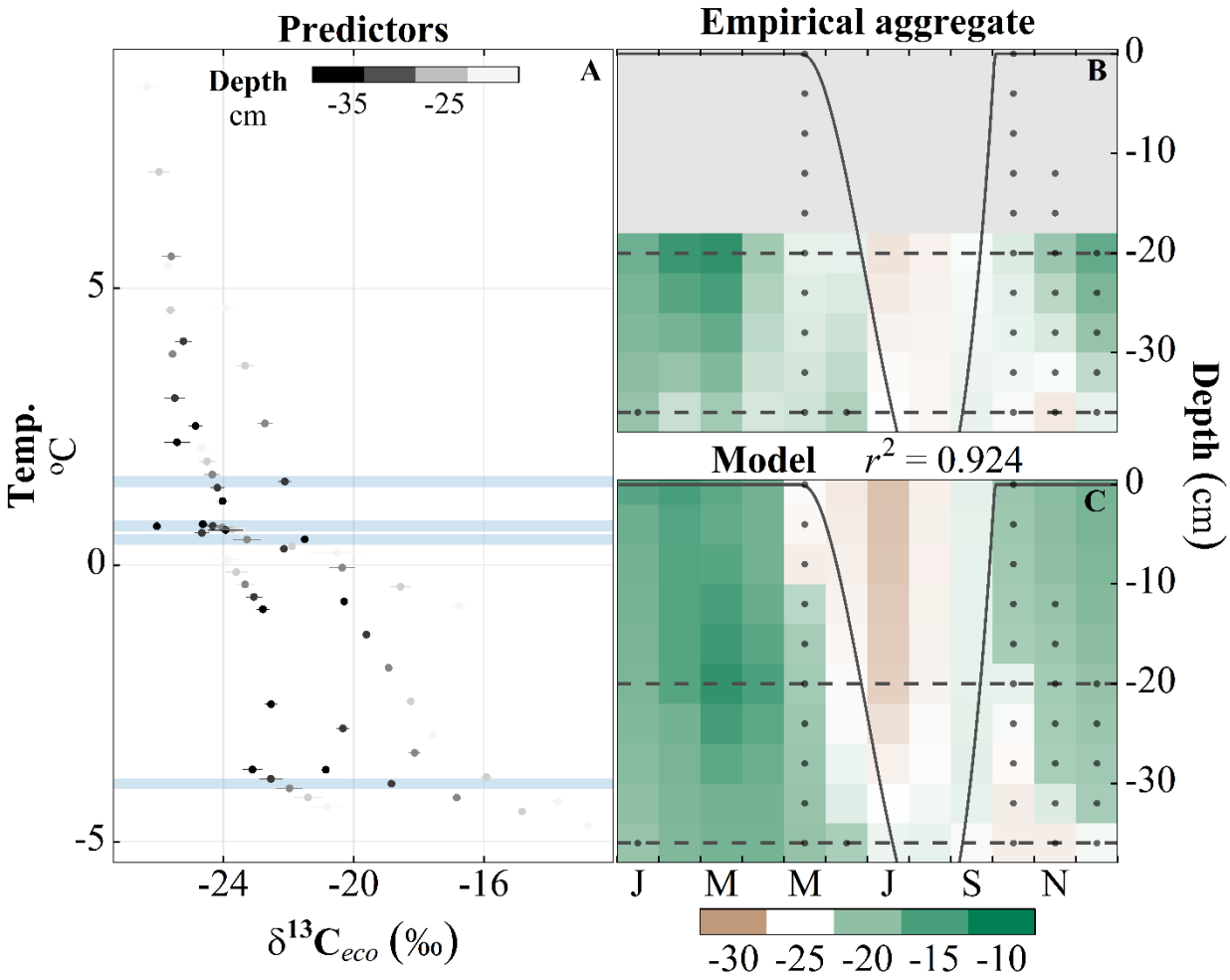

Fig. 3.13 (A) Summary of $\delta^{13}CO_{2\ eco}$ predictor, (B) interpolated response and (C) model prediction. Empirical $\delta^{13}CO_{2\ eco}$ results were aggregated by month of year and modeled as a function of temperature. Hinges calculated by *earth* model are shown as horizontal light blue bars. *Dashed horizontal lines* show mean depths of sampler inlets. *Spline* shows modeled probe thaw depth, while *dot pattern* shows temperature=0±1°C.

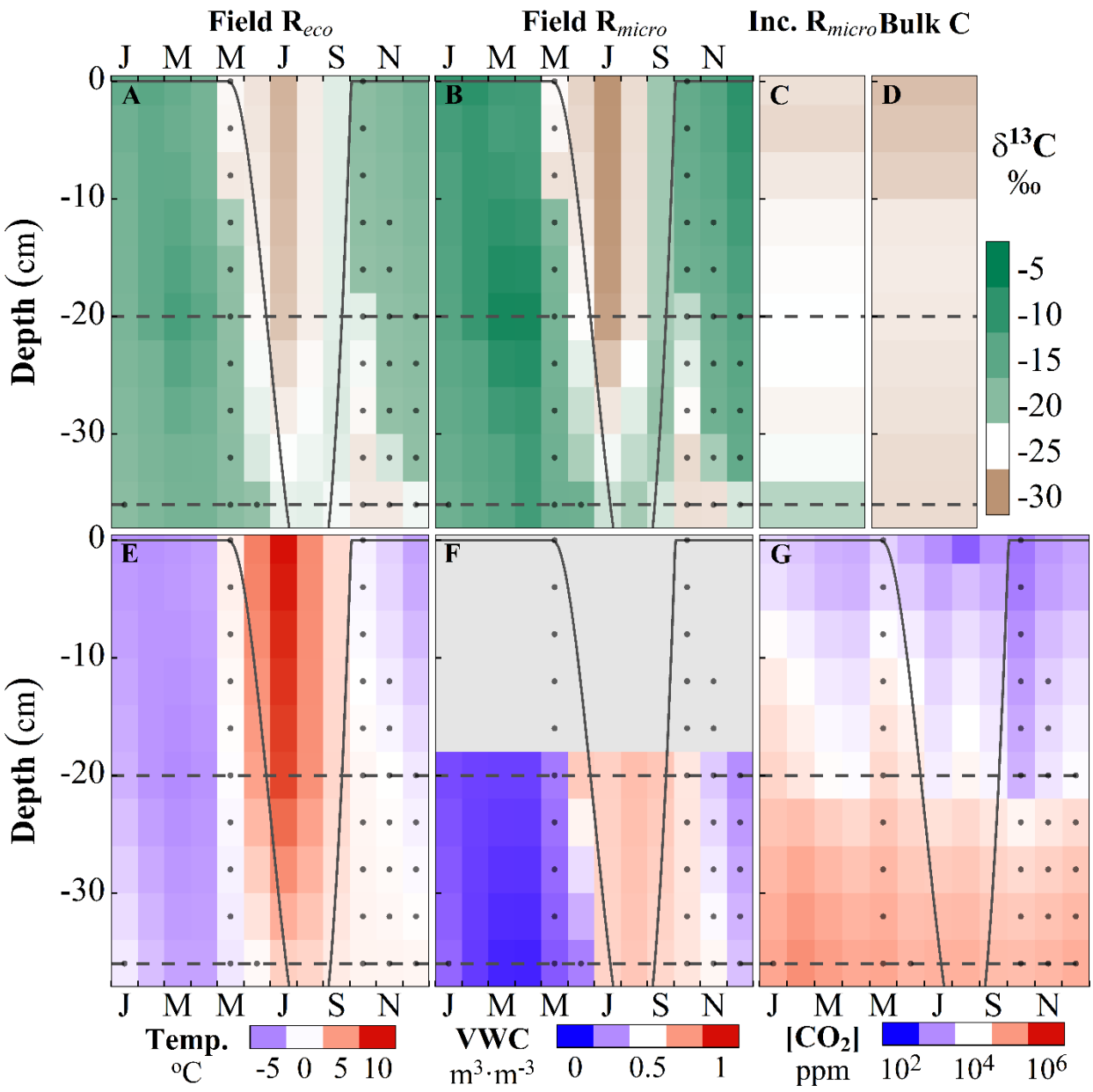

Fig. 3.14 Upper panels compare $\delta^{13}C$ of (A) soil CO_2 modeled from passive sampler observations, (B) microbial CO_2 modeled from (A) using temperature-dependent emissions, (C) microbial CO_2 from incubations, and (D) bulk soil organic matter as a function of depth (0 cm = top of O horizon) and month of year. Bottom panels (E-G) show linear interpolations of month of year mean values of environmental data from *in-situ* probes. Surface values for temperature and $[CO_2]$ were taken from Toolik EDC and the Imnavait Fen EC tower, respectively. Dashed horizontal lines show mean depths of access wells. Grey spline shows modeled thaw depth, while gray dots show temperature = 0±1°C.

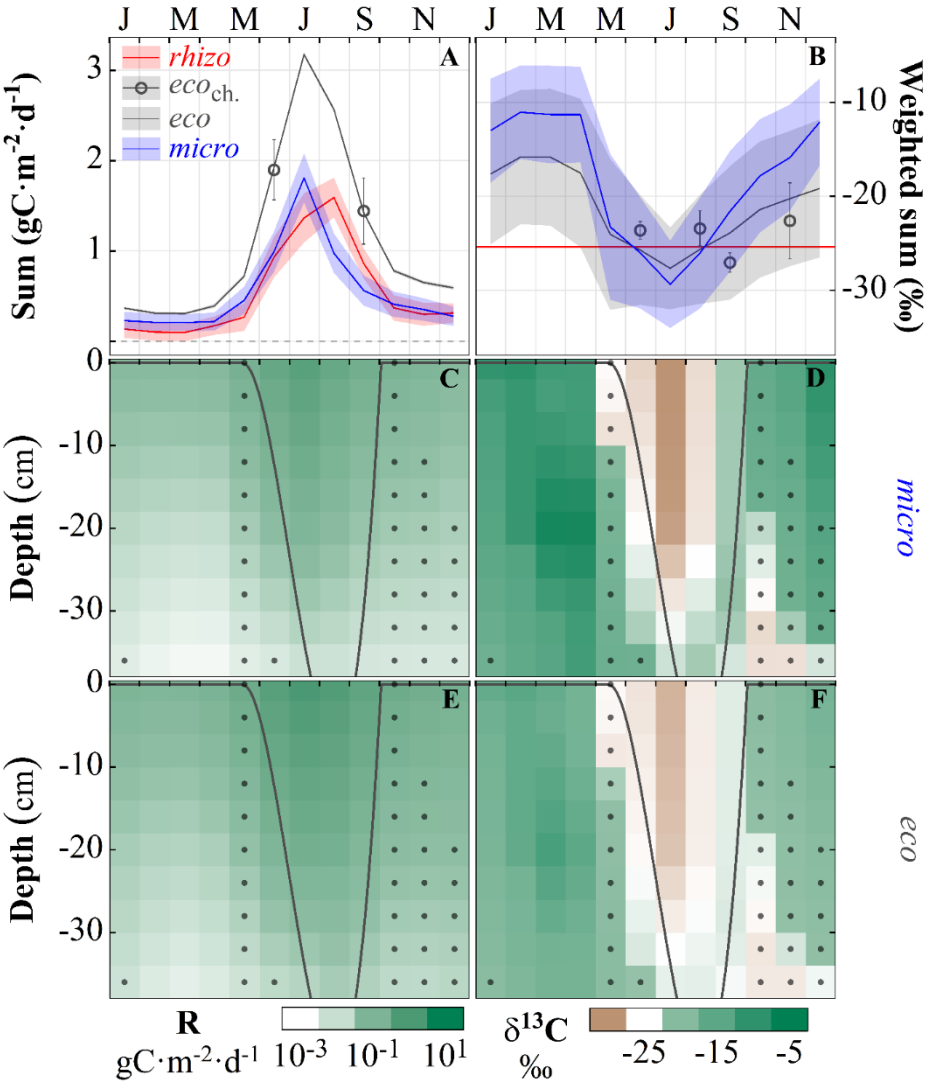

Fig. 3.15 (Top row) Flux (A) and $\delta^{13}C$ (B) of total surface CO_2 emissions (R_{eco}) and contributions from the rhizosphere (R_{rhizo}) and decomposition of organic matter by heterotrophic microorganisms (R_{micro}). (Middle row) Depth-resolved flux (C) and $\delta^{13}C$ (D) of microbial emissions (R_{micro}). (Bottom row) Depth-resolved flux (E) and $\delta^{13}C$ (F) of soil CO_2. (C) and (F) are model products, while (D) and (E) are derived by partitioning the fluxes in (A). Finally (B), root incubation CO_2 (red) is used with component groups (C+D or E+F) to produce weighted surface fluxes. Circles show month of year chamber mean, and all error indicators (bands and bars) show 95% CI. Gray spline shows modeled probe thaw depth, while gray dots show temperature=0±1ºC.

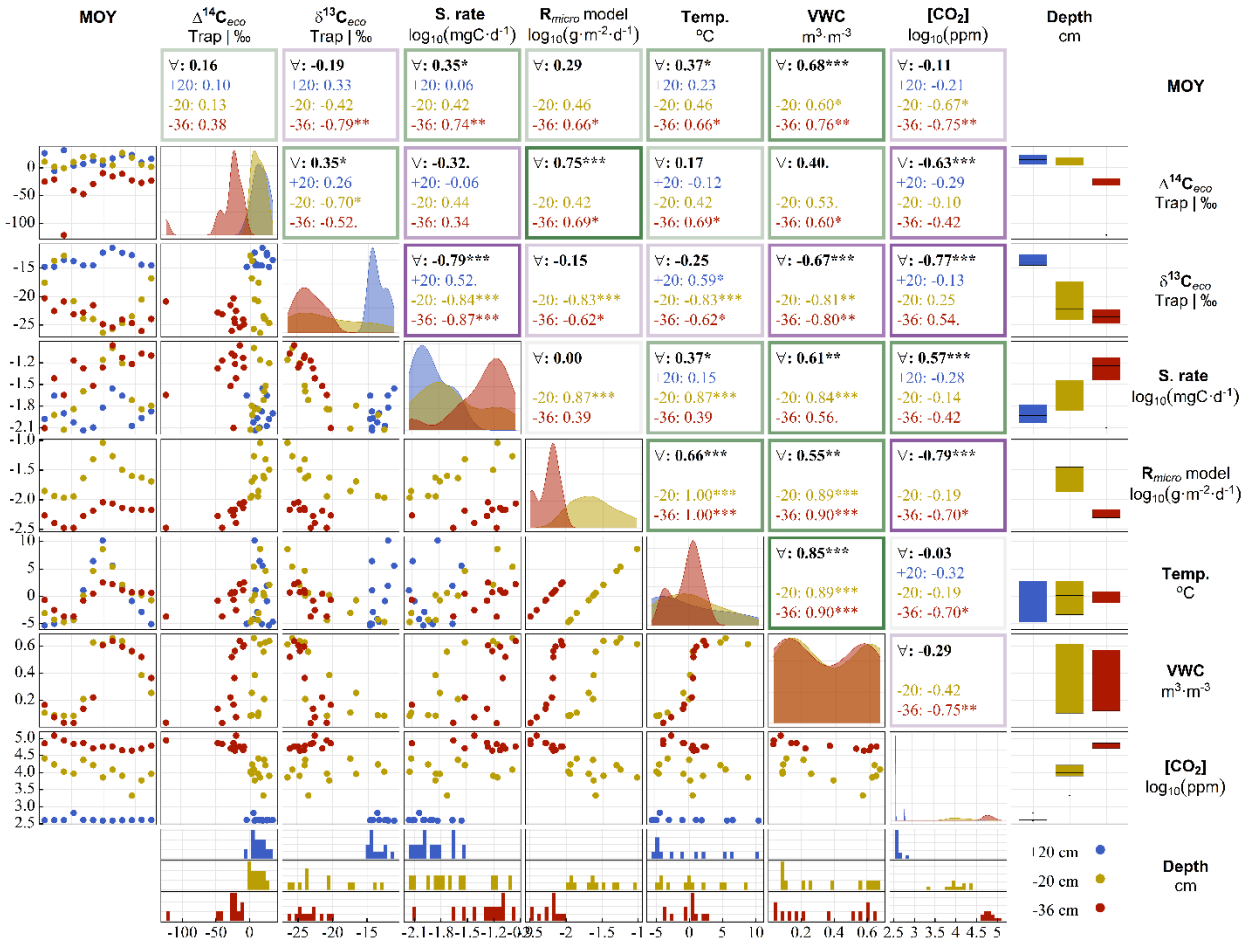

Fig. 3.16 Correlation matrix of month of year mean MS trap R_{eco} data, modeled R_{micro}, and sensory data. Diagonals show distribution, bottom panels show counts, above-diagonal panels list Pearson correlation coefficients (∀ is for all) with significance codes: [0 '***' 0.001 '**' 0.01 '*' 0.05 '.' 0.1 ' ' 1] and border colors are proportional to the ∀ correlation (purples indicating negative and greens positive).

Chapter 4: Increasing winter snow accelerates loss of organic carbon from permafrost soils

Adapted from:

Increasing winter snow accelerates loss of organic carbon from permafrost soils

Pedron S, Jespersen R G, Czimczik C I, Xu X, Khazinder Y, Homyak P M, Welker J M, *Nature*
In prep

4.1 Introduction

In addition to warming and permafrost thaw, the future Arctic is anticipated to experience significant increases in precipitation, as a consequence of moisture transport from lower latitudes and an increasingly ice free Arctic Ocean (Bintanja, 2018; Thomas *et al.*, 2018). About half of annual precipitation typically falls as snow (Liston *et al.*, 2011), with large interannual and regional variability (Callaghan *et al.*, 2011; Mudryk *et al.*, 2020; Wang *et al.*, 2013).

Changes in precipitation and surface hydrology will further impact permafrost thaw (Loranty *et al.*, 2018), and thus large amounts of organic carbon (C) (472±27 Pg C between the surface and 1 m depth (Hugelius *et al.*, 2014)) currently frozen in permafrost. Arctic warming, a longer unfrozen season, active layer depth (ALD) increases, and changing precipitation are expected to increase the exposure of these C stocks to microbial decomposition (Schuur *et al.*, 2015; Turetsky *et al.*, 2020). However, uncertainties around the magnitude and form of Arctic climate change, cold-season processes, and substrate quality complicate the overall picture.

Snow depth is a key biophysical variable that controls the functioning of ecosystems in cold season climates, including the cycling of C (Fahnestock *et al.*, 1999; Lupascu *et al.*, 2014c;

Welker *et al.*, 2000). During winter, a deeper snowpack protects plants from wind abrasion (Rieley *et al.*, 1995; Sturm *et al.*, 2001) and insulates the soil from cold air temperatures (Lafrenière *et al.*, 2013; Schimel *et al.*, 2004). Warmer soil temperatures (and prolonged availability of liquid water films) stimulate the activity of soil microorganisms (Nobrega & Grogan, 2007) – increasing N and phosphorus mineralization (Hobbie & Chapin, 1996; Mikan *et al.*, 2006; Schimel *et al.*, 2004; Schmidt *et al.*, 1999) and plant nutrient content (Leffler & Welker, 2013; Welker *et al.*, 2005), and result in a deeper ALD (Nowinski *et al.*, 2010; Pattison & Welker, 2014). During spring, deeper snowpack takes longer to melt or sublimate, which shortens the growing season (Borner *et al.*, 2008; Lupascu *et al.*, 2014c; Morgner *et al.*, 2010; Pattison & Welker, 2014; Welker *et al.*, 2000), increases the moisture content of soils (Lupascu *et al.*, 2014c), and causes soils to become saturated with water in regions with high ground ice content (Hinkel & Hurd Jr, 2006). Ecosystem respiration is temporarily enhanced under deepened snowpack during fall, but is reduced after several years of continuous deepened snow (likely due to significant depletion of belowground C stocks) (Semenchuk *et al.*, 2016). Deepened snow has also been shown to stimulate shrub growth in the low Arctic (Vankoughnett & Grogan, 2016), potentially due to an altered nitrogen (N) cycle caused by warmer soil temperatures beneath the snowpack (Pattison & Welker, 2014). Over time, deeper snowpack often causes a shift in plant community composition – turning graminoid-dominated tundra into shrub-dominated tundra (Semenchuk *et al.*, 2013; Wahren *et al.*, 2005). This “shrubification” impacts the distribution of snow on the landscape - trapped snow under shrubs lowers surface albedo, increases soil moisture during the growing season and soil temperature in winter (Jespersen *et al.*, 2018; Sturm *et al.*, 2001).

Carbon emissions during the non-growing season have been identified as an important component of the annual C balance (Euskirchen *et al.*, 2012; Fahnestock *et al.*, 1998; Morgner *et al.*, 2010; Oechel *et al.*, 2014, 1997; Raz-Yaseef *et al.*, 2017) that are transforming Arctic ecosystems into a net C source (Commane *et al.*, 2017; Natali *et al.*, 2019). However, the soil C pools which fuel microbial respiration from fall to spring are not well understood.

Radiocarbon (^{14}C) is often used as a tool used to investigate terrestrial C cycling in reservoirs including soil organic matter, respired CO_2, and dissolved C by tracking the passage of time between initial fixation by photosynthesis and measurement during land-atmosphere emissions. Growing season soil respiration is largely driven by plant roots and microorganisms that consume root exudates and have a similar ^{14}C signature to current ambient air, whereas much of the C stored frozen in Arctic soils is ancient (depleted in ^{14}C by radioactive decay).

To reduce the uncertainty in our understanding of non-growing season soil C emissions and the permafrost C feedback to climate change, we need direct, year-round observations of soil respiration sources from changing permafrost landscapes. Several influential experiments have clarified how warming might impact Arctic soils (Čapek *et al.*, 2015; Hartley *et al.*, 2008; Oechel *et al.*, 1997). However, Arctic climate change is multifaceted (AMAP, 2017; Box *et al.*, 2019), and impacts of changing precipitation are anticipated to be similarly dramatic to those of temperature (Loranty *et al.*, 2018; Lupascu *et al.*, 2014a; Mekonnen *et al.*, 2021). Across the Pan-Arctic, increases in precipitation are expected in the 21st century (i.e. (Min *et al.*, 2008)), and models suggest precipitation increases may be particularly dramatic during the cold season (+30-50%). Much less is known about how these anticipated increases in precipitation will influence soil C and N cycling and permafrost C stability.

In 1994, a snow fence experiment was established on the North Slope of the Brooks Range with the aim of understanding how increased snowfall would impact moist acidic tussock tundra, a prominent ecosystem in the Alaskan Arctic. The snow fence accumulates a drift on its leeward side proportional to its height. As a result, several zones of influence have developed in relation to their distance from the fence, each with unique biogeophysical responses to the altered snowpack depth and duration. In this study we coupled intensive soil sampling and physical measurements with a new device for in situ passive sampling of soil CO_2 for ^{14}C analysis to understand how 25 years of deepened snow have affected permafrost thaw and C and N cycling. Increased snow resulted in an 8.4% increase (5.0±4.3 cm) in active layer depth. However, a shift toward greater age in bulk soil $\Delta^{14}CO_2$ indicated that the soil under additional snow had also undergone subsidence and compaction (11 cm). Under additional snow, we observed greater active layer C and N stocks (+125% C (341±45 g C m^{-2}) and +162% N (21±2 g N m^{-2})) that are being decomposed as indicated by higher collection rates (0.27±0.05 mg C day^{-1}) and older age (-260±15‰ $\Delta^{14}C$) of soil CO_2. Together our results demonstrate that the additional snow significantly increased C and N cycling and the loss of permafrost C and increasing winter precipitation may accelerate the permafrost C feedback to climate change.

4.2 Methods

4.2.1 Snow fence experiment

Our study uses a 2.8 × 60 m wood fence (Toolik Field Station (TFS), AK, USA, "wet" snow fence, 68.6201 N, 149.60219 W, 753 m) installed in a moist acidic tussock (dominated by *Eriophorum vaginatum* L.) tundra (O horizon pH=3.7±0.1, B horizon 4.6±0.4 mean±se (Hobbie & Gough, 2002)). The fence accumulates a tapered snowdrift on its lee side (Pattison & Welker,

2014). The snow cover period extends from September through May. Total annual precipitation is near 300 mm (~200 mm summer and ~100 mm winter).

The accumulation of snow adjacent to the fence consequentially deprives the snowpack further downfield of some mass, creating a depletion zone as well (due to the topography of the site, however, this zone receives meltwater from the snow-enriched zones). The different zones are physically and conceptually separated into three zones (*Deep*, *Intermediate*, and *Depletion*, referring to snow depth) and a *Control* plot (ambient snow) is located directly southeast of the fence.

While the snow-enriched zones exhibit increased ALD and shifts in vegetation composition (with the *Intermediate* zone undergoing shrub (*Betula nana* L., *Salix pulchra* CHAM.) expansion), the *Depletion* zone shows decreased ALD and magnitude of maximum photosynthetic capacity. In this study, we focus on a comparison of the *Intermediate* zone ("*Snow*"), which receives 20–45% more snow (0.5-2 m) than the *Control* (DeFranco *et al.*, 2020; Jones *et al.*, 1998; Pattison & Welker, 2014; Walker *et al.*, 1999).

4.2.2 Sources of ecosystem respiration

We installed 24 access wells (diffusive silicone inlet attached to steel well, Pedron *et al.* (2021)) in June 2019 for soil $^{14}CO_2$ sampling within the *Control* and *Snow* zones. Access well inlet depths were chosen to sample the organic (-20 cm) and mineral (-50 cm) active layer, and the top of the permafrost table (-80 cm) (n=4 per depth and zone). Samples were collected from June 2019 to April 2021 over periods of 5-18 weeks using exchangeable molecular sieve (MS) traps (Pedron *et al.* 2021).

To episodically measure the flux and ^{14}C content of ecosystem respiration, we also installed 12 traditional dynamic soil chambers in June 2017 (*n*=3 tussocks and swales in both zones). Chamber bases were inserted into organic soils to about 2 cm depth and vegetation was left intact. We collected soil respiration samples on MS traps in Sept. 2017 (*n*=12), March & Aug. 2018 (*n*=4), June & Aug. 2019 (*n*=18), and July 2020 (*n*=16) and also CO_2 in air for isotopic analysis (*n*=15) using established techniques (Lupascu *et al.*, 2018, 2014b). We flushed chambers with ambient air before to attaching them to bases, and subsequently corrected isotopes for air volume. We quantified ecosystem CO_2 respiration fluxes by circulating chamber headspace gas through an infrared gas analyzer (LI-840, LI-1400, LI-COR Biosciences, Lincoln, NE, USA) at a rate of 0.5 L min^{-1}, calculating the slope of time vs. CO_2 concentration using linear regression.

At UC Irvine, we thermally desorbed CO_2 from access well (Pedron *et al.*, 2021) or chamber and air (Lupascu *et al* 2018, 2014a) MS traps on a vacuum line and converted the C to graphite by sealed-tube zinc reduction (Xu *et al.*, 2007). Graphite was then analyzed for $\Delta^{14}C$ using accelerator mass spectrometry (NEC 0.5MV 1.5SDH-2 AMS) with a measurement uncertainty of <3‰ from processing standards and blanks (Beverly *et al.*, 2010). We additionally analyzed samples with total yield >= 0.3 mg C for $\delta^{13}C$, with an uncertainty of 0.1‰ (GasBench II-DeltaPlus XL, Thermo, Waltham, MA, USA).

4.2.3 Ancillary data

To gauge the magnitude of increased snowpack depth and duration (i.e. the treatment effect) upon soil temperature and volumetric water content (VWC), we installed sensors (temperature from thermocouples, VWC from Decagon EC5, METER, USA) at equivalent depths to the passive trap inlet depths (-20 & -50 cm *n*=3 each zone/sensor, -80 cm *n*=2 each zone/sensor).

Meteorological stations in each zone also provide long-term (>10 yrs) data for air temperature, relative humidity, and wind direction and speed. The TFS science support team measures monthly winter snow depth over a grid encompassing the snow fence and *Control*.

Our team measured thaw depth in the *Control* and *Snow* zones from 2015 to 2020 by pushing a steel-tipped tile probe into randomly selected inter-tussock areas to the maximum depth. We also use public historic data from the snow fence collected by the Boreal Ecology Cooperative Research Unit between 1994-2002, as well as data shared personally by M. Ricketts (2012-2016). We compare our data to measurements collected between 1995-2020 by the Circumpolar Active Layer Monitoring (CALM) network (code U12A, i.e. the Toolik 1 km grid) for the points which surround the study area (but do not fall within the footprint). We model thaw depth as a 3-degree polynomial (day of year) + zone to capture the curve and treatment effect throughout the growing season. The fit is set to zero outside of the growing season (where the polynomial touches or crosses above zero).

4.2.4 Bulk soil properties and microbial C fluxes (incubations)

We harvested *n*=16 soil cores between 2015 and 2019 to compare treatment effects on bulk soil properties and for incubations. Cores were collected with either a powered auger (2015, *n*=12) or a hole saw modified to be driven by cordless drill (2019, *n*=4), and stored frozen in either capped plastic tubes or plastic bags.

In the lab, we separated cores into horizons, which were further divided for bulk analysis or incubations. Bulk soils were oven dried at 60^{o}C and powdered with ball and rotary mills for mineral and organic segments, respectively. Elemental (C & N) and stable isotope ($\delta^{13}C$ & $\delta^{15}N$) composition was determined by EA-IRMS (Fisons NA-1500NC, DeltaPlus XL, Thermo) along

with processing blanks and standards. We report measurement uncertainties (1σ) of 0.1‰ and 0.4‰ for $\delta^{13}C$ and $\delta^{15}N$ respectively, based on long term secondary standard records. Bulk $\Delta^{14}C$ subsamples were first converted to CO_2 by combusting in the presence of cupric oxide (900°C for 3h) and analyzed via AMS as described for soil CO_2 above.

Incubations of field-moist soils were performed in the dark at -20, 7, and 22°C. Samples were placed in 0.5-2 L glass mason jars with ports in the lids and flushed with CO_2-free air after a 24-hour period (to avoid capturing the initial respiration pulse). We measured [CO_2] at regular intervals using a LI-COR 820, and terminated incubations before 30% [CO_2] was reached (17-49 days). A subset of samples was analyzed for CH_4 and, or N_2O emissions at UC Riverside using a gas chromatograph (Shimadzu 2014A, Columbia, MD, USA) with thermal conductivity or electron capture detectors, respectively.

To calculate stocks at defined depths, and to inform models or averages with data spanning the top and bottom of each core segment (rather than just a mean segment depth), we aggregated soil data into 1-cm increments spanning the organic horizon surface (0 cm) to the bottom depth of the deepest *Snow* core (-88 cm). Core segments which overlap each depth step were averaged into that depth, creating a weighted average that includes multiple unique core segments, some of which were analyzed/incubated in duplicate.

We interpret the treatment effect upon C and N stocks in the context of three phenomena: an increase in thaw depth, subsidence due to the difference in volume occupied by ice and liquid water and physical compaction from the weight of snow, and changes in productivity and decomposition. While the change in thaw depth is easily measured, both subsidence and productivity/decomposition changes will influence bulk density, and therefore stocks as well. We

use bulk soil ^{14}C to disentangle these phenomena by constraining the subsidence component, understanding that subsidence will effectively bring (old) material that was once deeper into the current-day fixed-depth inventory. This is accomplished by extracting the treatment effect from a multivariate ^{14}C model (predicted by depth and treatment) and converting this ^{14}C value to a subsided depth using the slope of the model where it is closest to the surface. In other words, we approximate a shift in depth as a shift in ^{14}C by using the rate at which ^{14}C decays with depth during recent years. This inference assumes that (a) we can ignore any "freshening" influence of increased productivity upon substrate ^{14}C values, and (b) there is minimal lateral export of dissolved organic C.

With depth values for increased thaw and physical subsidence, we can then report the physical effects of the *Snow* treatment as the *Control* stocks at a depth equal to the measured *Control* ALD + thaw increase + subsidence. The biological effect is then taken as the difference between empirically measured *Snow* zone stocks and *Control* zone stocks at the depth of calculated physical effects. We model ^{14}C with an additive multivariate adaptive regression spline (R *earth* v5.3.0) to allow natural nodes in predictor and response variables (specifically, depth), while using cross-validated backwards pruning to minimize variables and over-fitting. We allow no interaction between depth and treatment (*degree*=1) so that the model only produces one treatment effect value.

4.3 Results and Discussion

4.3.1 Sources of ecosystem respiration

Samples collected from access wells in the *Snow* zone yield $\Delta^{14}CO_2$ that is older than the *Control* at all depths, regardless of season (Fig. 4.1A). Within each zone, $\Delta^{14}CO_2$ decays with

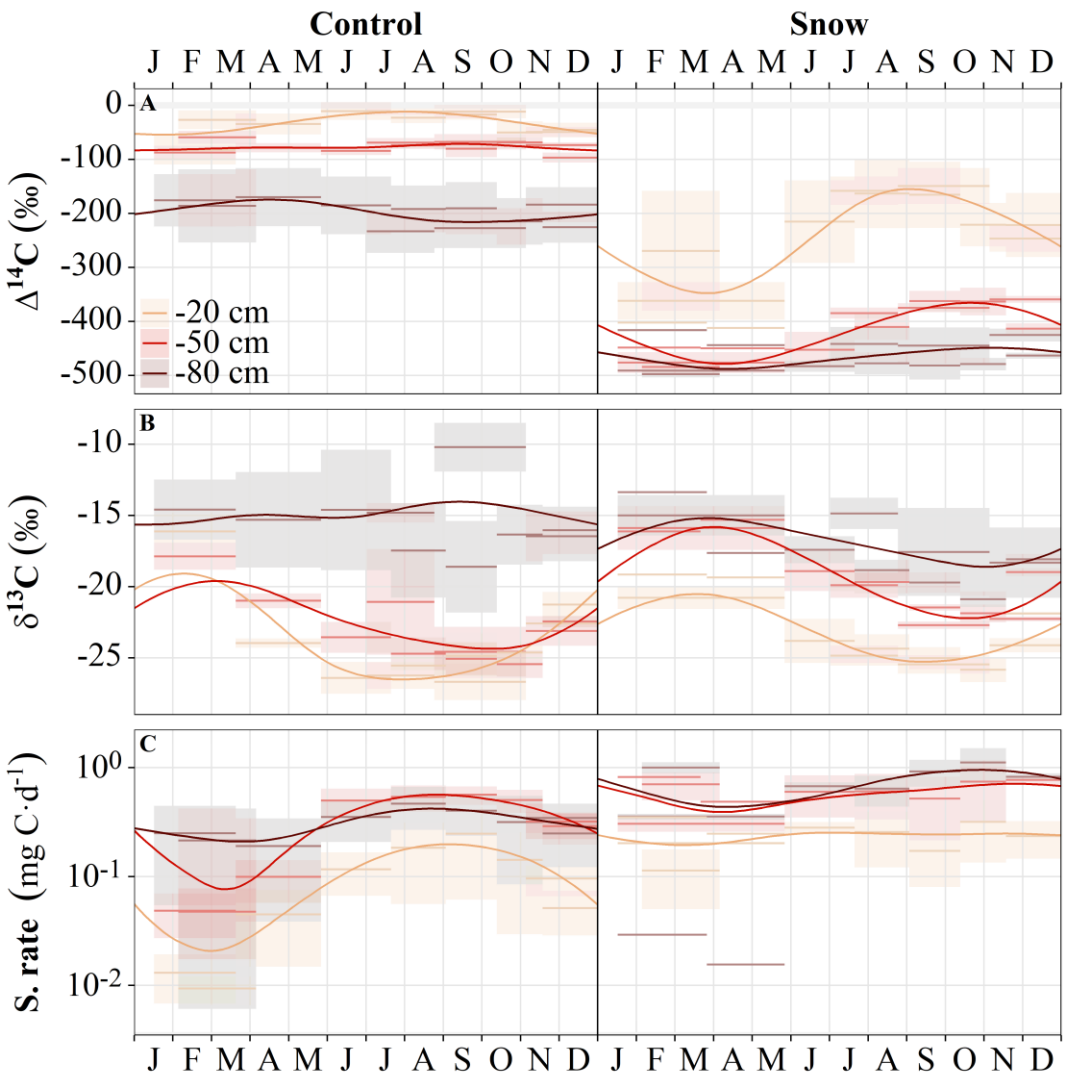

Fig. 4.1 Annual pattern of process-blank corrected (A) $\Delta^{14}C$, (B) $\delta^{13}C$ and (C) sampling rate of soil CO_2 in graminoid tundra (06/2019–04/2021). Horizontal segments (±se) span collection days for each sample. Local regressions are fit with R *loess* function using span=0.3.

depth as expected. We observe a much broader range of $\Delta^{14}CO_2$ in the *Snow* than *Control*, especially at -20 cm. This indication of a more active microbial community is supported by the consistently greater sampling rates in the *Snow* throughout the year, which are roughly an order of magnitude larger in the winter (Fig. 4.1C). The mean of captured $\delta^{13}CO_2$ is very similar between *Snow* and *Control*, with slightly more enriched values seen at -50 cm (*Control* = -22±0.6‰, *Snow* = -19±0.7‰ total mean±se). The $\delta^{13}CO_2$ enrichment with depth is also seen in

laboratory incubations, and further discussed in the following section. All data collected by the soil CO_2 samplers exhibit sinusoidal wave forms indicative of substrate (isotopes) and activity (sampling rate) seasonality. The periods of these wave forms are generally aligned as well, except for the deepest *Control* $\Delta^{14}CO_2$ and $\delta^{13}CO_2$. We posit that the seasonality describes a continuum of microbial substrate, with fresh material consumed during the growing season and older material during the other seasons when root exudate supply is diminished. $\Delta^{14}CO_2$ and $\delta^{13}CO_2$ are strongly correlated (Fig. 4.6, where significance codes indicate Pearson correlation p-values of: 0 '***' 0.001 '**' 0.01 '*' 0.05 '.' 0.1) at individual depths, within each zone (*Snow*=-0.56***, *Control*=-0.81***), and overall (-0.46***). This observed relationship allows for isotope fingerprinting and indicates that winter microbial CO_2 emissions are derived from (anaerobic) processes that fractionate $\delta^{13}C$, such as methanogenesis and methane oxidation.

4.3.2 Responses to snow addition

Increased snowpack depth and duration result in increased thaw depth (+8.4% ALD) from the start to end of season (Fig. 4.2A), beginning near the installation of the snow fence and continuing through present. This is an effect commonly observed in snow fence (winter warming) experiments (Hinkel & Hurd Jr, 2006; Lupascu *et al.*, 2018; Nobrega & Grogan, 2007), and accelerated at our site due to the presence of ground ice in the subsoil where melt and drainage promotes soil compaction and subsidence. A polynomial fit of the thaw depth data reveals an increase of 5.0±4.3 cm (-55±3.6 cm *Control*, -60±3.8 cm *Snow* for ALD polynomial fit±se (Fig. 4.2A), R^2=0.81, ~Aug. 29).

Sensory data support the observations of increased thaw depth, with greater VWC and temperature throughout the *Snow* zone column during the growing season (Fig. 4.3D&E,

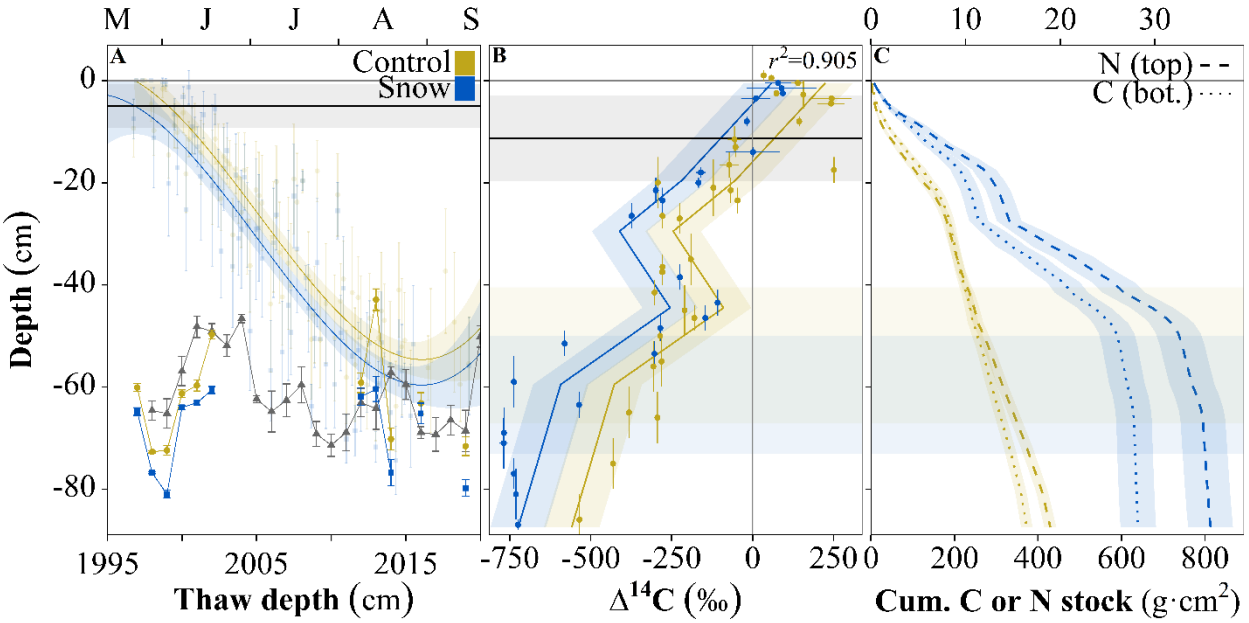

Fig. 4.2 Thaw probe measurements 1996-2020 as a function of day of year (with polynomial fit curves and horizontal line treatment effect ±se) (top) and maximum 10 August thaw depths for that year as a function of time (bottom, grey values are CALM U12A points immediately surrounding snow fence), (B) ^{14}C of bulk soil with earth model (fit lines) and the fit value converted to depth±se (horizontal line) over horizontal bands indicating range of August thaw depth, and (C) cumulative C and N stocks from 1-cm weighted averages (±se).

respectively). We also find that winter *Snow* zone temperatures are much higher than *Control*, due to thermal insulation from thicker snowpack (*Snow*=-0.86 to -2.11^{o}C, *Control*=-11.3 to -13.4^{o}C during March between -20 to -80 cm). These *Snow* temperatures fall well within the range at which microbes operate (Jansson & Taş, 2014), allowing decomposition throughout the winter. We average temperatures over each sampling period at each depth sampled and find significant Pearson correlations (Fig. S3) between ^{14}C and temperature within each zone (*Snow*=0.42***, *Control*=0.27**), and between ^{14}C and VWC within each zone (*Snow*=0.22**, *Control*=0.56***) and overall (0.18*). We also find strong correlations (of the opposite sign) between ^{13}C and temperature within each zone (*Snow*=-0.45***, *Control*=-0.30***) and overall (-0.32***), and between ^{13}C and VWC within each zone (*Snow*=-0.38***, *Control*=-0.49***) and overall (-0.43***). These correlations describe the relationship between microbial substrate

and the availability of energy and liquid water. As water availability decreases sharply in fall, microbes rapidly consume fresh material from the previous growing season and become limited to local material which may be mineral bound, the product of previous processing from an earlier season, and/or made of less nutritious material. As temperatures drop below freezing, there is less available energy for metabolism, which coincides with a strong decrease in sample collection rate in the *Control* (sampling rate:temperature correlation = 0.53***). In the *Snow* zone, where temperature range is less extreme, the relationship between temperature and sampling rate is not significant (correlation = 0.10). As all samplers are made with equivalent dimensions (despite being inserted to different depths), sampling rate should roughly equate to the magnitude

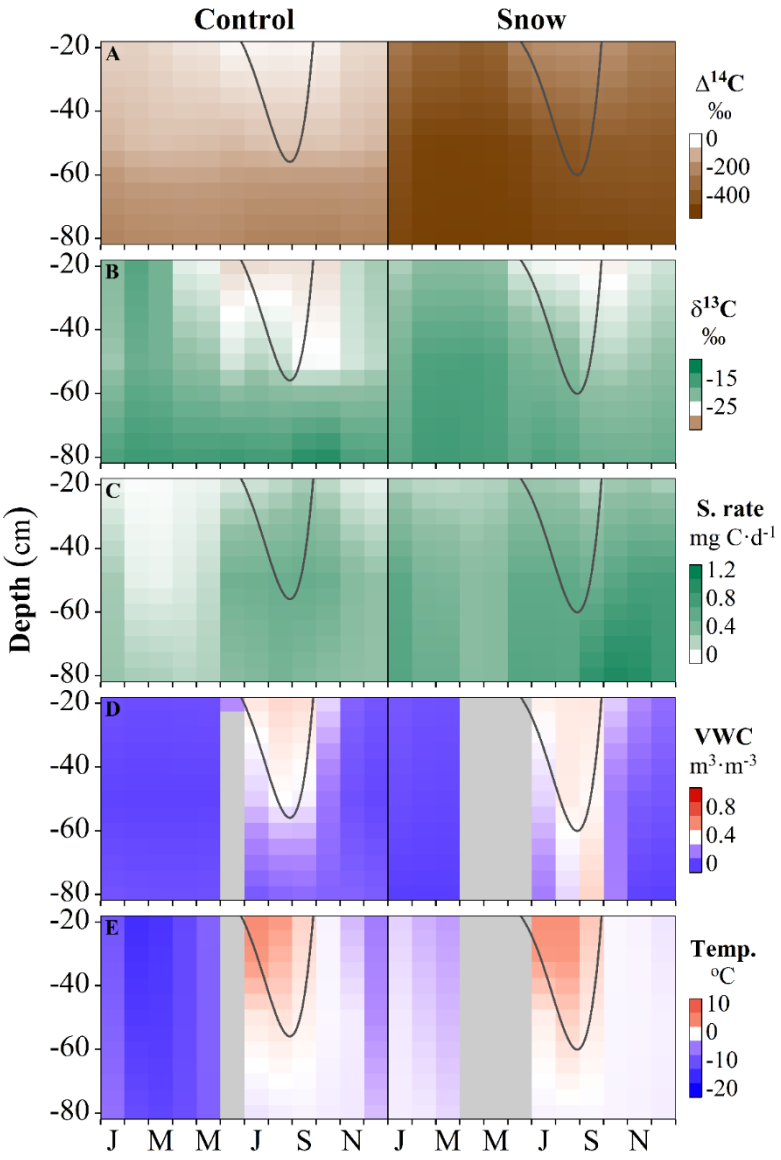

Fig. 4.3 Linear interpolations of (A-C) process-blank corrected soil CO_2 data and (D, E) ancillary *in-situ* probes. Surface values for temperature and [CO_2] were taken from Toolik EDC and the Imnavait Fen EC tower, respectively. Black spline shows modeled probe thaw depth.

of CO_2 production, implying that microbial activity in the *Snow* continues year-round, with little reduction during the cold season (Figs. 4.3C&E).

4.3.3 Bulk soils properties and microbial C fluxes (incubations)

We observe enhanced C and N stocks (Fig. 4.1C) in agreement with prior work (DeFranco *et al.*, 2020; Nowinski *et al.*, 2010). When considered in context with a greater C:N in *Snow* zone organic material (Fig. 4.4E), these results imply a greater degree of N cycling from the shift in vegetation composition and temperature, and the shift of plant- to microbial-derived soil organic matter (Cotrufo *et al.*, 2013). Moreover, we document an increase in bulk density (Fig. 4.4D) that reflects compaction of the soil column.

Ignoring physical and biological compaction, we measure increases of 342±30 mg C cm^2 and 21±2 mg N cm^2 in the seasonally thawed layer (125 and 162% increase, respectively). We further use bulk soil ^{14}C to say that, on average, the 55 cm column is 11±8 cm thinner than its original state. Combining the effects of thaw increase and subsidence introduces 16±9 cm of new material into the active layer (Table 4.1). We take the difference between empirical *Snow* stocks and combined physical effect effect stocks to conclude that enhanced biological activity has introduced 287±45 mg C cm^2 and 18±2.4 mg N cm^2 into the active layer, more than doubling the original stocks.

Microbial fluxes from soil incubations are younger on average than bulk soils at the same depth (relatively enriched $\Delta^{14}CO_2 < 0$, relatively depleted $\Delta^{14}CO_2 > 0$), in *Snow* and *Control*, indicating a preference for recently fixed material (Fig. 4.4A). The treatment effect is again evident, with *Snow* incubations producing aged respiration relative to equal depths in the *Control*. Respired $\delta^{13}CO_2$ (Fig. 4.4B) demonstrates a persistent enrichment commonly seen in

Table 4.1 Physical and biological effects of snow addition upon bulk soil C and N stocks (to maximum thaw). Physical effects are: increased thaw depth, subsidence (due to ground ice loss and compaction from additional snow mass), and combined thaw and subsidence. Biological compaction is the remaining stock increase after physical effects are removed (attributed to a shift in organic matter composition from plant to microbial origin and changes in root inputs).

		Snow	***Control***				***Effect***	
		Obs[1].	Obs[1].	+Thaw	+Sub[2].	+Thaw&Sub	Thaw&Sub	Bio.
ALD (cm)		-60	-55	-60	-66	-71		
C stock	mean	613	272	288	309	327	55	287
(g cm^2)	*se*	*43*	*13*	*13*	*13*	*14*	*19*	*45*
N stock	mean	34	13	14	15	16	3	18
(g cm^2)	*se*	*2.4*	*0.6*	*0.6*	*0.6*	*0.6*	*0.8*	*2.4*

[1]Thaw measured in August with tile probe; [2]Subsidence estimated from shift in bulk Δ^4C of topsoil between treatments

subsurface soils (Koarashi *et al.*, 2012). This enrichment may be attributable to decomposer preference of ^{12}C over ^{13}C, greater stability of ^{13}C-enriched material (Natelhoffer & Fry, 1988; Torn *et al.*, 2002), and the fact that recent assimilates will also have a

lower $^{13}C/^{12}C$ from ^{13}C-depleted fossil fuel dilution of atmospheric CO_2. Furthermore, soil fungal and microbial processes which catabolize ambient CO_2 (carboxylation/dark reactions) would enrich the decomposer in ^{13}C if it was consuming already-enriched CO_2, resulting in progressive enrichment with increasing levels of decomposition (Ehleringer *et al.*, 2000). This combination of processes should be amplified in isolation from fresh material, explaining the pore-space $\delta^{13}CO_2$ enrichment observed in the field as well. We observe no strong treatment effect from incubation $\delta^{13}CO_2$ within the active layer, and a slightly lower enrichment below the average depth of seasonal thaw.

Incubation CO_2 fluxes are greater in the *Snow* organic layer, and less below (Fig. 4.4F). These results, in agreement with the reduced $\delta^{13}CO_2$ fractionation below the active layer, seem to imply a less active microbial community at depth in *Snow*. Indeed, CH_4 and N_2O fluxes also demonstrate a negative treatment effect (Fig 4.4G&H, respectively). While it is clear that increased temperatures and water availability have had a dramatic impact upon the physical and biological processes controlling C and N cycling, more detailed investigation of the microbial community is necessary to understand the complex response to these new conditions.

4.4 Conclusions

Taking advantage of a 25-year snow addition experiment, we combine measurements of bulk soil properties and respired CO_2 to elucidate the impact of additional snow on permafrost thaw, C and N cycling in the active layer, and vulnerability of permafrost C stocks in the rapidly changing Arctic. We find that snow augmentation resulted in a deepening of the active layer, large increases in soil C and N stocks, and a transfer of permafrost C into the active layer that is being accessed by soil microorganisms. Our results suggest that soils have undergone physical compression from snow and subsidence from the loss of ground ice and biological compaction from a conversion of plant- to microbial-derived soil organic matter. Thus, increasing winter snowpack has the potential to accelerate soil C and N cycling and the loss of permafrost C beyond strictly temperature-driven estimates.

Acknowledgements

We thank the U.S. National Science Foundation for financial support (OPP #1836873 to J.M.W.). We are grateful to the staff of Toolik Field Station, E. Klein (UAA), the staff of the KCCAMS facility, B. Martinez, and L. Niu (UCI) for their support in the field or laboratory.

4.5 Supplement

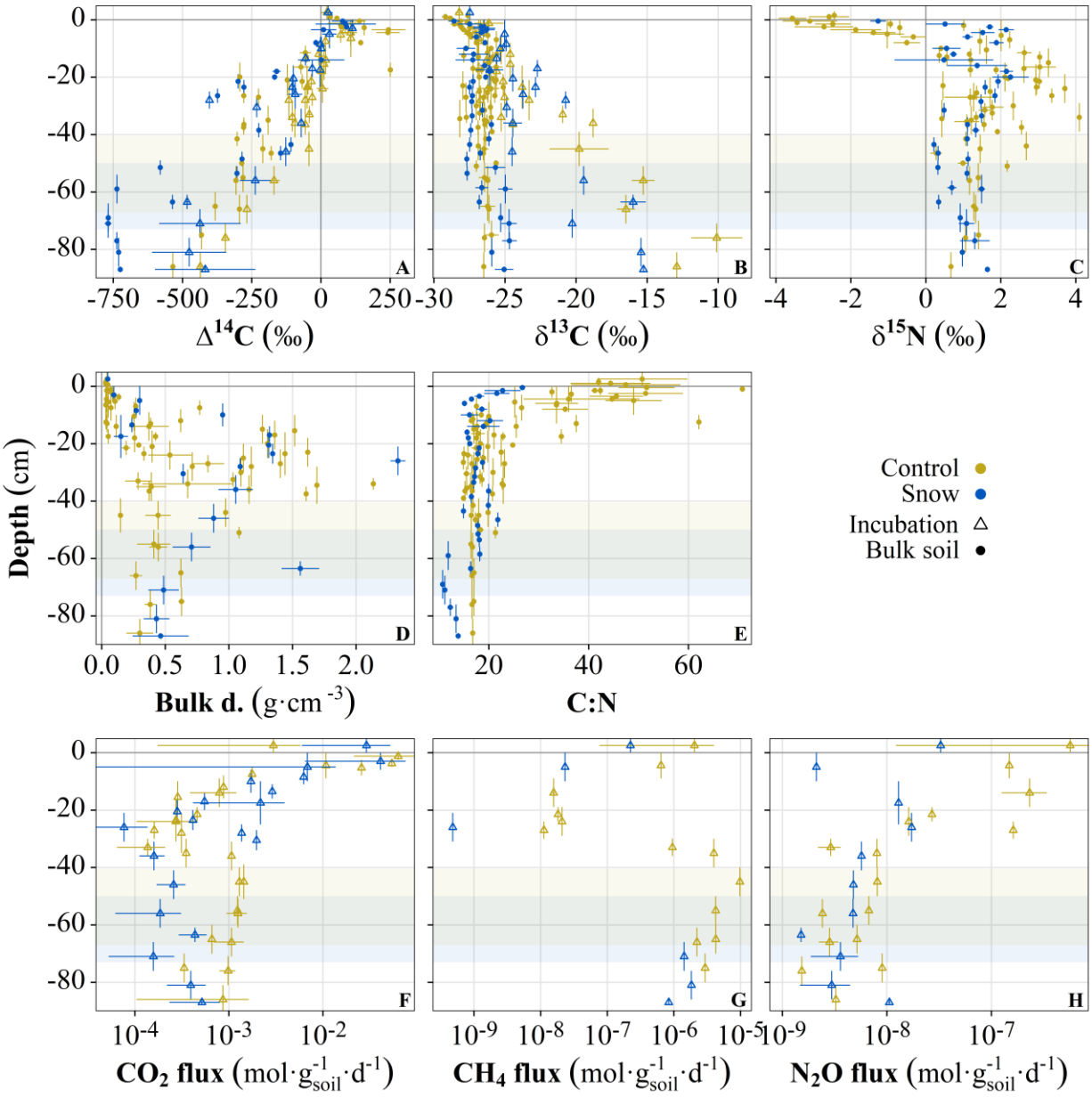

Fig. 4.4 Bulk soil and incubation averages at equivalent top and bottom segment depths, from cores collected at wet snow fence 2015-2019 (*n*=16). Vertical bars span top and bottom depth of segments, ±se (horizontal bar). Translucent horizontal rectangles indicate range of August thaw depth.

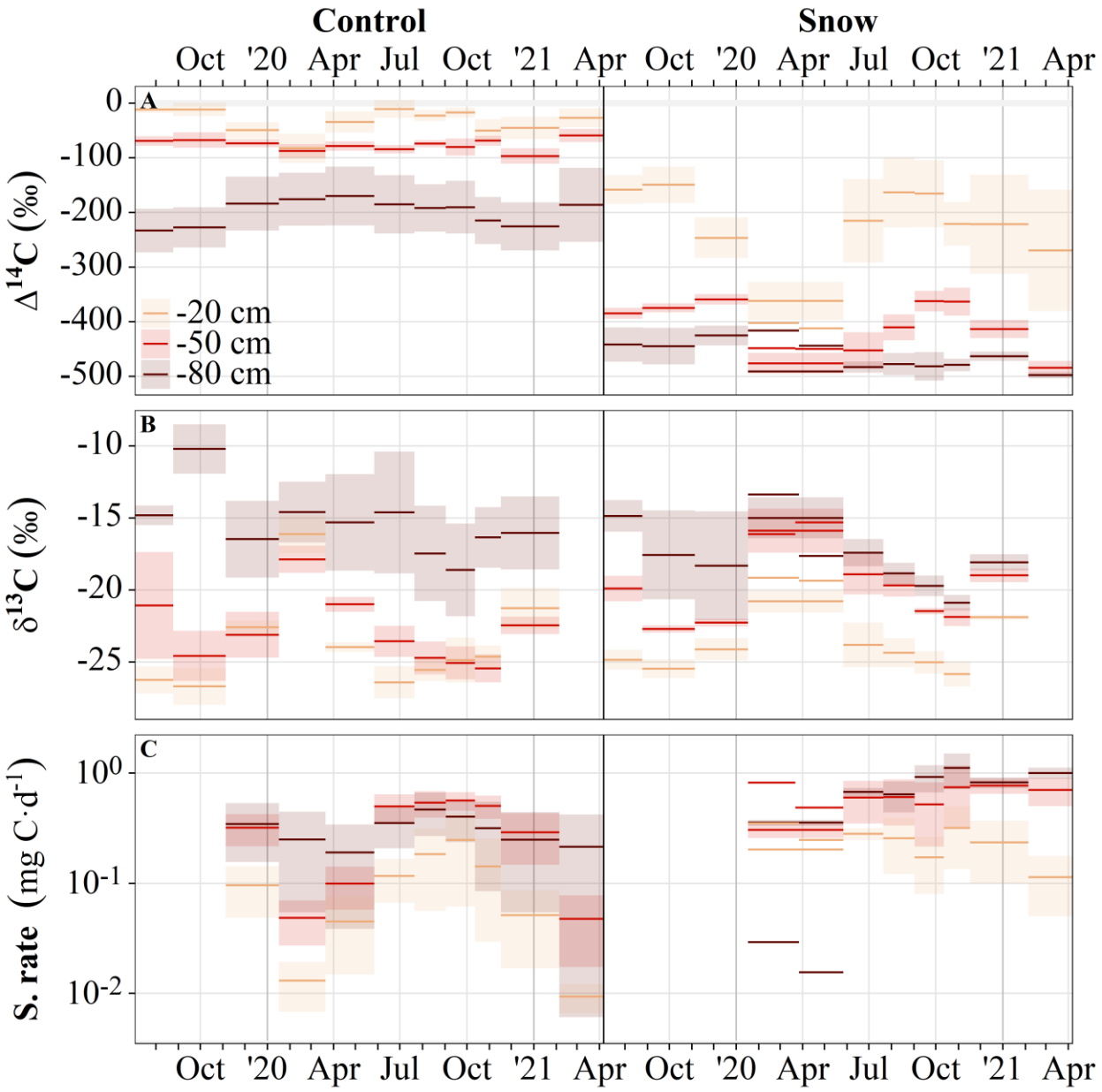

Fig. 4.5 Time series of process-blank corrected (A) $\Delta^{14}C$, (B) $\delta^{13}C$ and (C) sampling rate of soil CO_2 in graminoid tundra (06/2019–04/2021). Horizontal segments (±se) span collection dates for each sample.

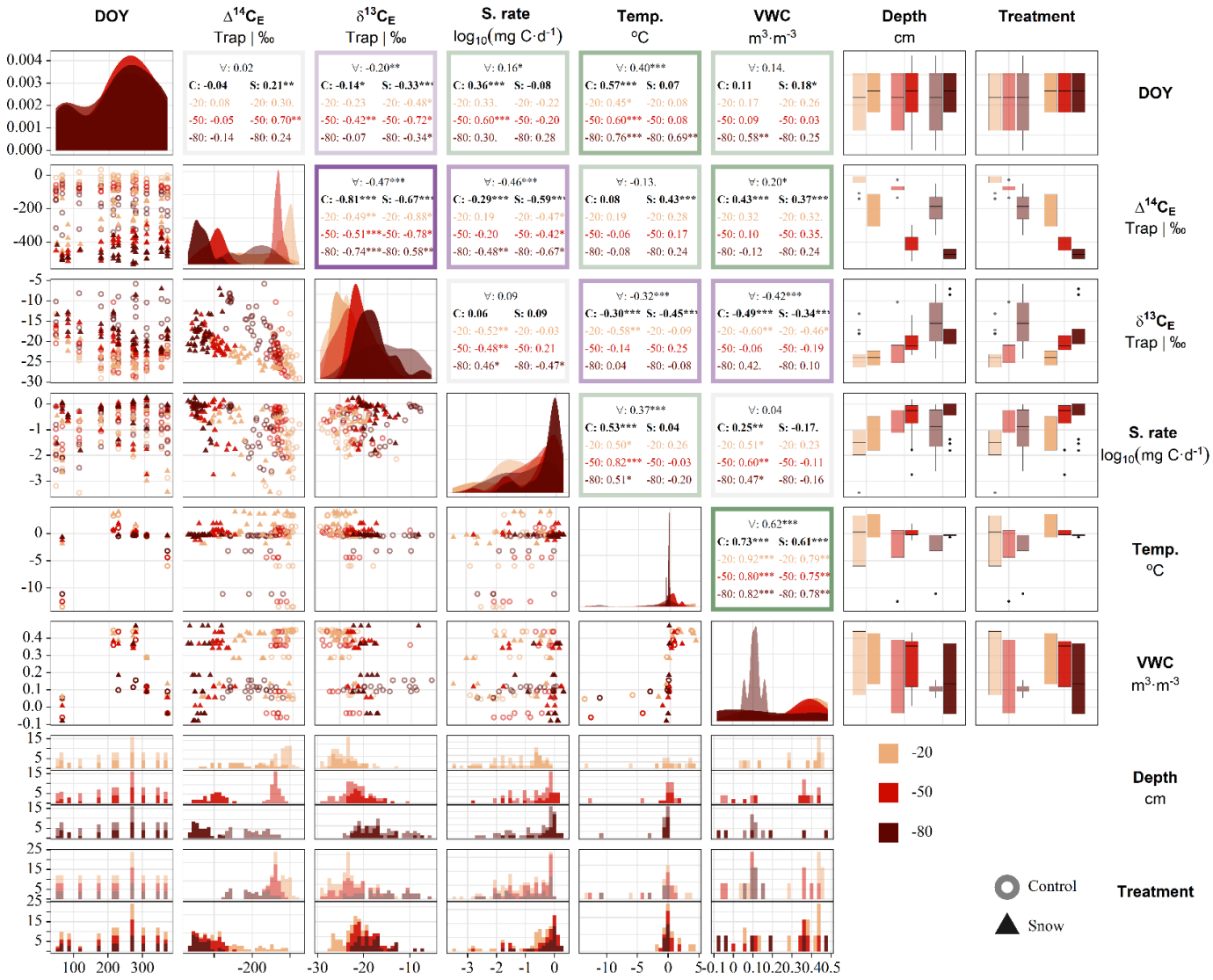

Fig. 4.6 Correlation matrix of soil CO_2 and sensory data. Diagonals show distribution, bottom panels show counts, above-diagonal panels list Pearson correlation coefficients (∀ for all, S for *Snow*, C for *Control*) with significance codes: [0 '***' 0.001 '**' 0.01 '*' 0.05 '.' 0.1] and border colors are proportional to the ∀ correlation (purples indicating negative and greens positive).

Chapter 5: Future directions and Conclusions

The aim of my dissertation was to improve our understanding of the biogeochemical cycling of carbon (C) and nitrogen (N) in permafrost soils. Therefore, a major aim of this work was to design and deploy a new sampler capable of lending insight to the seasonal dynamics of the Arctic C cycle. The following chapter summarizes the main scientific conclusions of this dissertation and provides a broader discussion of future research directions.

5.1 Summary of results

5.1.1 Design and evaluation of a passive sampler for radiocarbon analysis of soil CO_2 (Chapter 2)

In Chapter 2 I present a new design for a sampler capable of collecting soil-respired CO_2 year-round in time-integrated samples, which may be subsequently analyzed for radiocarbon (^{14}C – a proxy time since a C molecule was last in the atmosphere). To evaluate the performance, I subject the sampler to tests using certified reference materials under a range of temperature and [CO_2], varying dimensions to optimize efficiency. I then deploy the sampler in the Arctic to demonstrate its suitability for use under an extreme range of temperature and moisture conditions in organic and mineral soils. I show that the sampler accurately retains the isotopic signature of reference materials in laboratory full-process replication and collects CO_2 at a rate proportional to soil temperature in the field.

This new passive sampler was used in Chapters 3 and 4 of the dissertation and is expected to be used for future ^{14}C assessments of soil C cycling. I have constructed additional samplers that will be installed in Chile to study the implications of land use change on soil C dynamics (i.e. reforestation of formerly native Chilean forests with monocultures of non-native tree species),

disturbance (including fire) and in Finland to study the interactions between H_2O and C in a co-isotope ($\delta^{18}O$- $\Delta^{14}C$) ecohydrological catchment study.

5.1.2 Year-round observations of soil carbon sources (Chapter 3)

In Chapter 3 I assess the results of two full years of deployment of the sampler described in Chapter 2 in an Arctic graminoid tundra system. I combine these results with a laboratory incubation-derived microbial flux model to partition soil respiration into microbial and rhizosphere contributions and calculate the $\Delta^{14}CO_2$ of soil respiration within the active layer year-round at monthly resolution. This research shows that non-growing season emissions are primarily fueled by old C pools, while growing season emissions originate from a mixture of old C and C that was more recently fixed from the atmosphere by photosynthesis. This study demonstrates a shift from traditional approaches, where microbial $\Delta^{14}CO_2$ is prescribed per depth to calculate microbial flux contribution to soil respiration, to a seasonally dynamic view of microbial substrate use.

5.1.3 Impacts of Arctic wetting on climate-vulnerable permafrost C (Chapter 4)

In Chapter 4 I utilize a 25-year snow addition experiment to investigate the impacts of increased snowpack depth and duration on C and N cycling in Arctic graminoid tundra. By comparing soil C and N inventories under increased snow to those under ambient climate, and calculating the physical impacts of subsidence and thaw using bulk soil $\Delta^{14}C$ and thaw depth observations, I quantify the treatment effect upon C and N stocks from physical and biological responses. These results demonstrate that enhanced snow has a profound impact on active layer depth and the amounts of C (+125%) and N (+162%) that are seasonally thawed. I further show that significant amounts of old C are being actively respired under additional snow using soil incubations and the samplers from Chapter 2, suggesting that an increase in winter snowpack may

accelerate the cycling of C and N in permafrost soils and the loss of permafrost C beyond strictly temperature-driven estimates.

5.2 Future research directions

5.2.1 Regional-scale assessment of permafrost C emissions

While the current increase in atmospheric CO_2 and climate change are primarily driven by C emissions from fossil fuel burning (Friedlingstein *et al.*, 2020), C emissions from thawing permafrost in the Arctic may become a challenge for mitigating climate change under more aggressive fossil fuel mitigation scenarios. Permafrost thaw is projected to release up to 240 Pg C to the atmosphere by 2100 (Meredith *et al.*, 2019) and more in the coming centuries (McGuire *et al.*, 2018; Schuur *et al.*, 2015), and these changes are likely to be accelerated by abrupt thaw (Jones *et al.*, 2017; Turetsky *et al.*, 2019). Permafrost emissions may also play a larger role in land-atmosphere C cycling as CO_2-saturation of photosynthesis and increasing surface temperatures are likely to diminish the strength of the land's C sink in the future (Wang *et al.*, 2020).

With recent advances in greenhouse gas observing technology and microbial biogeochemistry and ecology, the non-growing season is now emerging as a key period for the annual C balance of Arctic ecosystems (Euskirchen *et al.*, 2012; Fahnestock *et al.*, 1998; Morgner *et al.*, 2010; Oechel *et al.*, 2014, 1997; Raz-Yaseef *et al.*, 2017) that has turned the Arctic into a net C source (Commane *et al.*, 2017; Natali *et al.*, 2019). However, large uncertainties remain in our understanding of permafrost and C dynamics in the Arctic.

In organic and acidic soils, the ^{14}C signature of bulk soil and soil-respired CO_2 provide important constraints on how rapidly soils may sequester or lose organic C in response to changes in net primary productivity or environmental conditions (He *et al.*, 2016; Shi *et al.*, 2020). In

permafrost soils, that contain C pools significantly depleted in ^{14}C, it can also be used to quantify emissions of ancient C from permafrost.

The passive sampler developed during my dissertation research lays the foundation for a more comprehensive assessment of the permafrost C feedback to climate change and complements similar advances made for Arctic lakes (Bogard *et al.*, 2019; Elder *et al.*, 2018). For the first time, it allows year-round collection of $\Delta^{14}CO_2$ from mineral soils. In future studies, the sampler could be powerful source of data if deployed in conjunction with eddy covariance towers and year-round observations of soil CO_2 concentration, temperature, and moisture. At the minimum, such studies would require sampling $\Delta^{14}CO_2$ at two depth (organic and mineral) and over periods of 1 to 2 months per sample.

Such data collected across the circumpolar permafrost region can provide important insights to permafrost C loss and benchmark datasets to further improve regional and global C cycle and climate models.

5.2.2 Permafrost thaw transitions

Roughly 20% of the exposed land area in the Northern Hemisphere (21×10^6 km^2) is underlain by permafrost (Obu *et al.*, 2019), the presence of perennially frozen ground beneath a seasonally thawed ("active") layer, that has been warming (globally 0.29 ± 0.12 °C (2007-2016); Biskaborn *et al* 2019) in response to rapid climate change (Box *et al.*, 2019; Overland *et al.*, 2019). While the surface of permafrost soils is subject to annual freeze–thaw cycles, and surface soils can remain thawed for much of the year due to the insulating effect of snow and thermal energy created by microbial activity, all C present in permafrost soils is considered "permafrost carbon" for C accounting purposes (Hugelius *et al.*, 2014; Tarnocai *et al.*, 2009). Many studies aimed at quantifying greenhouse gas emission from thawing permafrost soils to inform climate

models have been based on excess emissions from soils that have undergone active layer deepening (Elberling *et al.*, 2013; Voigt *et al.*, 2017).

However, above the perennially frozen ground ("true/isothermal permafrost"), permafrost soils do not merely consist of an active layer, but also a transient layer resulting from decadal scale fluctuations in active layer depth (permafrost table) and/or an intermediate layer, where chunks of soil are suspended in a matrix of ice (Ping *et al.*, 2015).

Three decades of thaw depth observations at Toolik Field Station (Chapter 4) reveal that the maximum summer thaw depth under moist acidic tussock tundra (i.e. 5 deepest measurements, ~late August), to which water and dissolved C, N and microbial biomass can be transported and roots can grow, is highly variable interannually (ranging from -43±5 to -73±0.5 cm within 1994-2020). Thaw depth also varies spatially within a single season: The active layer depth (max. annual thaw, DOY in 235-244) varies by 13±8% or 6.5±3.7 cm (n=11 site/date combinations) due to variability in microtopography, vegetation cover and type, and soil conditions. Furthermore, the timing and magnitude of thaw and freezing also varies significantly from year to year in response to summer insulation and precipitation, including the timing and amount of winter snow cover (Iijima *et al.*, 2010; Zhang, 2005).

My work shows that ^{14}C measurements (and for some soils stable isotope and C and N data) of the bulk soil organic matter can be used to determine the long-term position of the true permafrost table. This provides a novel opportunity to map active layer depth across the Arctic and to explore the climate-sensitivity of transition zone and isothermal permafrost C pools.

5.2.3 Arctic vegetation change

In Chapter 4 I explore the impact of changing precipitation (snow) in the Arctic on permafrost thaw and cycling of C and N. In addition to climate change, the Arctic is also undergoing a shift in the productivity and composition of vegetation.

As the Arctic continues to warm rapidly (Box *et al.*, 2019), erect (taller), deciduous shrubs have become more abundant in many graminoid tundra systems (Shevtsova *et al.*, 2020; Sturm *et al.*, 2001; Tape *et al.*, 2006). The causes of shrub expansion are complex (Martin *et al.*, 2017; Tape *et al.*, 2012) and include warming (Andreu-Hayles *et al.*, 2020), but also increases in soil nutrient (N) availability (Vankoughnett & Grogan, 2016), soil moisture (Ackerman *et al.*, 2017; Jespersen *et al.*, 2018), decreases in herbivory (Andruko *et al.*, 2020; Plante *et al.*, 2014), and disturbance events (Frost *et al.*, 2013; Racine *et al.*, 2004). While the recent "shrubification" of the Arctic tundra is known to include elements of range expansion, densification, and increases in canopy height, the ecosystem effects of these vegetation changes are less clear (Myers-Smith *et al.*, 2011). Specifically, vegetation cover and type are known to impact land energy partitioning, C storage, and permafrost distribution (Jorgenson *et al.*, 2010; Loranty *et al.*, 2018), raising the specter of climate-driven shifts in vegetation triggering important changes in these ecosystem properties.

Shrubification is generally expected to facilitate active layer deepening, permafrost thaw, and ultimately soil C emissions due to cold season processes (Sturm *et al.*, 2005). Tall shrubs trap snow and insulate soils from cool air temperatures in autumn and winter and protrude from the snow surface to lower the albedo of the land surface in spring (Jafarov *et al.*, 2018; Lawrence & Swenson, 2011; Vankoughnett & Grogan, 2016; Wilcox *et al.*, 2019). However, cold season shrub-snow interactions may change with climate warming if more frequent snowmelt events

occur in autumn, as these can decrease winter snow drifting and facilitate snow melt and surface cooling under taller vegetation (Barrere *et al.*, 2018).

It has also been proposed that shrubification may offset some of the C emissions associated with permafrost thaw. During the growing season tall shrubs are typically associated with cooler soils and a shallower, less dynamic active layer than under graminoids, which has been attributed to shading by the shrub canopy, insulation by understory vegetation (i.e. mosses) or organic soil horizons (Blok *et al.*, 2010), and reduced soil moisture as a result of high rates of shrub transpiration (Nauta *et al.*, 2015; Vankoughnett & Grogan, 2016). Shrub-induced soil drying may even lead to cooler soil temperatures year-round; however, the long-term implications of shrubification and surface hydrology on permafrost remain uncertain (Göckede *et al.*, 2017; Loranty *et al.*, 2018).

Adding to the complexity of assessing the consequences of Arctic shrubification is that the process involves several different shrubs, including alder (*Alnus* spp.), birch (*Betula* spp.), and willow (*Salix* spp.). These genera differ in C allocation strategy and chemical composition, which impacts their ability to expand and alter soil properties. For example, alders, which have N_2-fixing symbionts, have been shown to increase soil N, NO_3 production, and in some cases influence foliar N, growth, and diversity of nearby plants (Rhoades *et al.*, 2001; Wallace & Baltzer, 2020), and thus have been recognized as keystone species in the succession of nutrient-poor boreal ecosystems (Chapin *et al.*, 1994; Mitchell & Ruess, 2009) and Arctic tundra (Salmon *et al.*, 2019; Wallace & Baltzer, 2020). On the other hand birch has been shown to allocate a greater proportion of recent photosynthates to the rhizosphere (Street *et al.*, 2018), which together with large amounts of leaf litter, promotes microbial activity and N cycling year-round (Vankoughnett & Grogan, 2016) and may result in greater retention of C in soils (Lynch *et al.*,

2018). These species-specific differences in tissue composition also influence their palatability to herbivores, which in turn influences their potential expansion (Christie *et al.*, 2015; Olofsson *et al.*, 2009) as well as herbivore impacts on C cycling (Cahoon *et al.*, 2012).

Despite the ubiquity of Arctic shrubification and uncertainties surrounding its ecosystem consequences, few field studies have quantified the implications of shrubification on ecosystem and soil C sequestration. Some studies have proposed that shrubification has the potential to offset some of the C emissions associated with permafrost thaw. For instance, one modeling study predicted that a shift from graminoid and non-vascular to woody vegetation in North America under the RCP8.5 scenario would result in additional C sequestration during the 21st century, because the greater productivity of shrubs, lower decomposition rates of shrub litter, and shading of the soil surface during the growing-season compensated for warming-driven increases in heterotrophic respiration (Mekonnen *et al* 2018). In temperate climate regions, chronosequence studies found that woody encroachment into grasslands resulted in net ecosystem C gains in drier, but C losses in wetter regions (Jackson *et al.*, 2002). Analogous assessments of soil C stocks in permafrost soils are particularly complicated; cryoturbation, changes in microtopography that impact net radiation and surface hydrology, as well as buried horizons formed under previous vegetation types (legacy C) often prohibit direct comparisons of soils under graminoid and shrub tundra.

To advance our understanding of the impacts of shrubification on permafrost and C cycling, future studies could take advantage of the methodology developed in my dissertation research. For instance, I show that measurements of bulk soil organic matter ^{14}C provide another means to assess whether shrubification has promoted active layer deepening or subsidence to complement long-term observations of soil temperature and seasonal thaw.

5.2.4 Arctic H_2O-C interactions

As an intrinsic property of Arctic ecosystems (Obu *et al.*, 2019), with distribution and spatial extent influenced by climate, ecosystem properties, and surface hydrology (Jorgenson *et al.*, 2010), permafrost is a key control on Arctic biogeochemistry and hydrology. Arctic landscapes are a mosaic of tundra and wetland systems (Bogard *et al.*, 2019; Verpoorter *et al.*, 2012) that has accumulated vast quantities of C in sediments and soils (Hugelius *et al.*, 2014).

A major consequence of permafrost thaw is an increasing connectivity of the water (Walvoord & Kurylyk, 2016) and C cycles within Arctic landscapes, and aquatic systems are emerging as hotspots of permafrost soil C loss (Bowen *et al.*, 2020; Patzner *et al.*, 2020). Thus, improving our understanding of future Arctic-ecosystem permafrost distribution (Arp *et al.*, 2018) and impacts upon climate change and the global C cycle will require a landscape approach, that brings together expertise in C cycling in tundra, wetlands, streams, and lakes. In such studies, the sampler I developed during my graduate research can be combined with methodology recently developed for measuring the ^{14}C of CO_2 and CH_4 dissolved in lakes (Elder *et al.*, 2018).

5.3 Concluding Remarks

The near future holds important changes for the Arctic including increasing temperatures and precipitation, loss of permafrost areal extent, and deepening seasonal thaw in continuous permafrost regions. It is evident that there are already bidirectional impacts of these changes on Arctic biogeochemical cycles, including important climate forcers such as CO_2. As the Arctic transitions to an annual C source, global C budgets must attempt to fully constrain Arctic emissions, especially during the poorly understood winter and shoulder seasons (the short Arctic autumn and spring). This research contributes improved methods for understanding the age and

origin of seasonal permafrost soil CO_2 emissions. I have made novel contributions to soil CO_2 sampling technology, including a sampler designed to collect time-integrated samples from individual depths year-round, which can be used to partition soil respiration into contributions from rhizosphere and microbial endmembers. More work is underway to expand this technique into regions of distinct vulnerability and ecological interest, including H_2O-C linkages, to inform future understanding of the new Arctic and its role in the global C cycle.

REFERENCES

Ackerman, D., Griffin, D., Hobbie, S. E., & Finlay, J. C. (2017). Arctic shrub growth trajectories differ across soil moisture levels. *Global Change Biology*, *23*(10), 4294–4302. doi: 10.1111/gcb.13677

Affek, H. P., & Eiler, J. M. (2006). Abundance of mass 47 CO_2 in urban air, car exhaust, and human breath. *Geochimica et Cosmochimica Acta*, *70*(1), 1–12. doi: 10.1016/j.gca.2005.08.021

AMAP. (2017). Snow, Water, Ice and Permafrost in the Arctic (SWIPA) 2017. In *Arctic Monitoring and Assessment Programme (AMAP)*.

Andreu-Hayles, L., Gaglioti, B. V., Berner, L. T., Levesque, M., Anchukaitis, K. J., Goetz, S. J., & D'Arrigo, R. (2020). A narrow window of summer temperatures associated with shrub growth in Arctic Alaska. *Environmental Research Letters*, *15*(10), 105012. doi: 10.1088/1748-9326/ab897f

Andruko, R., Danby, R., & Grogan, P. (2020). *Recent Growth and Expansion of Birch Shrubs Across a Low Arctic Landscape in Continental Canada: Are These Responses More a Consequence of the Severely Declining Caribou Herd than of Climate Warming?* doi: 10.1007/s10021-019-00474-7

Aravena, R., Warner, B. G., Charman, D. J., Belyea, L. R., Mathur, S. P., & Dinel, H. (1993). Carbon isotopic composition of deep carbon gases in an ombrogenous peatland, northwestern Ontario, Canada. *Radiocarbon*, *35*(2), 271–276. doi: 10.1017/S0033822200064948

Arp, C. D., Jones, B. M., Engram, M., Alexeev, V. A., Cai, L., Parsekian, A., … Creighton, A. (2018). Contrasting lake ice responses to winter climate indicate future variability and trends on the Alaskan Arctic Coastal Plain. *Environmental Research Letters*, *13*(12), 125001. doi: 10.1088/1748-9326/aae994

Barrere, M., Domine, F., Belke-Brea, M., & Sarrazin, D. (2018). Snowmelt events in autumn can reduce or cancel the soil warming effect of snow-vegetation interactions in the arctic. *Journal of Climate*, *31*(23), 9507–9518. doi: 10.1175/JCLI-D-18-0135.1

Bertoni, G., Ciuchini, C., & Tappa, R. (2004). Measurement of long-term average carbon dioxide concentrations using passive diffusion sampling. *Atmospheric Environment*, *38*(11), 1625–1630. doi: 10.1016/j.atmosenv.2003.12.010

Beverly, R. K., Beaumont, W., Tauz, D., Ormsby, K. M., von Reden, K. F., Santos, G. M., … Southon, J. R. (2010). The Keck Carbon Cycle AMS laboratory, University of California, Irvine: Status report. *Radiocarbon*, *52*(2), 301–309. doi: 10.1017/S0033822200045343

Bieniek, P. A., Bhatt, U. S., Walker, D. A., Raynolds, M. K., Comiso, J. C., Epstein, H. E., … Ermold, W. (2015). Climate drivers linked to changing seasonality of Alaska Coastal tundra vegetation productivity. *Earth Interactions*, *19*(19), 1–29. doi: 10.1175/EI-D-15-0013.1

Bintanja, R. (2018). The impact of Arctic warming on increased rainfall. *Scientific Reports*, *8*(1), 16001. doi: 10.1038/s41598-018-34450-3

Biskaborn, B. K., Smith, S. L., Noetzli, J., Matthes, H., Vieira, G., Streletskiy, D. A., … Lantuit, H. (2019). Permafrost is warming at a global scale. *Nature Communications*, *10*(264), 1–11. doi: 10.1038/s41467-018-08240-4

Blok, D., Heijmans, M. M. P. D., Schaepman-Strub, G., Kononov, A. V., Maximov, T. C., & Berendse, F. (2010). Shrub expansion may reduce summer permafrost thaw in Siberian tundra. *Global Change Biology*, *16*(4), 1296–1305. doi: 10.1111/j.1365-2486.2009.02110.x

Bockheim, J. G. (2007). Importance of cryoturbation in redistributing organic carbon in permafrost-affected soils. *Soil Science Society of America Journal*, *71*(4), 1335–1342. doi: 10.2136/sssaj2006.0414n

Bogard, M. J., Kuhn, C. D., Johnston, S. E., Striegl, R. G., Holtgrieve, G. W., Dornblaser, M. M., … Butman, D. E. (2019). Negligible cycling of terrestrial carbon in many lakes of the arid circumpolar landscape. *Nature Geoscience*, *12*(3), 180–185. doi: 10.1038/s41561-019-0299-5

Borken, W., Savage, K., Davidson, E., & Trumbore, S. E. (2006). Effects of experimental drought on soil respiration and radiocarbon efflux from a temperate forest soil. *Global Change Biology*, *12*, 177–193. doi: 10.1111/j.1365-2486.2005.01058.x

Borner, A. P., Kielland, K., & Walker, M. D. (2008). Effects of Simulated Climate Change on Plant Phenology and Nitrogen Mineralization in Alaskan Arctic Tundra. *Arctic, Antarctic, and Alpine Research*, *40*(1), 27–38. doi: 10.1657/1523-0430(06-099)[BORNER]2.0.CO;2

Bowen, J. C., Ward, C. P., Kling, G. W., & Cory, R. M. (2020). Arctic Amplification of Global Warming Strengthened by Sunlight Oxidation of Permafrost Carbon to CO_2. *Geophysical Research Letters*, *47*(12), 1–8. doi: 10.1029/2020GL087085

Box, J. E., Colgan, W. T., Schmidt, N. M., Lund, M., Parmentier, F.-J. W., Brown, R., … Olsen, M. S. (2019). Key indicators of Arctic climate change: 1971–2017. *Environmental Research Letters*, *14*(4), 045010. doi: 10.1088/1748-9326/aafc1b

Burke, E. J., Zhang, Y., & Krinner, G. (2020). Evaluating permafrost physics in the Coupled Model Intercomparison Project 6 (CMIP6) models and their sensitivity to climate change. *Cryosphere*, *14*(9), 3155–3174. doi: 10.5194/tc-14-3155-2020

Cahoon, S. M. P., Sullivan, P. F., Post, E., & Welker, J. M. (2012). Large herbivores limit CO_2 uptake and suppress carbon cycle responses to warming in West Greenland. *Global Change Biology*, *18*(2), 469–479. doi: 10.1111/j.1365-2486.2011.02528.x

Callaghan, T. V., Johansson, M., Brown, R. D., Groisman, P. Y., Labba, N., Radionov, V., … Wood, E. F. (2011). Multiple Effects of Changes in Arctic Snow Cover. *AMBIO*, *40*(S1), 32–45. doi: 10.1007/s13280-011-0213-x

Čapek, P., Diáková, K., Dickopp, J. E., Bárta, J., Wild, B., Schnecker, J., … Šantrůčková, H. (2015). The effect of warming on the vulnerability of subducted organic carbon in arctic

soils. *Soil Biology and Biochemistry*, *90*, 19–29. doi: 10.1016/j.soilbio.2015.07.013

Chadburn, S. E., Burke, E. J., Cox, P. M., Friedlingstein, P., Hugelius, G., & Westermann, S. (2017). An observation-based constraint on permafrost loss as a function of global warming. *Nature Climate Change*, *7*(5), 340–344. doi: 10.1038/nclimate3262

Chapin, F. S. I. I., Walker, L. R., Fastie, C. L., & Sharman, L. C. (1994). Mechanisms of primary succession following deglaciation at Glacier Bay, Alaska. *Ecological Monographs*, *64*(2), 149–175. doi: 10.2307/2937039

Charman, D. J., Aravena, R., Bryant, C. L., & Harkness, D. D. (1999). Carbon isotopes in peat, DOC, CO_2, and CH_4 in a Holocene peatland on Dartmoor, southwest England. *Geology*, *27*(6), 539–542. doi: 10.1130/0091-7613(1999)027<0539:ciipdc>2.3.co;2

Christie, K. S., Bryant, J. P., Gough, L., Ravolainen, V. T., Ruess, R. W., & Tape, K. D. (2015, November 25). The Role of Vertebrate Herbivores in Regulating Shrub Expansion in the Arctic: A Synthesis. *BioScience*, Vol. 65, pp. 1123–1133. Oxford University Press. doi: 10.1093/biosci/biv137

Clymo, R. S., & Bryant, C. L. (2008). Diffusion and mass flow of dissolved carbon dioxide, methane, and dissolved organic carbon in a 7-m deep raised peat bog. *Geochimica et Cosmochimica Acta*, *72*(8), 2048–2066. doi: 10.1016/j.gca.2008.01.032

Commane, R., Lindaas, J., Benmergui, J., Luus, K. A., Chang, R. Y.-W., Daube, B. C., … Wofsy, S. C. (2017). Carbon dioxide sources from Alaska driven by increasing early winter respiration from Arctic tundra. *Proceedings of the National Academy of Sciences*, *114*(21), 5361–5366. doi: 10.1073/pnas.1618567114

Cotrufo, M. F., Wallenstein, M. D., Boot, C. M., Denef, K., & Paul, E. (2013). The Microbial Efficiency-Matrix Stabilization (MEMS) framework integrates plant litter decomposition with soil organic matter stabilization: Do labile plant inputs form stable soil organic matter? *Global Change Biology*, *19*(4), 988–995. doi: 10.1111/gcb.12113

Czimczik, C. I., Trumbore, S. E., Carbone, M. S., & Winston, G. C. (2006). Changing sources of soil respiration with time since fire in a boreal forest. *Global Change Biology*, *12*(6), 957–971. doi: 10.1111/j.1365-2486.2006.01107.x

Czimczik, C. I., & Welker, J. M. (2010). Radiocarbon content of CO_2 respired from high arctic tundra in Northwest Greenland. *Arctic, Antarctic, and Alpine Research*, *42*(3), 342–350. doi: 10.1657/1938-4246-42.3.342

Davidson, G. R. (1995). The stable isotopic composition and measurement of carbon in soil CO_2. *Geochimica et Cosmochimica Acta*, *59*(12), 2485–2489. doi: 10.1016/0016-7037(95)00143-3

DeFranco, K. C., Ricketts, M. P., Blanc-Betes, E., Welker, J. M., Gonzalez-Meler, M. A., & Sturchio, N. C. (2020). Deeper snow increases the net soil organic carbon accrual rate in moist acidic tussock tundra: 210Pb evidence from Arctic Alaska. *Arctic, Antarctic, and Alpine Research*, *52*(1), 461–475. doi: 10.1080/15230430.2020.1802864

Ehleringer, J. R., Buchmann, N., & Flanagan, L. B. (2000). Carbon isotope ratios in belowground carbon cycle processes. In *FEATURE Ecological Applications* (Vol. 412). John Wiley & Sons, Ltd. doi: 10.1890/1051-0761(2000)010[0412:CIRIBC]2.0.CO;2

Elberling, B., Michelsen, A., Schädel, C., Schuur, E. A. G., Christiansen, H. H., Berg, L., … Sigsgaard, C. (2013). Long-term CO_2 production following permafrost thaw. *Nature Climate Change*, *3*(10), 890–894. doi: 10.1038/nclimate1955

Elder, C. D., Xu, X., Walker, J. C., Schnell, J. L., Hinkel, K. M., Townsend-Small, A., … Czimczik, C. I. (2018). Greenhouse gas emissions from diverse Arctic Alaskan lakes are dominated by young carbon. *Nature Climate Change*, *8*(2), 166–171. doi: 10.1038/s41558-017-0066-9

Environmental Data Center Team. (2020). *Meteorological monitoring program at Toolik, Alaska. Toolik Field Station; Institute of Arctic Biology; University of Alaska Fairbanks; Fairbanks; AK 99775*.

Estop-Aragonés, C., Czimczik, C. I., Heffernan, L., Gibson, C., Walker, J. C., Xu, X., & Olefeldt, D. (2018). Respiration of aged soil carbon during fall in permafrost peatlands enhanced by active layer deepening following wildfire but limited following thermokarst. *Environmental Research Letters*, *13*(8), 85002. doi: 10.1088/1748-9326/aad5f0

Euskirchen, E., Bret-Harte, M., Shaver, G., Edgar, C., & Romanovsky, V. (2019). Arctic Observatory Network: Imnavait Fen Eddy Covariance. *Arctic Observatory Network.*

Euskirchen, E. S., Bret-Harte, M. S., Scott, G. J., Edgar, C., & Shaver, G. R. (2012). Seasonal patterns of carbon dioxide and water fluxes in three representative tundra ecosystems in northern Alaska. *Ecosphere*, *3*(1), 4. doi: 10.1890/ES11-00202.1

Fahnestock, J. T., Jones, M. H., Brooks, P. D., Walker, D. A., & Welker, J. M. (1998). Winter and early spring CO_2 efflux from tundra communities of northern Alaska. *Journal of Geophysical Research*, *103*(D22), 23–27. doi: 10.1029/98JD00805

Fahnestock, J. T., Jones, M. H., & Welker, J. M. (1999). Wintertime CO_2 efflux from Arctic soils: Implications for annual carbon budgets. *Global Biogeochemical Cycles*, *13*(3), 775–779. doi: 10.1029/1999GB900006

Friedlingstein, P., O'Sullivan, M., Jones, M. W., Andrew, R. M., Hauck, J., Olsen, A., … Zaehle, S. (2020). Global Carbon Budget 2020. *Earth System Science Data*, *12*(4), 3269–3340. doi: 10.5194/essd-12-3269-2020

Frost, G. V., Epstein, H. E., Walker, D. A., Matyshak, G., & Ermokhina, K. (2013). Patterned-ground facilitates shrub expansion in Low Arctic tundra. *Environmental Research Letters*, *8*(1), 15035–15044. doi: 10.1088/1748-9326/8/1/015035

Garnett, M. H., Dinsmore, K. J., & Billett, M. F. (2012). Annual variability in the radiocarbon age and source of dissolved CO_2 in a peatland stream. *Science of the Total Environment*, *427–428*(May), 277–285.

Garnett, M. H., & Hardie, S. M. L. (2009). Isotope (^{14}C and ^{13}C) analysis of deep peat CO_2 using

a passive sampling technique. *Soil Biology and Biochemistry*, *41*(12), 2477–2483. doi: 10.1016/j.soilbio.2009.09.004

Garnett, M. H., Hardie, S. M. L., & Murray, C. (2011). Radiocarbon and stable carbon analysis of dissolved methane and carbon dioxide from the profile of a raised peat bog. *Radiocarbon*, *53*(April), 71–83.

Garnett, M. H., Hartley, I. P., Hopkins, D. W., Sommerkorn, M., & Wookey, P. A. (2009). A passive sampling method for radiocarbon analysis of soil respiration using molecular sieve. *Soil Biology and Biochemistry*, *41*(7), 1450–1456. doi: 10.1016/j.soilbio.2009.03.024

Gentsch, N., Mikutta, R., Alves, R. J. E., Barta, J., Capek, P. ˇ, Gittel, A., … Guggenberger, G. (2015). Storage and transformation of organic matter fractions in cryoturbated permafrost soils across the Siberian Arctic. *Biogeosciences*, *12*, 4525–4542. doi: 10.5194/bg-12-4525-2015

Göckede, M., Kittler, F., Jung Kwon, M., Burjack, I., Heimann, M., Kolle, O., … Zimov, S. (2017). Shifted energy fluxes, increased Bowen ratios, and reduced thaw depths linked with drainage-induced changes in permafrost ecosystem structure. *Cryosphere*, *11*(6), 2975–2996. doi: 10.5194/tc-11-2975-2017

Gonfiantini, R. (1984). Stable isotope reference samples for geochemical and hydrological investigations. *The International Journal of Applied Radiation and Isotopes*, *35*(5), 426. doi: 10.1016/0020-708X(84)90059-0

Graven, H., Keeling, R. F., & Rogelj, J. (2020). Changes to carbon isotopes in atmospheric CO_2 over the Industrial Era and into the future. *Global Biogeochemical Cycles*, *34*(11), e2019GB006170. doi: 10.1029/2019GB006170

Grogan, P., & Chapin, F. S. (1999). Arctic soil respiration: Effects of climate and vegetation depend on season. *Ecosystems*, *2*(5), 451–459. doi: 10.1007/s100219900093

Hartley, I. P., Garnett, M. H., Sommerkorn, M., Hopkins, D. W., & Wookey, P. A. (2013). The age of CO_2 released from soils in contrasting ecosystems during the arctic winter. *Soil Biology and Biochemistry*, *63*, 1–4. doi: 10.1016/j.soilbio.2013.03.011

Hartley, I. P., Hopkins, D. W., Garnett, M. H., Sommerkorn, M., & Wookey, P. A. (2008). Soil microbial respiration in arctic soil does not acclimate to temperature. *Ecology Letters*, *11*(10), 1092–1100. doi: 10.1111/j.1461-0248.2008.01223.x

He, Y., Trumbore, S. E., Torn, M. S., Harden, J. W., Vaughn, L. J. S., Allison, S. D., & Randerson, J. T. (2016). Radiocarbon constraints imply reduced carbon uptake by soils during the 21st century. *Science*, *353*(6306), 1419–1424. doi: 10.1126/science.aad4273

Hicks Pries, C. E., Castanha, C., Porras, R. C., & Torn, M. S. (2017). The whole-soil carbon flux in response to warming. *Science*, *355*(6332), 1420–1423. doi: 10.1126/science.aal1319

Hicks Pries, C. E., Schuur, E. A. G., & Crummer, K. G. (2013). Thawing permafrost increases old soil and autotrophic respiration in tundra: Partitioning ecosystem respiration using $\delta^{13}C$ and $\Delta^{14}C$. *Global Change Biology*, *19*(2), 649–661. doi: 10.1111/gcb.12058

Hicks Pries, C. E., Schuur, E. A. G., Natali, S. M., & Crummer, K. G. (2016). Old soil carbon losses increase with ecosystem respiration in experimentally thawed tundra. *Nature Climate Change*, *6*(2), 214–218. doi: 10.1038/nclimate2830

Hinkel, K. M., & Hurd Jr, J. K. (2006). Permafrost destabilization and thermokarst following snow fence installation, Barrow, Alaska, USA. *Arctic, Antarctic, and Alpine Research*, *38*(4), 530–539.

Hirsch, A. I., Trumbore, S. E. ., & Goulden, M. L. (2004). The surface CO_2 gradient and pore-space storage flux in a high-porosity litter layer. *Tellus B: Chemical and Physical Meteorology*, *56*(4), 312–321. doi: 10.3402/tellusb.v56i4.16449

Hirsch, A. I., Trumbore, S. E., & Goulden, M. L. (2002). Direct measurement of the deep soil respiration accompanying seasonal thawing of a boreal forest soil. *Journal of Geophysical Research: Atmospheres*, *107*(D23), WFX 2-1-WFX 2-10. doi: 10.1029/2001JD000921

Hobbie, S. E., & Chapin, F. S. (1996). Winter regulation of tundra litter carbon and nitrogen dynamics. *Biogeochemistry*, *35*(2), 327–338. doi: 10.1007/BF02179958

Hobbie, S. E., & Gough, L. (2002). Foliar and soil nutrients in tundra on glacial landscapes of contrasting ages in northern Alaska. *Oecologia*, *131*(3), 453–462. doi: 10.1007/s00442-002-0892-x

Högberg, P. (1997). Tansley review no. 95 natural abundance in soil-plant systems. *New Phytologist*, Vol. 137, pp. 179–203. doi: 10.1046/j.1469-8137.1997.00808.x

Högberg, P., & Read, D. J. (2006). Towards a more plant physiological perspective on soil ecology. *Trends in Ecology and Evolution*, *21*(10), 548–554. doi: 10.1016/j.tree.2006.06.004

Hugelius, G., Strauss, J., Zubrzycki, S., Harden, J. W., Schuur, E. A. G., Ping, C. L., … Kuhry, P. (2014). Estimated stocks of circumpolar permafrost carbon with quantified uncertainty ranges and identified data gaps. *Biogeosciences*, *11*(23), 6573– 6593. doi: doi:10.5194/bg-11-6573-2014

Iijima, Y., Fedorov, A. N., Park, H., Suzuki, K., Yabuki, H., Maximov, T. C., & Ohata, T. (2010). Abrupt increases in soil temperatures following increased precipitation in a permafrost region, central Lena River basin, Russia. *Permafrost and Periglacial Processes*, *21*(1), 30–41. doi: 10.1002/ppp.662

Jacinthe, P. A., & Groffman, P. M. (2001). Silicone rubber sampler to measure dissolved gases in saturated soils and waters. *Soil Biology and Biochemistry*, *33*(7–8), 907–912. doi: 10.1016/S0038-0717(00)00236-4

Jackson, R. B., Banner, J. L., Jobbaágy, E. G., Pockman, W. T., & Wall, D. H. (2002). Ecosystem carbon loss with woody plant invasion of grasslands. *Nature*, *418*(6898), 623–626. doi: 10.1038/nature00910

Jafarov, E. E., Coon, E. T., Harp, D. R., Wilson, C. J., Painter, S. L., Atchley, A. L., & Romanovsky, V. E. (2018). Modeling the role of preferential snow accumulation in through

talik development and hillslope groundwater flow in a transitional permafrost landscape. *Environmental Research Letters*, *13*(10), 105006. doi: 10.1088/1748-9326/aadd30

Jansson, J. K., & Taş, N. (2014, May 12). The microbial ecology of permafrost. *Nature Reviews Microbiology*, Vol. 12, pp. 414–425. Nature Publishing Group. doi: 10.1038/nrmicro3262

Jeffries, M. O., Overland, J. E., & Perovich, D. K. (2013). The Arctic shifts to a new normal. *Physics Today*, *66*(10), 35–40. doi: 10.1063/PT.3.2147

Jespersen, R. G., Leffler, A. J., Oberbauer, S. F., & Welker, J. M. (2018). Arctic plant ecophysiology and water source utilization in response to altered snow: isotopic (δ18O and δ2H) evidence for meltwater subsidies to deciduous shrubs. *Oecologia*, *187*(4), 1009–1023. doi: 10.1007/s00442-018-4196-1

Jones, M. C., Harden, J., O'Donnell, J., Manies, K., Jorgenson, T., Treat, C., & Ewing, S. (2017). Rapid carbon loss and slow recovery following permafrost thaw in boreal peatlands. *Global Change Biology*, *23*(3), 1109–1127. doi: 10.1111/gcb.13403

Jones, M. H., Fahnestock, J. T., Walker, D. A., Walker, M. D., & Welker, J. M. (1998). Carbon dioxide fluxes in moist and dry arctic tundra during the snow-free season: Responses to increases in summer temperature and winter snow accumulation. *Arctic and Alpine Research*, *30*(4), 373–380. doi: 10.1080/00040851.1998.12002912

Jorgenson, M. T., Romanovsky, V., Harden, J., Shur, Y., O'Donnell, J., Schuur, E. A. G., … Marchenko, S. (2010). Resilience and vulnerability of permafrost to climate change. *Canadian Journal of Forest Research*, *40*(7), 1219–1236. doi: 10.1139/X10-060

Kammann, C., Grünhage, L., & Jäger, H.-J. (2001). A new sampling technique to monitor concentrations of CH_4 , N_2O and CO_2 in air at well-defined depths in soils with varied water potential. *European Journal of Soil Science*, *52*(2), 297–303. doi: 10.1046/j.1365-2389.2001.00380.x

Kammermeyer, K. (1957). Silicone rubber as a selective barrier. *Industrial & Engineering Chemistry*, *49*(10), 1685–1686.

Koarashi, J., Hockaday, W. C., Masiello, C. A., & Trumbore, S. E. (2012). Dynamics of decadally cycling carbon in subsurface soils. *Journal of Geophysical Research: Biogeosciences*, *117*(3). doi: 10.1029/2012JG002034

Koven, C. D., Riley, W. J., & Stern, A. (2013). Analysis of permafrost thermal dynamics and response to climate change in the CMIP5 earth system models. *Journal of Climate*, *26*(6), 1877–1900. doi: 10.1175/JCLI-D-12-00228.1

Lafrenière, M. J., Laurin, E., & Lamoureux, S. F. (2013). The Impact of Snow Accumulation on the Active Layer Thermal Regime in High Arctic Soils. *Vadose Zone Journal*, *12*(1), 0. doi: 10.2136/vzj2012.0058

Lawrence, D. M., & Swenson, S. C. (2011). Permafrost response to increasing Arctic shrub abundance depends on the relative influence of shrubs on local soil cooling versus large-scale climate warming. *Environmental Research Letters*, *6*(4), 045504. doi: 10.1088/1748-

9326/6/4/045504

Lee, H., Schuur, E. A. G., & Vogel, J. G. (2010). Soil CO_2 production in upland tundra where permafrost is thawing. *Journal of Geophysical Research*, *115*(G1). doi: 10.1029/2008jg000906

Leffler, A. J., & Welker, J. M. (2013). Long-term increases in snow pack elevate leaf N and photosynthesis in *Salix arctica* : responses to a snow fence experiment in the High Arctic of NW Greenland. *Environmental Research Letters*, *8*(2), 025023. doi: 10.1088/1748-9326/8/2/025023

Levin, I., Naegler, T., Kromer, B., Diehl, M., Francey, R. J., Gomez-Pelaez, A. J., … Worthy, D. E. (2010). Observations and modelling of the global distribution and long-term trend of atmospheric $^{14}CO_2$. *Tellus B*, *62*(1), 26–46. doi: 10.1111/j.1600-0889.2009.00446.x

Liston, G. E., Hiemstra, C. A., Liston, G. E., & Hiemstra, C. A. (2011). The Changing Cryosphere: Pan-Arctic Snow Trends (1979–2009). *Journal of Climate*, *24*(21), 5691–5712. doi: 10.1175/JCLI-D-11-00081.1

Loranty, M. M., Abbott, B. W., Blok, D., Douglas, T. A., Epstein, H. E., Forbes, B. C., … Walker, D. A. (2018, August 31). Reviews and syntheses: Changing ecosystem influences on soil thermal regimes in northern high-latitude permafrost regions. *Biogeosciences*, Vol. 15, pp. 5287–5313. Copernicus GmbH. doi: 10.5194/bg-15-5287-2018

Lupascu, M., Czimczik, C. I., Welker, M. C., Ziolkowski, L. A., Cooper, E. J., & Welker, J. M. (2018). Winter ecosystem respiration and sources of CO_2 from the High Arctic tundra of Svalbard: Response to a deeper snow experiment. *Journal of Geophysical Research: Biogeosciences*, *123*(8), 2627–2642. doi: 10.1029/2018JG004396

Lupascu, M., Welker, J. M., Seibt, U., Maseyk, K., Xu, X., & Czimczik, C. I. (2014a). High Arctic wetting reduces permafrost carbon feedbacks to climate warming. *Nature Climate Change*, *4*(1), 51–55. doi: 10.1038/nclimate2058

Lupascu, M., Welker, J. M., Seibt, U., Xu, X., Velicogna, I., Lindsey, D. S., & Czimczik, C. I. (2014b). The amount and timing of precipitation control the magnitude, seasonality and sources (^{14}C) of ecosystem respiration in a polar semi-desert, northwestern Greenland. *Biogeosciences*, *11*(16), 4289–4304. doi: 10.5194/bg-11-4289-2014

Lupascu, M., Welker, J. M., Xu, X., & Czimczik, C. I. (2014c). Rates and radiocarbon content of summer ecosystem respiration in response to long-term deeper snow in the High Arctic of NW Greenland. *Journal of Geophysical Research: Biogeosciences*, *119*(6), 1180–1194. doi: 10.1002/2013JG002494

Lynch, L. M., Machmuller, M. B., Cotrufo, M. F., Paul, E. A., & Wallenstein, M. D. (2018). Tracking the fate of fresh carbon in the Arctic tundra: Will shrub expansion alter responses of soil organic matter to warming? *Soil Biology and Biochemistry*, *120*, 134–144. doi: 10.1016/j.soilbio.2018.02.002

Mann, W. B. (1983). An international reference material for radiocarbon daring. *Radiocarbon*, *25*(2), 519–527.

Mariotti, A., Germon, J. C., Hubert, P., Kaiser, P., Letolle, R., Tardieux, A., & Tardieux, P. (1981). Experimental determination of nitrogen kinetic isotope fractionation: Some principles; illustration for the denitrification and nitrification processes. *Plant and Soil*, (62), 413–430.

Martin, A. C., Jeffers, E. S., Petrokofsky, G., Myers-smith, I. H., & Macias-Fauria, M. (2017). Shrub growth and expansion in the Arctic tundra : an assessment of controlling factors using an evidence-based approach. *Environmental Research Letters*, *12*, 085007.

McGuire, A. D., Lawrence, D. M., Koven, C., Clein, J. S., Burke, E., Chen, G., … Zhuang, Q. (2018). Dependence of the evolution of carbon dynamics in the northern permafrost region on the trajectory of climate change. *Proceedings of the National Academy of Sciences of the United States of America*, *115*(15), 3882–3887. doi: 10.1073/pnas.1719903115

Mekonnen, Z. A., Riley, W. J., & Grant, R. F. (2018). Accelerated Nutrient Cycling and Increased Light Competition Will Lead to 21st Century Shrub Expansion in North American Arctic Tundra. *Journal of Geophysical Research: Biogeosciences*, *123*(5), 1683–1701. doi: 10.1029/2017JG004319

Mekonnen, Z. A., Riley, W. J., Grant, R. F., & Romanovsky, V. E. (2021). Changes in precipitation and air temperature contribute comparably to permafrost degradation in a warmer climate. *Environmental Research Letters*, *16*(2), 24008. doi: 10.1088/1748-9326/abc444

Meredith, M., Sommerkorn, M., Cassotta, S., Derksen, C., Ekaykin, A., Hollowed, A., … Schurr, E. A. G. (2019). Chapter 3: Polar regions. *IPCC Special Report on the Ocean and Cryosphere in a Changing Climate*.

Mikan, C., Schimel, J. P., Michaelson, G., Welker, J., Romanovsky, V. E., Fahnestock, J., & Ping, C.-L. (2006). Cold-season production of CO_2 in Arctic soils: Can laboratory and field estimates be reconciled through a simple modeling approach? *Arctic, Antarctic, and Alpine Research*, *38*(2), 249–256. doi: 10.1657/1523-0430(2006)38[249:cpocia]2.0.co;2

Min, S.-K., Zhang, X., & Zwiers, F. (2008). Human-induced Arctic moistening. *Science*, *320*(5875), 518–520. doi: 10.1126/science.1153468

Mitchell, J. S., & Ruess, R. W. (2009). N2 fixing alder (Alnus viridis spp. fruticosa) effects on soil properties across a secondary successional chronosequence in interior Alaska. *Biogeochemistry*, *95*(2), 215–229. doi: 10.1007/s10533-009-9332-x

Mook, W. G., Bommerson, J. C., & Staverman, W. H. (1974). Carbon isotope fractionation between dissolved bicarbonate and gaseous carbon dioxide. *Earth and Planetary Science Letters*, *22*(2), 169–176. doi: 10.1016/0012-821X(74)90078-8

Morgner, E., Elberling, B., Strebel, D., & Cooper, E. J. (2010). The importance of winter in annual ecosystem respiration in the High Arctic: effects of snow depth in two vegetation types. *Polar Research*, *29*(1), 58–74.

Mudryk, L., Chereque, A. E., Brown, R., Derksen, C., Luojus, K., & Decharme, B. (2020). *NOAA Arctic Report Card 2020*. doi: 10.25923/p6ca-v923

Mueller, C. W., Rethemeyer, J., Kao-Kniffin, J., Löppmann, S., Hinkel, K. M., & G. Bockheim, J. (2015). Large amounts of labile organic carbon in permafrost soils of northern Alaska. *Global Change Biology*, *21*(7), 2804–2817. doi: 10.1111/gcb.12876

Muhr, J., Franke, J., & Borken, W. (2010). Drying-rewetting events reduce C and N losses from a Norway spruce forest floor. *Soil Biology and Biochemistry*, *42*(8), 1303–1312. doi: 10.1016/j.soilbio.2010.03.024

Myers-Smith, I. H., Forbes, B. C., Wilmking, M., Hallinger, M., Lantz, T., Blok, D., … Hik, D. S. (2011). Shrub expansion in tundra ecosystems: dynamics, impacts and research priorities. *Environmental Research Letters*, *6*(4), 045509. doi: 10.1088/1748-9326/6/4/045509

Natali, S. M., Schuur, E. A. G., Trucco, C., Hicks Pries, C. E., Crummer, K. G., & Baron Lopez, A. F. (2011). Effects of experimental warming of air, soil and permafrost on carbon balance in Alaskan tundra. *Global Change Biology*, *17*(3), 1394–1407. doi: 10.1111/j.1365-2486.2010.02303.x

Natali, S. M., Watts, J. D., Rogers, B. M., Potter, S., Ludwig, S. M., Selbmann, A. K., … Zona, D. (2019). Large loss of CO_2 in winter observed across the northern permafrost region. *Nature Climate Change*, *9*(11), 852–857. doi: 10.1038/s41558-019-0592-8

Natelhoffer, K. J., & Fry, B. (1988). Controls on Natural Nitrogen-15 and Carbon-13 Abundances in Forest Soil Organic Matter. *Soil Science Society of America Journal*, *52*(6), 1633–1640. doi: 10.2136/sssaj1988.03615995005200060024x

Nations, U. (2015). *UNFCCC, Adoption of the Paris agreement. COP*. Paris.

Nauta, A. L., Heijmans, M. M. P. D., Blok, D., Limpens, J., Elberling, B., Gallagher, A., … Berendse, F. (2015). Permafrost collapse after shrub removal shifts tundra ecosystem to a methane source. *Nature Climate Change*, *5*(1), 67–70. doi: 10.1038/nclimate2446

Nobrega, S., & Grogan, P. (2007). Deeper Snow Enhances Winter Respiration from Both Plant-associated and Bulk Soil Carbon Pools in Birch Hummock Tundra. *Ecosystems*, *10*(3), 419–431. doi: 10.1007/s10021-007-9033-z

Nowinski, N. S., Taneva, L., Trumbore, S. E., & Welker, J. M. (2010). Decomposition of old organic matter as a result of deeper active layers in a snow depth manipulation experiment. *Oecologia*, *163*(3), 785–792. doi: 10.1007/s00442-009-1556-x

Obu, J., Westermann, S., Bartsch, A., Berdnikov, N., Christiansen, H. H., Dashtseren, A., … Zou, D. (2019). Northern Hemisphere permafrost map based on TTOP modelling for 2000–2016 at 1 km^2 scale. *Earth-Science Reviews*, *193*(April), 299–316. doi: 10.1016/j.earscirev.2019.04.023

Oechel, W. C., Laskowski, C. A., Burba, G., Gioli, B., & Kalhori, A. A. M. (2014). Annual patterns and budget of CO_2 flux in an Arctic tussock tundra ecosystem. *Journal of Geophysical Research: Biogeosciences*, *119*(3), 323–339. doi: 10.1002/2013JG002431

Oechel, W. C., Vourlitis, G., & Hastings, S. J. (1997). Cold season CO_2 emission from arctic soils. *Global Biogeochemical Cycles*, *11*(2), 163–172.

Olofsson, J., Oksanen, L., Callaghan, T., Hulme, P. E., Oksanen, T., & Suominen, O. (2009). Herbivores inhibit climate-driven shrub expansion on the tundra. *Global Change Biology*, *15*(11), 2681–2693. doi: 10.1111/j.1365-2486.2009.01935.x

Osterkamp, T. E. (2003). Establishing long-term permafrost observatories for active-layer and permafrost investigations in Alaska: 1977-2002. *Permafrost and Periglacial Processes*, *14*(4), 331–342. doi: 10.1002/ppp.464

Overland, J., Dunlea, E., Box, J. E., Corell, R., Forsius, M., Kattsov, V., … Wang, M. (2019). The urgency of Arctic change. *Polar Science*, *21*(November 2018), 6–13. doi: 10.1016/j.polar.2018.11.008

Pattison, R. R., & Welker, J. M. (2014). Differential ecophysiological response of deciduous shrubs and a graminoid to long-term experimental snow reductions and additions in moist acidic tundra, Northern Alaska. *Oecologia*, *174*(2), 339–350. doi: 10.1007/s00442-013-2777-6

Patzner, M. S., Mueller, C. W., Malusova, M., Baur, M., Nikeleit, V., Scholten, T., … Bryce, C. (2020). Iron mineral dissolution releases iron and associated organic carbon during permafrost thaw. *Nature Communications*, *11*(1), 1–11. doi: 10.1038/s41467-020-20102-6

Pedron, S., Xu, X., Walker, J. C., Ferguson, J. C., Jespersen, R. G., Welker, J. M., … Czimczik, C. I. (2021). Time-integrated collection of CO_2 for ^{14}C analysis from soils. *Radiocarbon*, *In press*.

Ping, C. L., Bockheim, J. G., Kimble, J. M., Michaelson, G. J., & Walker, D. A. (1998). Characteristics of cryogenic soils along a latitudinal transect in Arctic Alaska. *Journal of Geophysical Research Atmospheres*, *103*(D22), 28917–28928. doi: 10.1029/98JD02024

Ping, C. L., Jastrow, J. D., Jorgenson, M. T., Michaelson, G. J., & Shur, Y. L. (2015). *Permafrost soils and carbon cycling*. *1*, 147–171. doi: 10.5194/soil-1-147-2015

Plante, S., Champagne, E., Ropars, P., Boudreau, S., Lévesque, E., Tremblay, B., & Tremblay, J. P. (2014). Shrub cover in northern Nunavik: Can herbivores limit shrub expansion? *Polar Biology*, *37*(5), 611–619. doi: 10.1007/s00300-014-1461-6

Plaza, C., Pegoraro, E., Bracho, R., Celis, G., Crummer, K. G., Hutchings, J. A., … Schuur, E. A. G. (2019). Direct observation of permafrost degradation and rapid soil carbon loss in tundra. *Nature Geoscience*, *12*(8), 627–631. doi: 10.1038/s41561-019-0387-6

Pörtner, H.-O., Roberts, D. C., Masson-Delmotte, V., Zhai, P., Tignor, M., Poloczanska, E., … Weyer, N. M. (2019). IPCC, 2019: Summary for Policymakers. *IPCC Special Report on the Ocean and Cryosphere in a Changing Climate*.

Post, E., Alley, R. B., Christensen, T. R., Macias-Fauria, M., Forbes, B. C., Gooseff, M. N., … Wang, M. (2019). The polar regions in a 2°C warmer world. *Science Advances*, *5*(12), eaaw9883. doi: 10.1126/sciadv.aaw9883

Pulliainen, J., Luojus, K., Derksen, C., Mudryk, L., Lemmetyinen, J., Salminen, M., … Norberg, J. (2020). Patterns and trends of Northern Hemisphere snow mass from 1980 to 2018.

Nature, *581*(7808), 294–298. doi: 10.1038/s41586-020-2258-0

Racine, C., Jandt, R., Meyers, C., Dennis, J., Peninsula, S., & Charles Racine, U. (2004). Tundra Fire and Vegetation Change along a Hillslope on the Seward Peninsula. *Arctic, Antarctic, and Alpine Research*, *36*(1), 1–10. doi: 10.1657/1523-0430(2004)036[0001:TFAVCA]2.0.CO;2

Raz-Yaseef, N., Torn, M. S., Wu, Y., Billesbach, D. P., Liljedahl, A. K., Kneafsey, T. J., … Wullschleger, S. D. (2017). Large CO_2 and CH_4 emissions from polygonal tundra during spring thaw in northern Alaska Naama. *Geophysical Research Letters*, *44*, 504–513. doi: 10.1002/2016GL071220

Reimer, P. J., Bard, E., Bayliss, A., Beck, J. W., Blackwell, P. G., Ramsey, C. B., … van der Plicht, J. (2013). IntCal13 and Marine13 radiocarbon age calibration curves 0–50,000 years cal BP. *Radiocarbon*, *55*(4), 1869–1887. doi: 10.2458/azu_js_rc.55.16947

Rhoades, C., Oskarsson, H., Binkley, D., & Stottlemyer, B. (2001). Alder (alnus crispa) effects on soils in ecosystems of the agashashok river valley, northwest Alaska. *Ecoscience*, *8*(1), 89–95. doi: 10.1080/11956860.2001.11682634

Rieley, G., Welker, J. M., Callaghan, T. V., & Eglinton, G. (1995). Epicuticular waxes of two arctic species: Compositional differences in relation to winter snow cover. *Phytochemistry*, *38*(1), 45–52. doi: 10.1016/0031-9422(94)00649-E

Robb, W. L. (1968). Thin silicone membranes- Their permeation properties and some applications. *Annals of the New York Academy of Sciences*, *146*(1), 119–137. doi: 10.1111/j.1749-6632.1968.tb20277.x

Roth, V. N., Lange, M., Simon, C., Hertkorn, N., Bucher, S., Goodall, T., … Gleixner, G. (2019). Persistence of dissolved organic matter explained by molecular changes during its passage through soil. *Nature Geoscience*, *12*(9), 755–761. doi: 10.1038/s41561-019-0417-4

Salmon, V. G., Breen, A. L., Kumar, J., Lara, M. J., Thornton, P. E., Wullschleger, S. D., & Iversen, C. M. (2019). Alder distribution and expansion across a tundra hillslope: Implications for local N cycling. *Frontiers in Plant Science*, *10*, 1099. doi: 10.3389/fpls.2019.01099

Santos, G. M., Southon, J. R., Griffin, S., Beaupre, S. R., & Druffel, E. R. M. (2007). Ultra small-mass AMS ^{14}C sample preparation and analyses at KCCAMS/UCI Facility. *Nuclear Instruments and Methods in Physics Research, Section B: Beam Interactions with Materials and Atoms*, *259*(1), 293–302. doi: 10.1016/j.nimb.2007.01.172

Schädel, C., Schuur, E. A. G., Bracho, R., Elberling, B., Knoblauch, C., Lee, H., … Turetsky, M. R. (2014). Circumpolar assessment of permafrost C quality and its vulnerability over time using long-term incubation data. *Global Change Biology*, *20*(2), 641–652. doi: 10.1111/gcb.12417

Schimel, J. P., Bilbrough, C., & Welker, J. M. (2004). Increased snow depth affects microbial activity and nitrogen mineralization in two Arctic tundra communities. *Soil Biology and Biochemistry*, *36*(2), 217–227. doi: 10.1016/J.SOILBIO.2003.09.008

Schimel, J. P., & Clein, J. S. (1995). Microbial response to freeze-thaw cycles in tundra and taiga soils. *Soil Biology and Biochemistry*, *28*(8), 1061–1066. doi: 10.1016/0038-0717(96)00083-1

Schirrmeister, L., Grosse, G., Schnelle, M., Fuchs, M., Krbetschek, M., Ulrich, M., … Schwamborn, G. (2011a). Late Quaternary paleoenvironmental records from the western Lena Delta, Arctic Siberia. *Palaeogeography, Palaeoclimatology, Palaeoecology*, *299*(1–2), 175–196. doi: 10.1016/j.palaeo.2010.10.045

Schirrmeister, L., Grosse, G., Wetterich, S., Overduin, P. P., Strauss, J., Schuur, E. A. G., & Hubberten, H. W. (2011b). Fossil organic matter characteristics in permafrost deposits of the northeast Siberian Arctic. *Journal of Geophysical Research: Biogeosciences*, *116*(3), 0–02. doi: 10.1029/2011JG001647

Schmidt, I. K., Jonasson, S., & Michelsen, A. (1999). Mineralization and microbial immobilization of N and P in arctic soils in relation to season, temperature and nutrient amendment. *Applied Soil Ecology*, *11*(2–3), 147–160. doi: 10.1016/S0929-1393(98)00147-4

Schmidt, M. W. I., Torn, M. S., Abiven, S., Dittmar, T., Guggenberger, G., Janssens, I. A., … Trumbore, S. E. (2011, October 6). Persistence of soil organic matter as an ecosystem property. *Nature*, Vol. 478, pp. 49–56. Nature Publishing Group. doi: 10.1038/nature10386

Schuur, E. A. G., McGuire, A. D., Schädel, C., Grosse, G., Harden, J. W., Hayes, D. J., … Vonk, J. E. (2015). Climate change and the permafrost carbon feedback. *Nature*, *520*(7546), 171–179. doi: 10.1038/nature14338

Schuur, E. A. G., & Trumbore, S. E. (2006). Partitioning sources of soil respiration in boreal black spruce forest using radiocarbon. *Global Change Biology*, *12*(2), 165–176. doi: 10.1111/j.1365-2486.2005.01066.x

Schuur, E. A. G., Vogel, J. G., Crummer, K. G., Lee, H., Sickman, J. O., & Osterkamp, T. E. (2009). The effect of permafrost thaw on old carbon release and net carbon exchange from tundra. *Nature*, *459*(7246), 556–559. doi: 10.1038/nature08031

Scott, E. M. (2003). Part 2: The Third International Radiocarbon Intercomparison (Tiri). *Radiocarbon*, *45*(2), 293–328. doi: 10.1017/S0033822200032677

Semenchuk, P. R., Christiansen, C. T., Grogan, P., Elberling, B., & Cooper, E. J. (2016). Long-term experimentally deepened snow decreases growing-season respiration in a low- and high-arctic tundra ecosystem. *Journal of Geophysical Research: Biogeosciences*, *121*(5), 1236–1248. doi: 10.1002/2015JG003251

Semenchuk, P. R., Elberling, B., & Cooper, E. J. (2013). Snow cover and extreme winter warming events control flower abundance of some, but not all species in high arctic Svalbard. *Ecology and Evolution*, *3*(8), 2586–2599. doi: 10.1002/ece3.648

Shevtsova, I., Heim, B., Fuchs, M., Runge, A., Morgenstern, A., Grosse, G., … Lashchinskiy, N. (2020). *Mapped arctic vegetation communities and soil nutrient regimes in the Permafrost landscape of the Central Lena delta, RU*. Hamburg. doi: http://dx.doi.org/10.2312/BzPM_0739_2020

Shi, Z., Allison, S. D., He, Y., Levine, P. A., Hoyt, A. M., Beem-Miller, J., … Randerson, J. T. (2020). The age distribution of global soil carbon inferred from radiocarbon measurements. *Nature Geoscience*, *13*(8), 555–559. doi: 10.1038/s41561-020-0596-z

Sierra, C. A., Müller, M., Metzler, H., Manzoni, S., & Trumbore, S. E. (2017). The muddle of ages, turnover, transit, and residence times in the carbon cycle. *Global Change Biology*, *23*(5), 1763–1773. doi: 10.1111/gcb.13556

Sokol, N. W., Kuebbing, S. E., Karlsen-Ayala, E., & Bradford, M. A. (2019). Evidence for the primacy of living root inputs, not root or shoot litter, in forming soil organic carbon. *New Phytologist*, *221*(1), 233–246. doi: 10.1111/nph.15361

Steffen, W. (2006). The Arctic in an Earth System Context: From Brake to Accelerator of Change. *Ambio*, *35*, 153–159. doi: 10.1579/0044-7447(2006)35[153:TAIAES]2.0.CO;2

Stewart, K. J., Coxson, D., & Siciliano, S. D. (2011). Small-scale spatial patterns in N_2-fixation and nutrient availability in an arctic hummock-hollow ecosystem. *Soil Biology and Biochemistry*, *43*(1), 133–140. doi: 10.1016/j.soilbio.2010.09.023

Strauss, J., Schirrmeister, L., Wetterich, S., Borchers, A., & Davydov, S. P. (2012). Grain-size properties and organic-carbon stock of Yedoma Ice Complex permafrost from the Kolyma lowland, northeastern Siberia. *Global Biogeochemical Cycles*, *26*(3). doi: 10.1029/2011GB004104

Street, L. E., Garnett, M. H., Subke, J. A., Baxter, R., Dean, J. F., & Wookey, P. A. (2020). Plant carbon allocation drives turnover of old soil organic matter in permafrost tundra soils. *Global Change Biology*, *26*(8), 4559–4571. doi: 10.1111/gcb.15134

Street, L. E., Subke, J. A., Baxter, R., Dinsmore, K. J., Knoblauch, C., & Wookey, P. A. (2018). Ecosystem carbon dynamics differ between tundra shrub types in the western Canadian Arctic. *Environmental Research Letters*, *13*(8), 084014. doi: 10.1088/1748-9326/aad363

Stuiver, M., & Polach, H. (1977). Discussion Reporting of ^{14}C Data. *Radiocarbon*, *19*(3), 355–363.

Sturm, M., Douglas, T., Racine, C., & Liston, G. E. (2005). Changing snow and shrub conditions affect albedo with global implications. *Journal of Geophysical Research*, *110*(G1), 1004. doi: 10.1029/2005jg000013

Sturm, M., Holmgren, J., McFadden, J. P., Liston, G. E., Chapin, F. S., Racine, C. H., … Racine, C. H. (2001). Snow–Shrub Interactions in Arctic Tundra: A Hypothesis with Climatic Implications. *Journal of Climate*, *14*(3), 336–344. doi: 10.1175/1520-0442(2001)014<0336:SSIIAT>2.0.CO;2

Tape, K. D., Hallinger, M., Welker, J. M., & Ruess, R. W. (2012). Landscape Heterogeneity of Shrub Expansion in Arctic Alaska. *Ecosystems*, *15*(5), 711–724. doi: 10.1007/s10021-012-9540-4

Tape, K., Sturm, M., & Racine, C. (2006). The evidence for shrub expansion in Northern Alaska and the Pan-Arctic. *Global Change Biology*, *12*(4), 686–702. doi: 10.1111/j.1365-

2486.2006.01128.x

Tarnocai, C., Canadell, J. G., Schuur, E. A. G., Kuhry, P., Mazhitova, G., & Zimov, S. (2009). Soil organic carbon pools in the northern circumpolar permafrost region. *Global Biogeochemical Cycles*, *23*(2), n/a-n/a. doi: 10.1029/2008GB003327

Thode, H. G., Shima, M., Rees, C. E., & Krishnxmurty, K. V. (1965). Carbon-13 isotope effects in systems containing carbon dioxide, bicarbonate, carbonate, and metal ions. *Canadian Journal of Chemistry*, *43*(3), 582–595.

Thomas, E. K., Castañeda, I. S., McKay, N. P., Briner, J. P., Salacup, J. M., Nguyen, K. Q., & Schweinsberg, A. D. (2018). A Wetter Arctic Coincident With Hemispheric Warming 8,000 Years Ago. *Geophysical Research Letters*, *45*(19), 10,637-10,647. doi: 10.1029/2018GL079517

Torn, M. S., Lapenis, A. G., Timofeev, A., Fischer, M. L., Babikov, B. V., & Harden, J. W. (2002). Organic carbon and carbon isotopes in modern and 100-year-old-soil archives of the Russian steppe. *Global Change Biology*, *8*(10), 941–953. doi: 10.1046/j.1365-2486.2002.00477.x

Treat, C. C., Natali, S. M., Ernakovich, J., Iversen, C. M., Lupascu, M., Mcguire, A. D., … Waldrop, M. P. (2015). A pan-Arctic synthesis of CH_4 and CO_2 production from anoxic soil incubations. *Global Change Biology*, *21*(7), 2787–2803. doi: 10.1111/gcb.12875

Trent, V. A., Medlin, J. H., Coleman, S. L., & Stanton, R. W. (1982). Chemical analyses and physical properties of 12 coal samples from the Pocahontas field, Tazewell County, Virginia, and McDowell County, West Virginia. *U.S. Geological Survey Bulletin*, *Bulletin*(1528). doi: 10.3133/b1528

Trumbore, S., Czimczik, C. I., Sierra, C. A., Muhr, J., & Xu, X. (2015). Non-structural carbon dynamics and allocation relate to growth rate and leaf habit in California oaks. *Tree Physiology*, *35*(11), 1206–1222. doi: 10.1093/TREEPHYS/TPV097

Trumbore, S. E. (2000). Age of soil organic matter and soil respiration: Radiocarbon constraints on belowground C dynamics. *Ecological Applications*, *10*(2), 399–411. doi: 10.1890/1051-0761(2000)010[0399:AOSOMA]2.0.CO;2

Trumbore, S. E. (2006). Carbon respired by terrestrial ecosystems - recent progress and challenges. *Global Change Biology*, *12*(2), 141–153. doi: 10.1111/j.1365-2486.2006.01067.x

Trumbore, S. E. (2009). Radiocarbon and soil carbon dynamics. *Annual Review of Earth and Planetary Sciences*, *37*(1), 47–66. doi: 10.1146/annurev.earth.36.031207.124300

Trumbore, S. E., Sierra, C. A., & Hicks Pries, C. E. (2016). Radiocarbon nomenclature, theory, models, and interpretation: Measuring age, determining cycling rates, and tracing source pools. In *Radiocarbon and Climate Change: Mechanisms, Applications and Laboratory Techniques* (pp. 45–82). Springer International Publishing. doi: 10.1007/978-3-319-25643-6_3

Turetsky, M. R., Abbott, B. W., Jones, M. C., Anthony, K. W., Olefeldt, D., Schuur, E. A. G., … McGuire, A. D. (2020). Carbon release through abrupt permafrost thaw. *Nature Geoscience*, *13*(2), 138–143. doi: 10.1038/s41561-019-0526-0

Turetsky, M. R., Jones, M. C., Walter Anthony, K. M., Olefeldt, D., Schuur, E. A. G., Koven, C. D., … Grosse, G. (2019). Permafrost collapse is accelerating carbon release. *Nature*, *569*, 32–24.

Vankoughnett, M. R., & Grogan, P. (2016). Plant production and nitrogen accumulation above- and belowground in low and tall birch tundra communities: the influence of snow and litter. *Plant and Soil*, *408*(1–2), 195–210. doi: 10.1007/s11104-016-2921-2

Verpoorter, C., Kutser, T., & Tranvik, L. (2012). Automated mapping of water bodies using landsat multispectral data. *Limnology and Oceanography: Methods*, *10*(DECEMBER), 1037–1050. doi: 10.4319/lom.2012.10.1037

Voigt, C., Marushchak, M. E., Lamprecht, R. E., Jackowicz-Korczyński, M., Lindgren, A., Mastepanov, M., … Biasi, C. (2017). Increased nitrous oxide emissions from Arctic peatlands after permafrost thaw. *Proceedings of the National Academy of Sciences of the United States of America*, *114*(24), 6238–6243. doi: 10.1073/pnas.1702902114

Wahren, C.-H. A., Walker, M. D., & Bret-Harte, M. S. (2005). Vegetation responses in Alaskan arctic tundra after 8 years of a summer warming and winter snow manipulation experiment. *Global Change Biology*, *11*(4), 537–552. doi: 10.1111/j.1365-2486.2005.00927.x

Walker, J. C., Xu, X., Fahrni, S. M., Lupascu, M., & Czimczik, C. I. (2015). Developing a passive trap for diffusive atmospheric $^{14}CO_2$ sampling. *Nuclear Instruments and Methods in Physics Research, Section B: Beam Interactions with Materials and Atoms*, *361*, 632–637. doi: 10.1016/j.nimb.2015.05.030

Walker, M. D., Walker, D. A., Welker, J. M., Arft, A. M., Bardsley, T., Brooks, P. D., … Turner, P. L. (1999). Long-term experimental manipulation of winter snow regime and summer temperature in arctic and alpine tundra. In *PROCESSES Hydrol. Process* (Vol. 13). doi: 10.1002/(SICI)1099-1085(199910)13:14/15

Wallace, C. A., & Baltzer, J. L. (2020). Tall Shrubs Mediate Abiotic Conditions and Plant Communities at the Taiga–Tundra Ecotone. *Ecosystems*, *23*(4), 828–841. doi: 10.1007/s10021-019-00435-0

Walvoord, M. A., & Kurylyk, B. L. (2016). Hydrologic Impacts of Thawing Permafrost-A Review. *Vadose Zone Journal*, *15*(6), vzj2016.01.0010. doi: 10.2136/vzj2016.01.0010

Wang, T., Peng, S., Lin, X., & Chang, J. (2013). Declining snow cover may affect spring phenological trend on the Tibetan Plateau. *Proceedings of the National Academy of Sciences of the United States of America*, *110*(31), E2854-5. doi: 10.1073/pnas.1306157110

Wang, T., Yang, D., Yang, Y., Piao, S., Li, X., Cheng, G., & Fu, B. (2020). Permafrost thawing puts the frozen carbon at risk over the Tibetan Plateau. *Science Advances*, *6*(19), 3513–3519. doi: 10.1126/sciadv.aaz3513

Wang, Y., & LeVan, M. D. (2009). Adsorption equilibrium of carbon dioxide and water vapor on zeolites 5a and 13X and silica gel: Pure components. *Journal of Chemical and Engineering Data*, *54*(10), 2839–2844. doi: 10.1021/je800900a

Watanabe, K., & Wake, T. (2009). Measurement of unfrozen water content and relative permittivity of frozen unsaturated soil using NMR and TDR. *Cold Regions Science and Technology*, *59*(1), 34–41. doi: 10.1016/j.coldregions.2009.05.011

Welker, J. M., Fahnestock, J. T., Henry, G. H. R., O'Dea, K. W., & Chimner, R. A. (2004). CO_2 exchange in three Canadian High Arctic ecosystems: Response to long-term experimental warming. *Global Change Biology*, *10*(12), 1981–1995. doi: 10.1111/j.1365-2486.2004.00857.x

Welker, J. M., Fahnestock, J. T., & Jones, M. H. (2000). Annual CO_2 Flux in Dry and Moist Arctic Tundra: Field Responses to Increases in Summer Temperatures and Winter Snow Depth. *Climatic Change*, *44*(1/2), 139–150. doi: 10.1023/A:1005555012742

Welker, J. M., Fahnestock, J. T., Sullivan, P. F., & Chimner, R. A. (2005). Leaf mineral nutrition of Arctic plants in response to warming and deeper snow in northern Alaska. *Oikos*, *109*(1), 167–177. doi: 10.1111/j.0030-1299.2005.13264.x

Whiticar, M. J., Faber, E., & Schoell, M. (1986). Biogenic methane formation in marine and freshwater environments: CO_2 reduction vs. acetate fermentation-Isotope evidence. *Geochimica et Cosmochimica Acta*, *50*(5), 693–709. doi: 10.1016/0016-7037(86)90346-7

Wilcox, E. J., Keim, D., de Jong, T., Walker, B., Sonnentag, O., Sniderhan, A. E., … Marsh, P. (2019). Tundra shrub expansion may amplify permafrost thaw by advancing snowmelt timing. *Arctic Science*, *5*(4), 202–217. doi: 10.1139/as-2018-0028

Winston, G. C., Sundquist, E. T., Stephens, B. B., & Trumbore, S. E. (1997). Winter CO_2 fluxes in a boreal forest. *Journal of Geophysical Research*, *102*(24), 28795–28804. doi: 10.1029/97jd01115

Wotte, A., Wischhöfer, P., Wacker, L., & Rethemeyer, J. (2017a). $^{14}CO_2$ analysis of soil gas: Evaluation of sample size limits and sampling devices. *Nuclear Instruments and Methods in Physics Research, Section B: Beam Interactions with Materials and Atoms*, *413*, 51–56. doi: 10.1016/j.nimb.2017.10.009

Wotte, A., Wordell-Dietrich, P., Wacker, L., Don, A., & Rethemeyer, J. (2017b). $^{14}CO_2$ processing using an improved and robust molecular sieve cartridge. *Nuclear Instruments and Methods in Physics Research, Section B: Beam Interactions with Materials and Atoms*, *400*, 65–73. doi: 10.1016/j.nimb.2017.04.019

Xu, X., Trumbore, S. E., Zheng, S., Southon, J. R., McDuffee, K. E., Luttgen, M., & Liu, J. C. (2007). Modifying a sealed tube zinc reduction method for preparation of AMS graphite targets: Reducing background and attaining high precision. *Nuclear Instruments and Methods in Physics Research Section B: Beam Interactions with Materials and Atoms*, *259*(1), 320–329. doi: 10.1016/J.NIMB.2007.01.175

Zhang, H., & Cloud, A. (2006). The Permeability Characteristics of Silicone Rubber. *SAMPE*

Fall Technical Conference: Global Advances in Materials and Process Engineering, Coating and Sealants Section, 1–10.

Zhang, T. (2005, December 1). Influence of the seasonal snow cover on the ground thermal regime: An overview. *Reviews of Geophysics*, Vol. 43, p. 4002. John Wiley & Sons, Ltd. doi: 10.1029/2004RG000157

APPENDIX

5.4 Schematics

Schematics 5.4.1-5.4.4 describe the components and dimensions of the passive CO_2 sampling system from Chapter 2. Access well v1.0 was used in initial calibrations and tests, and for results in Chapter 3, while v2.0 was used in Chapter 4. The molecular sieve trap was used as the exchangeable CO_2 capture device for both access wells, while the heater (representing 1 of 2 identical halves) was used to thermally desorb captured CO_2 in the laboratory.

The soil core device (5.4.5) was used to collect soil samples in Chapters 2 & 3.

5.4.1 Access well v1.0

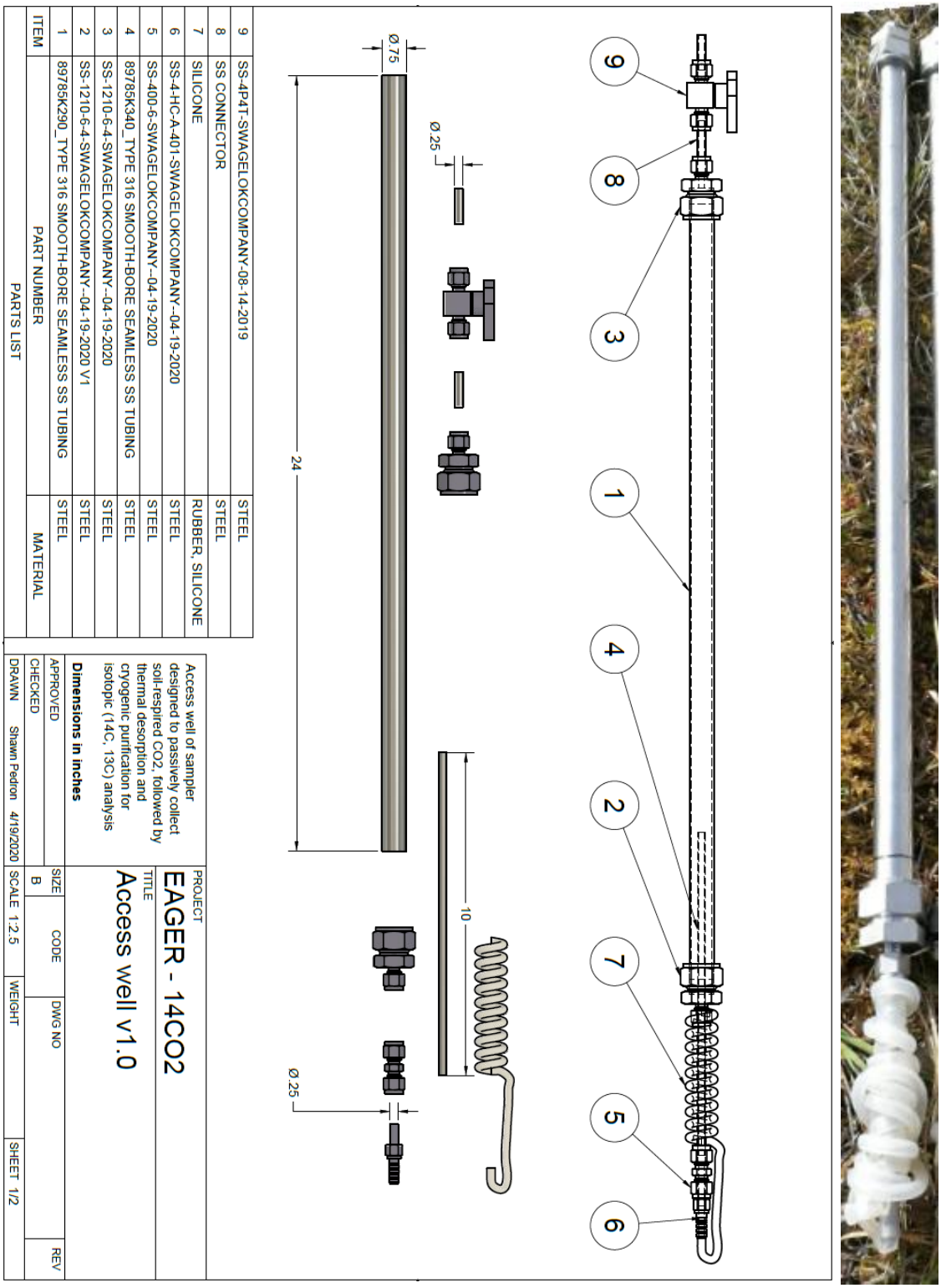

ITEM	PART NUMBER	MATERIAL
9	SS-4P4T-SWAGELOKCOMPANY-08-14-2019	STEEL
8	SS CONNECTOR	STEEL
7	SILICONE	RUBBER, SILICONE
6	SS-4-HC-A-401-SWAGELOKCOMPANY--04-19-2020	STEEL
5	SS-400-6-SWAGELOKCOMPANY--04-19-2020	STEEL
4	89785K340_TYPE 316 SMOOTH-BORE SEAMLESS SS TUBING	STEEL
3	SS-1210-6-4-SWAGELOKCOMPANY--04-19-2020	STEEL
2	SS-1210-6-4-SWAGELOKCOMPANY--04-19-2020 V1	STEEL
1	89785K290_TYPE 316 SMOOTH-BORE SEAMLESS SS TUBING	STEEL

PARTS LIST

Access well of sampler designed to passively collect soil-respired CO_2, followed by thermal desorption and cryogenic purification for isotopic (^{14}C, ^{13}C) analysis

Dimensions in inches

APPROVED	
CHECKED	
DRAWN	Shawn Pedron 4/19/2020

PROJECT: EAGER - 14CO2

TITLE: Access well v1.0

SIZE	CODE	DWG NO	REV
B			

SCALE 1:2.5	WEIGHT	SHEET 1/2

5.4.2 Access well v2.0

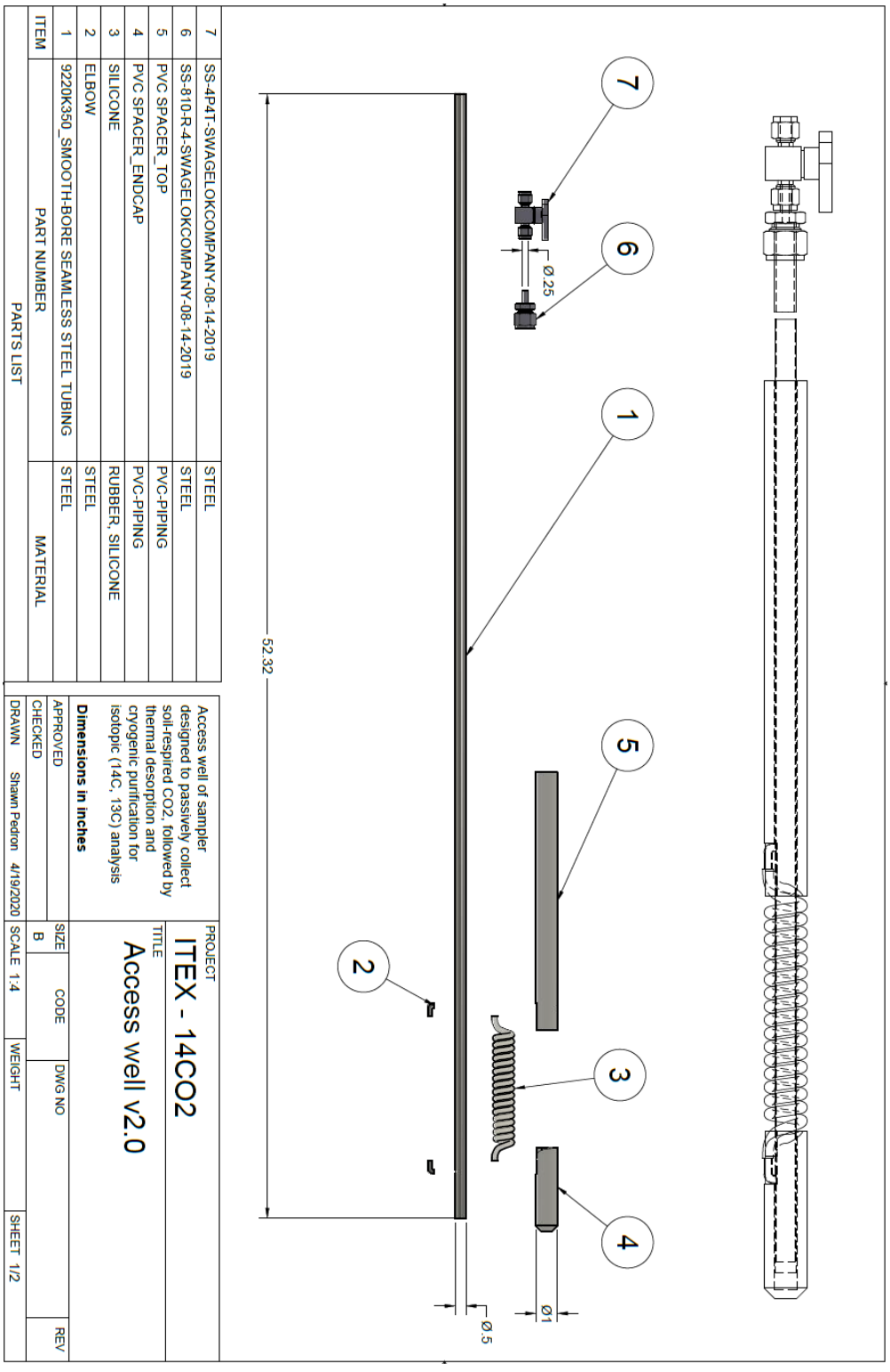

ITEM	PART NUMBER	MATERIAL
7	SS-4P4T-SWAGELOKCOMPANY-08-14-2019	STEEL
6	SS-810-R-4-SWAGELOKCOMPANY-08-14-2019	STEEL
5	PVC SPACER_TOP	PVC-PIPING
4	PVC SPACER_ENDCAP	PVC-PIPING
3	SILICONE	RUBBER, SILICONE
2	ELBOW	STEEL
1	9220K350_SMOOTH-BORE SEAMLESS STEEL TUBING	STEEL

PARTS LIST

Access well of sampler designed to passively collect soil-respired CO2, followed by thermal desorption and cryogenic purification for isotopic (14C, 13C) analysis

Dimensions in inches

APPROVED	
CHECKED	
DRAWN	Shawn Pedron 4/19/2020

PROJECT: ITEX - 14CO2

TITLE: Access well v2.0

SIZE	CODE	DWG NO	REV
B			
SCALE 1:4	WEIGHT	SHEET 1/2	

5.4.3 Molecular sieve trap

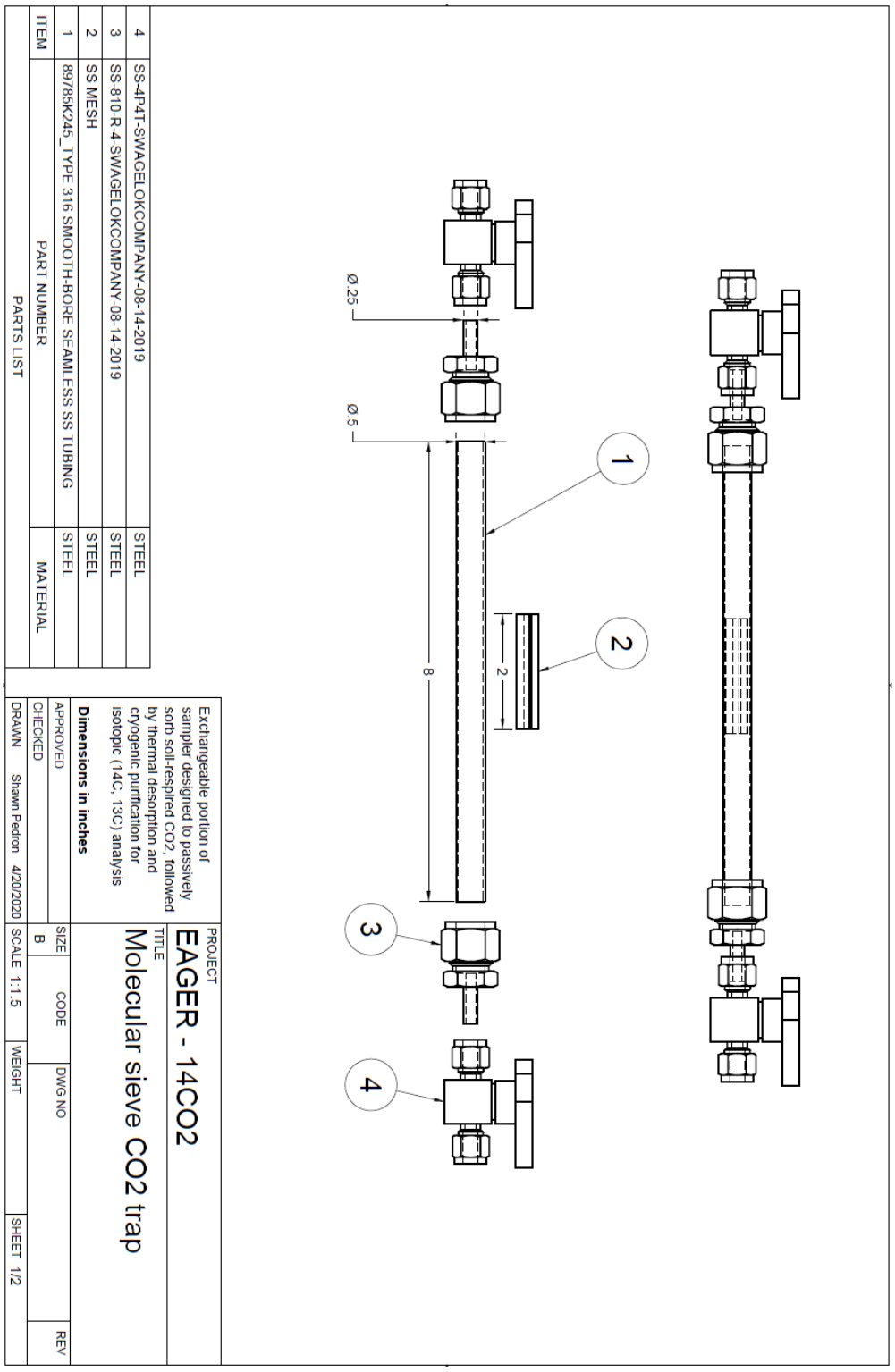

ITEM	PART NUMBER	MATERIAL
4	SS-4P4T-SWAGELOKCOMPANY-08-14-2019	STEEL
3	SS-810-R-4-SWAGELOKCOMPANY-08-14-2019	STEEL
2	SS MESH	STEEL
1	89785K245_TYPE 316 SMOOTH-BORE SEAMLESS SS TUBING	STEEL

PARTS LIST

Exchangeable portion of sampler designed to passively sorb soil-respired CO2, followed by thermal desorption and cryogenic purification for isotopic (14C, 13C) analysis

Dimensions in inches

APPROVED			
CHECKED			
DRAWN	Shawn Pedron	4/20/2020	

PROJECT: EAGER - 14CO2

TITLE: Molecular sieve CO2 trap

SIZE	CODE	DWG NO	REV
B			

SCALE 1:1.5	WEIGHT	SHEET 1/2

5.4.4 Clamshell heater

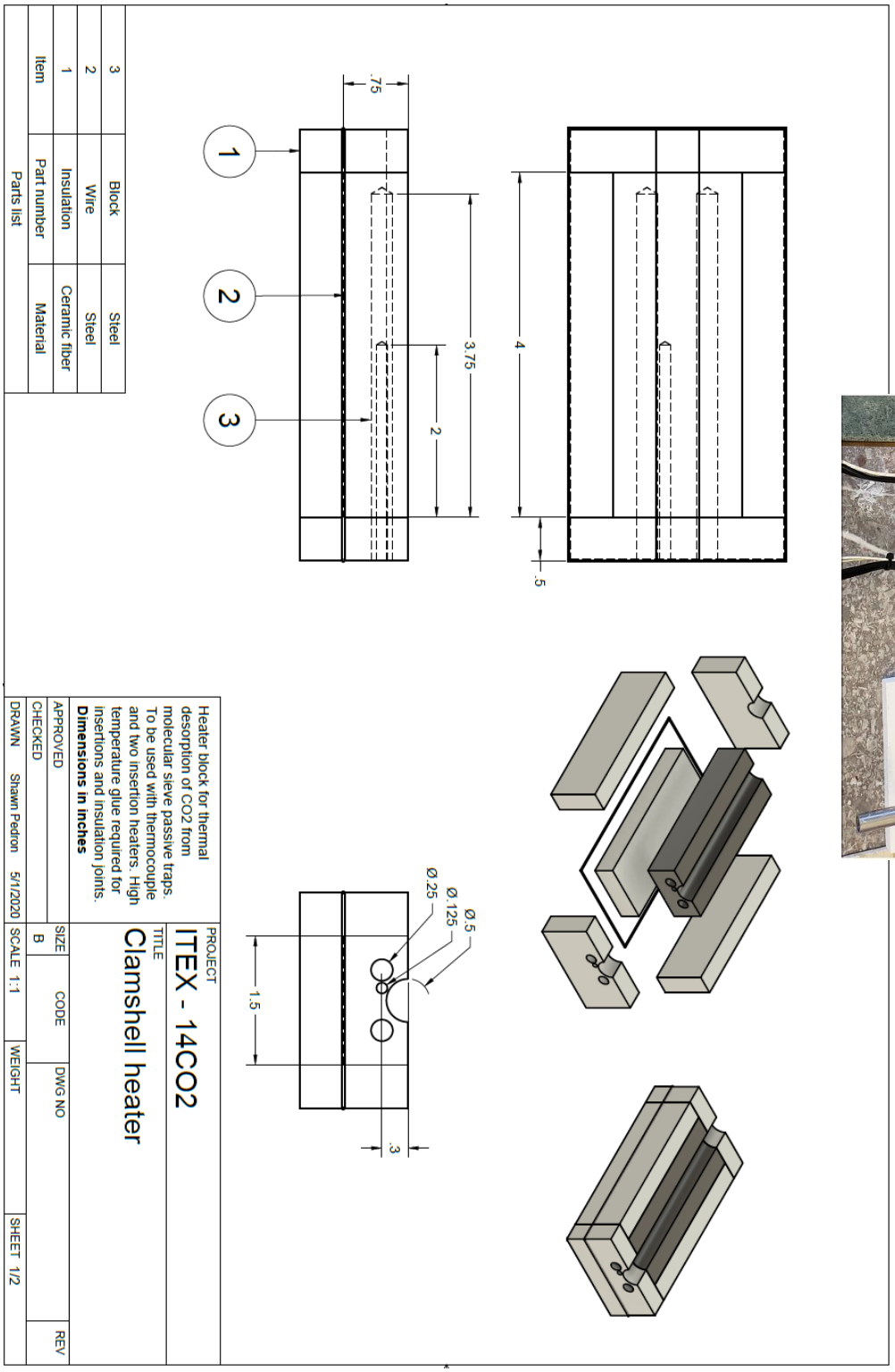

5.4.5 Soil core device

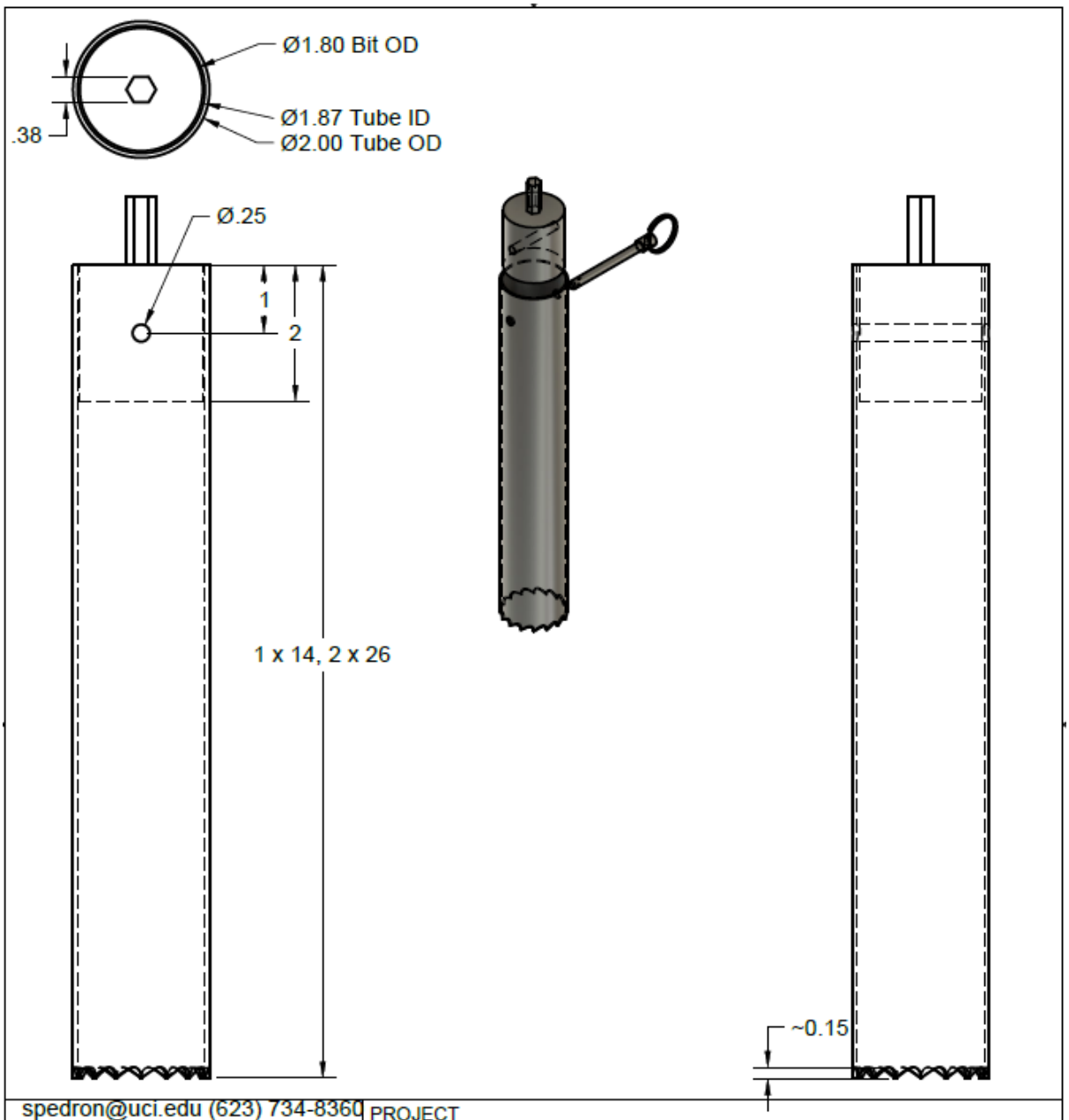

spedron@uci.edu (623) 734-8360

McMaster parts:
89975K360_HIGH-PRESSURE WELDED STEEL TUBING

95165A041_HEAVY DUTY QUICK-RELEASE PIN

PROJECT
Dept. ESS - P.I. Goulden

TITLE
Soil corer
McMaster parts - Dim. in inches

APPROVED	SIZE	CODE	DWG NO	REV
CHECKED	A	FG18442		
DRAWN Shawn Pedron 8/6/2019	SCALE 1:2	WEIGHT	SHEET 2/2	

5.5 MS trap assembly

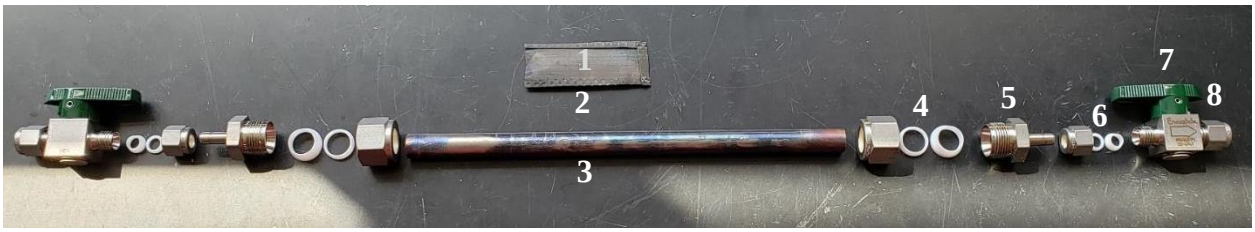

Parts

	Vendor	Part #	Dimensions	Part	#/sampler
1	Sigma Aldrich	20304	13X, 45-60 mesh, 50g	Molecular Sieve matrix (1.5g/trap)	0.06
2	McMaster Carr	9319T188	325x325 mesh, 0.0017”	SS wire cloth (envelope, 1.5"x6"/trap)	0.04
3	McMaster Carr	89785K843	1/2" OD	SS tubing, 6 ft (8"/trap)	0.11
4	Swagelok	T-800-SET	1/2"	PTFE ferrules (2/trap, 1/access well)	5
5	Swagelok	SS-810-R-4	1/2" to 1/4"	Reducer (2/trap, 1/access well)	5
6	Swagelok	T-400-SET	1/4"	PTFE ferrules (2/trap, 1/access well)	5
7	Swagelok	SS-4P4T	1/4"	2-way valve (2/trap, 1/access well)	5
8	Swagelok	B-400-P	1/4"	Brass Plug (2/trap)	4

Tools

- Scissors
- Pencil, sharpie, ruler
- Gloves (work + nitrile)
- Bench-mounted vise
- Tube cutter
- Lab oven (≤600^{o}C)

Procedure

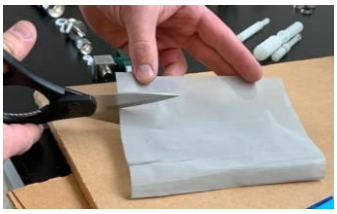

1. Cut raw materials to appropriate dimensions.
    a. SS tubing is cut to ~8” length
        i. Measure raw tubing, marking in 8” increments
        ii. Clamp in vise (between a cloth)
        iii. Cut with tube cutter (work gloves)
    b. SS cloth is cut into 1.5” by 6” rectangles
        i. Mark grid on raw sheet using ruler and pencil
        ii. Cut with regular scissors

2. Fold SS cloth into envelopes
    a. Fold in half (6” -> 3”)
    b. Fold one long edge about 1 mm over itself, crimp in vice
    c. Fold same edge again, crimp in vice
    d. Fold opposite edge in opposite direction, crimp in vice
    e. Fold opposite again, crimp in vice
    f. Final product should resemble a narrow envelope. Slide sharpie inside to form it into more of a tall cup

3. Pre-bake materials in oven (ambient/lab atmosphere) to oxidize residual organics from fabrication
    a. SS tubing and envelopes: 500^{o}C for 1 hr
        i. Do not wrap in Al foil, it will fuse to the steel!
        ii. Place in ceramic / Pyrex tray or beaker
        iii. Handle envelopes with nitrile gloves post-baking (latex snags but suit yourself)
    b. MS material: 600^{o}C for 1 hr
        i. Do not exceed 700^{o}C, or the MS will decompose
        ii. Place in Pyrex beaker, bowl, or dish, uncovered
        iii. After baking, move to desiccator to avoid excess H_2O absorption

4. Weigh cool MS material into cool envelopes
    a. Weigh by difference using a plastic tray or weigh paper
    b. 1.5 g MS is about the max each envelope can handle and still fit in ½” tube. This theoretically holds up to ~70 mg CO_2-C, if not competing with H_2O (Wang & LeVan, 2009)
    c. Fold top over ~1 mm, crimp in vise, fold once more, crimp in vise

5. Insert completed envelope into SS tube
    a. Place envelope and tube parallel on bench. Align center

    b. Place a spacing device (pen or glass rod, the closer to tube ID the better) with the tip touching one end of the envelope, parallel to the tube. Mark it where it aligns with the end of the tube
    c. With fingers pinch envelope into “U” shape lengthwise, forming a kind of long trough. You may need to shake it a bit to evenly distribute the MS within
    d. Slide envelope into tube, center using spacer
6. Attach ½” to ¼” reducers to either end of tube
    a. If you anticipate taking apart traps, replace ½” steel ferrules (as-shipped) with PTFE (Swagelok T-800-SET). Otherwise, you will not be able to re-use the trap if disassembled, as steel ferrules permanently warp the tube (by design)! Xiaomei has wisdom about limited PTFE ferrule lifetime and general ferrule tightening technique.
    b. PTFE ferrules will reduce the heat that reaches the valves during cleaning, but will also need to be tightened periodically as the heat causes loosening
    c. Ferrules should be tightened until you feel resistance, and then 1/4 turn more.

7. Attach SS-4P4T valves to ¼” end of reducers, replacing steel ferrules (as-shipped) with PTFE (T-400-SET). Cap and store/transport with brass plugs to minimize air infiltration.

Traps must be cleaned at least once before sampling. Ideally, load CRM onto a random selection of traps and test (Pedron *et al.*, 2021).